521 | Mai 1992

SCHRIFTENREIHE SCHIFFBAU

Jörg Denker, Thomas Knaack und Jürgen Kux

Experimental and Numerical Investigations of HSVA-Tanker -2 Flow Field

TUHH
Technische Universität Hamburg-Harburg

Experimental and Numerical Investigations of HSVA-Tanker-2 Flow Field

Jörg Denker, Thomas Knaack, Jürgen Kux, Hamburg, Technische Universität Hamburg-Harburg, 1992

Schriftenreihe Schiffbau
Schwarzenbergstraße 95c
D-21073 Hamburg

http://www.tuhh.de/vss

INSTITUT FÜR SCHIFFBAU DER UNIVERSITÄT HAMBURG

Bericht Nr. 521

Experimental and Numerical Investigations of HSVA-Tanker-2 Flow Field

Jörg Denker, Thomas Knaack, Jürgen Kux

Mai 1992

Abstract

The flow around the double-model of a ship hull was investigated experimentally and numerically. The hull form was designed by SSPA with the purpose to serve as second test case in the competition of computational methods, the 1991 SSPA-CTH-IIHR Workshop on Ship Viscous Flow, and was characterized by U-shaped stern sections in order to get a more uniform flow in the propeller plane.

The experiments were performed in the wind-tunnel. The distribution of the mean velocity was investigated by three-component LDV-measurements at 5 stations, leading to detailed surveys (800 points scanned). Turbulence was investigated too and charts of the distribution of turbulent kinetic energy k in the downstream stern region could be drawn. The directional field of wall shear stresses was visualized with paint in the stern region and wall-pressure was recorded there by pressure taps.

The numerical investigation centered around a detailed computation of the three-dimensional turbulent boundary layer by a program of the Cebeci-type (using a simple algebraic turbulence model and as outer velocity field the output of a potential theoretic computation with one half of the hull approximated by more than 1800 panels). Wall pressure values and boundary-layer velocity profiles show fair agreement with experiment for the upstream stations.

Zusammenfassung

Die Umströmung eines Schiff-Doppelmodells wurde experimentell und numerisch untersucht. Die Rumpfform wurde in der SSPA entworfen. Sie diente als zweiter Testfall für die Konkurrenz der Berechnungsverfahren im 1990 SSPA-CTH-IIHR Workshop Ship Viscous Flow. Die Rumpfform ist im Hinterschiffsbereich durch mehr U-förmige Spanten gekennzeichnet. Dadurch soll eine gleichmäßigere Strömung in der Propellerebene erreicht werden.

Die Experimente wurden im Windkanal durchgeführt. Die Verteilung der mittleren Geschwindigkeit im Strömungsfeld wurde mit einem Dreikomponenten-LDV-System in 5 Spantebenen an (im Mittel) 800 Punkten pro Ebene gemessen. Auch die Turbulenz wurde untersucht und Isolinienbilder für die kinetische Energie der Turbulenz k wurden für die hinteren Meßebenen erstellt. Das Richtungsfeld der Wandschubspannungen im Hinterschiffsbereich wurde mit Anstrichbildern sichtbar gemacht und der Wanddruck in diesem Bereich über Druckanbohrungen an einer Reihe von Orten bestimmt.

Schwerpunkt der numerischen Untersuchungen war die Berechnung der dreidimensionalen turbulenten Grenzschicht mit einem Rechenprogramm nach Cebeci. Das Grenzschichtprogramm enthält ein einfaches algebraisches Turbulenzmodell und verwendet die Ergebnisse einer potentialtheoretischen Berechnung der Außenströmung unter Aufteilung der Rumpfoberfläche in ca. 1800 Paneele. Wanddruck-Werte und Geschwindigkeitsprofile in der Grenzschicht zeigen befriedigende Übereinstimmung für die weiter stromaufwärts liegenden Spantebenen.

Contents

1 Introduction

Naval hydrodynamics is a challenge to the application of fluid dynamics, as well in the experimental field as in the numerical field.

The flow field around a ship hull has the free surface of the water as one of its boundaries, the moving surface of the hull (moving as a reaction to the pressure- and friction-forces) as another boundary. The real problem is thus an extreamly instationary one, even when the ship (or model) is not maneuvering. If we include the propeller, the problem becomes still more involved. The propeller works in the extremely nonhomogeneous turbulent wake originated by the detaching three-dimensional boundary layer which has developed along the hull, a wake which is influenced by both propeller effects, the suction action and the blade-induced velocities.

Experiments are needed to understand the details of the complex flow field and to provide reliable data sets suited to serve as test cases for the numerical methods. Full-scale experiments are expensive and it is unlikely that a domain of appropriate size can be scanned. Though data sets have been obtained in the boundary layer (single location) and in the near wake in front of the propeller (over restricted areas in transverse planes) for several full scale ships with one of the Laser- Doppler-Velocimetry (LDV) systems of the Institut für Schiffbau (IfS), these sets do not provide enough data to be used for a thorough test. Therefore data sets appropriate to be used as test cases are mainly obtained from model experiments.

Main goal of ship research is the optimization of the hull form say in relation to resistance and propulsion efficiency. In order to achieve this the model should be varied and measured again and again. Since this is expensive in the experiment, it is generally only done in numerical simulation. Today the state of the art is that when a boundary layer calculation is performed generally the problem is simplified by ignoring the effects of the free surface, the propeller, the rudder and other appendages. When a double model of a ship hull is investigated in the wind tunnel, the same simplifications are introduced.

At the IfS over several years systematic investigations of the flow field around such a double model of a high block-coefficient hull, the HSVA-tanker, (sometimes called Hoffmann-tanker) had been performed. Detailed measurements were thus available for a flow where the boundary layer and its separation and the so called nominal wake (with the above mentioned simplifications) were scrutinized. This data set was felt to be appropriate to serve as a first test case in a workshop, the 1990 SSPA-CTH-IIHR Workshop on SHIP VISCOUS FLOW. It was a competition of different calculation methods and codes, the participants being provided with a common set of input data and expected to present as results pressure distributions and the velocity fields in certain planes where values had been measured.

The investigation of a second model flow would well be convenient, it was considered, in order to have a second test case. So measurements and computations relating to the flow around this second model, called the mystery case, were performed. They are the theme of this report. In fact since the measurements took place later than the deadline for the delivery of the computational data, nobody could have knowledge on the details of the flow field, the case thus being really a mystery case. It was agreed to choose

a hull-form with the fore half having the same body plan than the first test case (the original HSVA-tanker) and with lines for the aft part with frames more U-shaped than the V-shaped frames of the first one. It was expected that this would lead to an increased effect of boundary layer separation. This case is now called, when data is being circulated by the IfS, the HSVA-tanker-2. The model was manufactured with funds granted by the german research council Deutsche Forschungsgemeinschaft.

The experimental investigation was accompanied by a corresponding numerical study. The velocity field around this double model was computed by first applying a potential-theoretic method to obtain the outer flow (neglecting viscosity and vorticity there) and then by applying three-dimensional boundary layer methods to obtain the (viscosity and turbulence dominated) details of the field near to the body.

2 Model, HSVA-tanker-2

The second hull form was designed merely to serve as a test case in the mentioned workshop and, (as the first test case) will never be built as a real ship. The idea was (and here we draw from the proceedings Larsson [11]) to enable an evaluation of how good existing calculation methods perform in predicting changes of the stern flow caused by minor modifications of the afterbody lines. Modifications of this kind are common as means to make the velocity distribution at the propeller plane more uniform; thus improving the propulsion and cavitation characteristics of the propeller.

From a comparison of the distribution patterns of the longitudinal component of the mean velocity of the nominal wake at the propeller plane it was deduced that a minor change in the afterbody lines from more V-shaped to more U-shaped sections lead to quite different velocity distributions. The mystery case hull-form was therefore obtained by modifying the stern sections of the original HSVA-tanker (test case 1) so that they became more U-shaped. The forebody is identical to that of the original HSVA model and the length between perpendiculars is the same, but the stem post, now straight and vertical, has been moved slightly backwards and there is no hub as for the original model hull. Due to these changes the propeller plane was assumed to have moved backwards by $X/L = 0.013$, as compared to the original hull, and measured as well as computed results for this new hull were requested at planes displaced this much backwards (this not to be applied to the check station $X/L = 0.646$, which remained unchanged. InFig. 1 the body plan of HSVA-tanker-2 is shown.

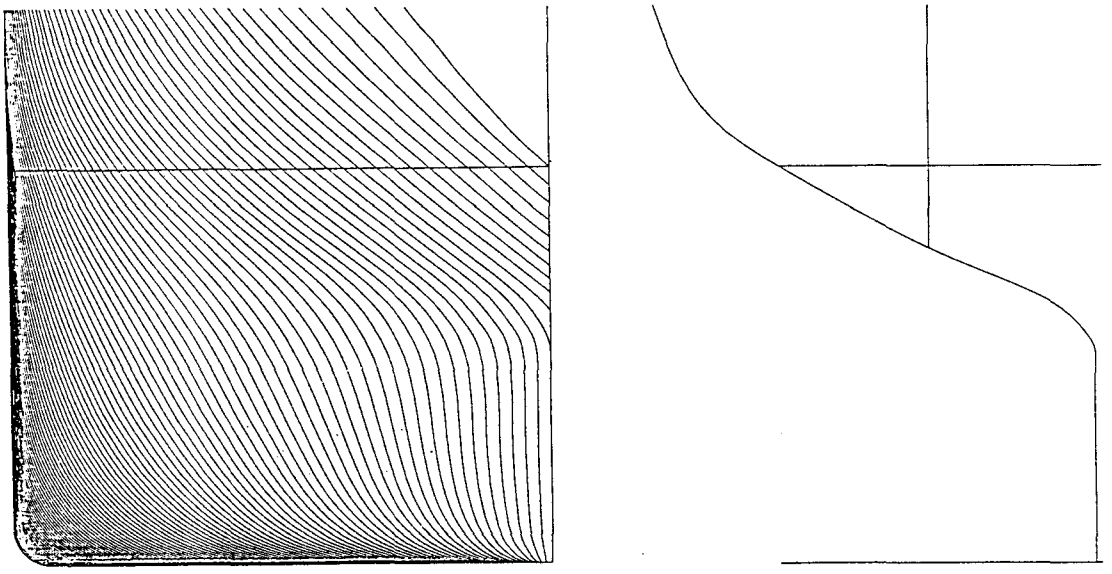

Figure 1: Body plan and contour of HSVA-tanker-2 hull (only stern)

3 Experimental Set Up

The length between perpendiculars of the double model of the HSVA-tanker-2 investigated in the wind tunnel is $L_{pp} = 2663mm$ (in this report termed simply as L) while the model beam is $400mm$ and the draught is $150mm$.
The measurements were made in the open test section of the wind tunnel of the IfS. Corresponding to the limitations of numerical investigations the model is investigated without rudder, propeller and appendages. The incident velocity is $U_\infty = 27\ \frac{m}{s}$. With the model length this leads to a Reynolds number of $5 \cdot 10^6$.
The model is fixed in a measuring cage (slotted wall) with a lenght of $5m$ and a diameter of $1.2m$. Wires are used to support the model, they are located at $520mm$ ($X/L = 0.195$) and $2160mm$ ($X/L = 0.811$).
In order to compare wind tunnel investigations of the original HSVA-tanker with those from HSVA-tanker-2, size and blockage of both models have not been changed.

While velocity of the original HSVA-tanker was measured by using a five-hole pressure probe (Hoffmann [3], Wieghardt [8]), velocity and turbulence parameters at HSVA-tanker-2 were determined by Laser-Doppler-Velocimetry (LDV). A three-component three-colour velocimeter using glasfibers was employed. All three components of the mean volocity vector and all six components of the Reynolds stress tensor can be determined simulataniously. In consideration of the duration of measurements, this investigation was restricted to the three diagonal components of the Reynolds tensor. Development and capacity of the LDV-system and measurements of the Reynolds stresses at

the original HSVA-tanker are decribed by Knaack [6] in detail.

Some important specificition of this Laser-Velocimeter are (Magnitudes are given as well in mm as nondimensionalized by L_{PP}):

- Optical components from TSI 9100-12 optics are used. The focal length of the front lenses is $1.2m$.
- Signal processing was performed by counters.
- The accuracy of the velocity is 1% in relation to the absolute value of the velocity vector. The components of the Reynolds tensor can be determined within 5%.
- Diameter of the measuring volume is $0.1mm$ (3.710^{-5}), its lenght is $0.3mm$ (1.110^{-4}).
- At incidence of the laser beams normal to the hull surface (at the side wall), smallest wall distance was 1 mm ($3.7\,10^{-4}$). This smallest wall distance was limited due to reflexions of the incident laser beams at the hull surface. Below the keel – laser beams and hull surface being parallel – measurements down to a distance of 0.1 mm ($3.7\,10^{-5}$) were possible.

All measurements are controlled by computer. This allows the accuracy of positioning to be $0.01mm$, which is less than the roughness of the model surface.

At each location 500 samples of the momentaneous values of all three components of the velocity vector were stored. A Gaussian distribution was adjusted to the measured probability distribution of the components of the velocity vector. By thus the mean and the standard deviation was given.

For the Laser-Velocimeter measurements seeding was neccessary. Upstream of the nuzzle an atomiser produces water droplets with 5% glycerine.

25 pressure taps were built into the model surface in order to measure the wall pressure. (For coordinates of locations refer to appendix B). Inside diameter of the pressure taps is $1mm$.

Surface flow visualisation was done by painting a film of oil and sooth on the hull surface at the stern of the ship. Photographs of the directional field of wall shear stresses (limiting streamlines) were taken.

4 Numerical Methods

In naval hydrodynamics we are faced with one of the application fields of CFD, though numerical ship hydrodynamics presents a series of features not present in other CFD areas.

The Reynolds-number for the full-scale ship is of the order of magnitude of 10^9 . Experimental data here is scarce and therefore ship rersearch has largely been model research. The Reynolds-number for the model-scale is of the order of 10^6. Numerical methods have to be tested against experimental data obtained at this scale and the assumption is made, that they remain valid in their prognostics for the full scale case.

As stated in the introduction, following the idea of Prandtl, here the outer flow was calculated applying potential theory and then the near-wall flow by boundary layer theory.

For the calculation of the velocity field by potential theory a singularity-method was applied in this study. The code has been developed at the IfS, being in use meanwhile for many years. It is based on the original work of A.M.O.Smith and his group [2]. It is a so called panel method, where only sources and sinks are used as singularities, these being localized on plane quadrilateral elements, the panels, which approximate the bounding surfaces (the body or walls), here the surface of the double-hull. More than 1800 panels are distributed over a quarter of this double-hull. A feature of the method allows to take into consideration the symmetries of the flow-problem, thus raising precision for a given number of panels or, stated differently, lowering the number of panels required for a prescribed accuracy. Once the distribution of the sources and sinks on the panelized surface has been determined from the boundary conditions (velocity component normal to the bounding wall equal to zero or equal to a prescribed blowing or suction), the velocity vector may be computed in arbitraryly selected points of space, and only there, where it is needed. An outer flow field with the velocity calculated by potential theory applies to model- and full-scale, i.e. is independent of the geometrical scale and is valid for different speeds, as long as dynamically induced changes in trim and sinkage do not need to be considered.

In order to simulate the suction by the propeller, and only this action of the propeller is considered in the frame of this project, an arrangement of sources and sinks is used. Geometrically this arrangement has more or less the size of the propeller with suction on the panels on its front side and blowing on those on its rear. This leads to different potential-theoretic velocity fields depending on whether this arrangement is included into the computation or not.

The boundary layer may be treated at different degrees of approximation. When a three-dimensional method is applied, the velocity vector in the boundary layer is obtained with its two components parallel to the wall in the direction of the wall coordinates obtained from (simplified) momentum equations while the third component normal to the wall may be derived from the continuity equation since the equation for the momentum balance in direction normal to the wall is neglected. The velocity parallel to the wall is generally shown as profiles over the distance from the wall of the component in direction of the outer flow and the component at right angles to this, the so called cross-flow.

The first three-dimensional boundary layer method applied was that forewarded by Cebeci [1], and only plots with results obtained by this method will be presented (for further details compare Kux [10]). Each calculation has to be performed for both, the model-scale, the only case where appropriate experimental data is available, and the full-scale case, being the one really of interest. This again has to be done with and without the mentioned simulation of the propeller suction action.

Cebeci's method uses nonorthogonal coordinates on the wall. The wall- curvature is not considered. The metrical tensor for the chosen coordinate system on the wall surface, i.e. the one resulting from the panelization, is computed and the geodetic curvature of the coordinate lines is taken into account. The terms of the boundary layer equations are approximated by a suitable difference scheme, this discretized equations are linearized by Newton's method and the resulting system of linear algebraic equations (its matrix presenting tridiagonal block structure) solved by the block elimination method by Keller. The turbulence model used, is a simple algebraic one, the two-deck model by Cebeci (based on the idea of Van Driest).

Another boundary-layer method investigated was the method by Monnoyer [12]. Several ideas forewarded 1971 by Kux [7], have been included in this method. Even the question of adecuate definition of the "loss thicknesses" as integral parameters is addressed, though presently not applied in the method. It is termed a second order method, which is correct since certain terms of the order of magnitude $O(\delta)$, with δ as the boundary-layer thickness, are not dropped. Nevertheless in the equation of motion for the component perpendicular to the wall certain terms have been discarded for the turbulent case. The turbulence model chosen is the algebraic model by Baldwin and Lomax, thus a model comparable to the one used in the Cebeci-method. Different schemes for the finite difference approximation are applied depending on the sign of the velocity component in the direction of the coordinate transverse to the mean flow direction. The resulting system of linear equations again has a matrix with tridiagonal box structure. The method requires a constant step size in the mentioned transverse coordinate (here along the frames). (This requirement is necessary to keep the truncation error low to second order.)

Several important features have been developed in this project and are now included in the method. Some of them will be explained here. The system of coordinate lines on the surface of the body, here the double hull, is given and derives from the panelization on which the potential theoretic calculation was based. The flow over a threedimensional body derived from this calculation has a velocity field with vectors at the wall having components in the two surface coordinate directions. The first coordinate direction is generally chosen in a way that it corresponds more or less to the mean lengthwise velocity. Since this is not known a priori, a component in the direction of the second coordinate, generally chosen girthwise along the frames, has to be expected almost everywhere on the body surface. This component will be zero in symmetry planes of the body if we only consider the case of zero incidence angle (no drift, no maneuvering). It will thus be zero along the water-line and the keel (supposed to be coordinate-lines). But it will eventually also become zero inbetween, as we cannot assume this component to have only one sign over the girth for all stations. This special case of vanishing girthwise component requires a special equation. In Cebecis method this equaton is obtained by taking the derivative of the original equations with respect to the second coordinate. This equation has been applied only at the keel and the water-line while it has been ignored at the location

(or locations) on the girth inbetween where the second component vanishes without a blow-up ocurring there in the computation.

Evidently this requires an adaptive computational net, which in the neighbourhood of the location of the change of sign of the second component replaces the original net by a new one which has at each station a mesh point (or points) placed girthwise at the location of this change of sign, allowing the application of the special equation there. Such an adaptive net has not been constructed for the application of the equations of Cebecis method in this investigation though it has been successfully used in a related investigation in our group. In principle even the first component could change its sign, which in the original net leads to a break down of the computation. An adaptive net which takes this into consideration too, would become severely distorted as compared to the original one.

The computational procedure which is used to obtain the derivatives for the special equation (vanishing transverse component) was improved since it leads to considerable errors when the surface is curved and the step size (mesh width) is large. Now the derivatives are obtained from spline approximations. As the derivatives are obtained at each station there may be a certain scatter in lengthwise direction. An optional smoothing by spline approximation has therefore also been provided.

Critical regions (very steep adverse pressure gradients, etc.) may cause a break-down of the computation. It is therefore necessary to start either from one or the other side of the domain along the second coordinate, trying to narrow down the gap where computation fails as far as possible. This possibility has been included now too.

Further features which have been installed are an optional automatic stepsize reduction in direction of the first coordinate if there are convergence- difficulties and a data-saving for restarts in case of machine failure (typically necessary when running the programm on smaller computers).

5 Results

Experiments were carried out from December 1990 till March 1991. Measurements of the pressure distribution in the wake of the model are planned, but did not take place until the publication of this report.

Computations were partially performed in a project "Development of Computational Methods in Fluid Dynamics" sponsored by Stiftung Volkswagenwerk (Kux [10]), which was finished in May 1991.

Locations of station and kind of investigation is shown in table 1.

CHECK STATIONS							
LOCATION	EXPERIMENT					COMPUTATION	
	wall	velocity		turbulence		potential	boundary
X/L	pressure	$\overline{u}$	$\overline{v}$, $\overline{w}$	$\overline{u'^2}$	k	flow	layer
0.128		X		X		X	X
0.646	X	X		X		X	X
0.917	X					X	
0.921		X	X	X	X		
0.964	X					X	
0.989		X	X	X	X		
1.018		X	X	X	X		

Table 1:

Results are presented in different manners in this report. I) We display a summary of results at different stations in a kind of graphics, which was used in the proceedings of 1990 SSPA-CTH-IIHR workshop. II) We show the information about the spatial structure of our results.
All parameters of the flow field are dimensionless using undisturbed incident velocity U_∞ and length of the model L. Figures displaying spatial distribution in transverse planes at stations of constant X/L are plotted by using a coordinate system labeled according to model scale. Length of the wind tunnel model is $L = 2663mm$. The origin is located at the intersection of the fore perpendicular with the construction waterline.

Experiments and computations, limitations and further calculations — in order to compare different data sets — are described in appendix A.

5.1 Wall Pressure

To get detailed information about the wall pressure of the model in the experiment, it would be necessary to build in a great number of pressure taps. For example, there are 239 pressure taps in the hull of the original HSVA-tanker.
Due to the limitation of budget and the delay in manufacturing of wind tunnel model of HSVA-tanker-2, the pressure taps were restricted in number. 25 taps were located

at three transverse stations $X/L = 0.646$, 0.917, 0.964 and a horizontal line half way between the waterline and the keel.
Station $X/L = 0.646$ was the initial check station for computations on the SSPA workshop. Assuming a small gradient of c_p along the girth at this station, we searched for stations of interest for the location of the few remaining pressure taps. Computing c_p by potential theory before the wind tunnel model was manufactured, lead to station $X/L = 0.964$, where the maximum of transverse gradient of "numerical c_p" (ref. Fig. 2) was found and station $X/L = 0.917$, where "numerical c_p" changes sign near half draught.
Coordinates of the location of the pressure taps and results of experiments are enclosed in appendix B.

c_p was calculated by potential theory using 1820 panels. To compare the results with measurements, computed values were interpolated onto the location of the pressure taps.

In figure 2 the calculated pressure distribution on the hull is displayed as contures of constant pressure coefficient c_p. This figure includes the locations of the pressure taps in the experiment. In order to get a better resolution the transverse coordinate is expanded by a factor 4.
Distributions of pressure at stations $X/L = 0.128$, 0.646, 0.917 and 0.964 are presented in Fig. 3 to 6. Girthwise distribution is shown in figure "a" and c_p plotted as arrows in normal direction to the shape of the hull in figure "b" (experiment) and "c" (computation) for each station.

At station $X/L = 0.128$ (Fig. 3) there are no results from experiment. Maximum of "numerical c_p", located at the keel, decreases in direction to the waterline. A local minimum is located at the turn of the bilge.
At station $X/L = 0.646$ (Fig. 4) there is a small transverse gradient in computed and measured data. Near to the keel and near to the waterline "numerical c_p" is a little bit smaller than "experimental c_p".
At station $X/L = 0.917$ (Fig. 5) the minimum of "experimental c_p" is smaller than "numerical c_p". This leads to a difference of girthwise location of the point, where the two c_p change sign, while values of c_p near the keel and waterline correspond very well.
Girthwise distribution of "experimental c_p" at station $X/L = 0.964$ (Fig. 6) shows almost constant values (results of 3 pressure taps) from 0% to 30% of the girth, though "numerical c_p" changes sign. Looking for possible errors in the experiment, these pressure taps were investigated and measurements were carried out again. This lead to the same results. No significant error in the experiment could be determined.

The difference could be caused by a local separation. Visualisation of limiting streamlines (to be discussed later) indicates backflow in that region. Local separation near to the keel around station $X/L = 0.964$ would cause the minimum of c_p to be farther upstream than calculated. This would also explain the difference at station $X/L = 0.917$ (smaller values of "experimental c_p").
Measurements of the velocity close to the wall will be necessary in order to get more information about seperation, but have not yet taken place.

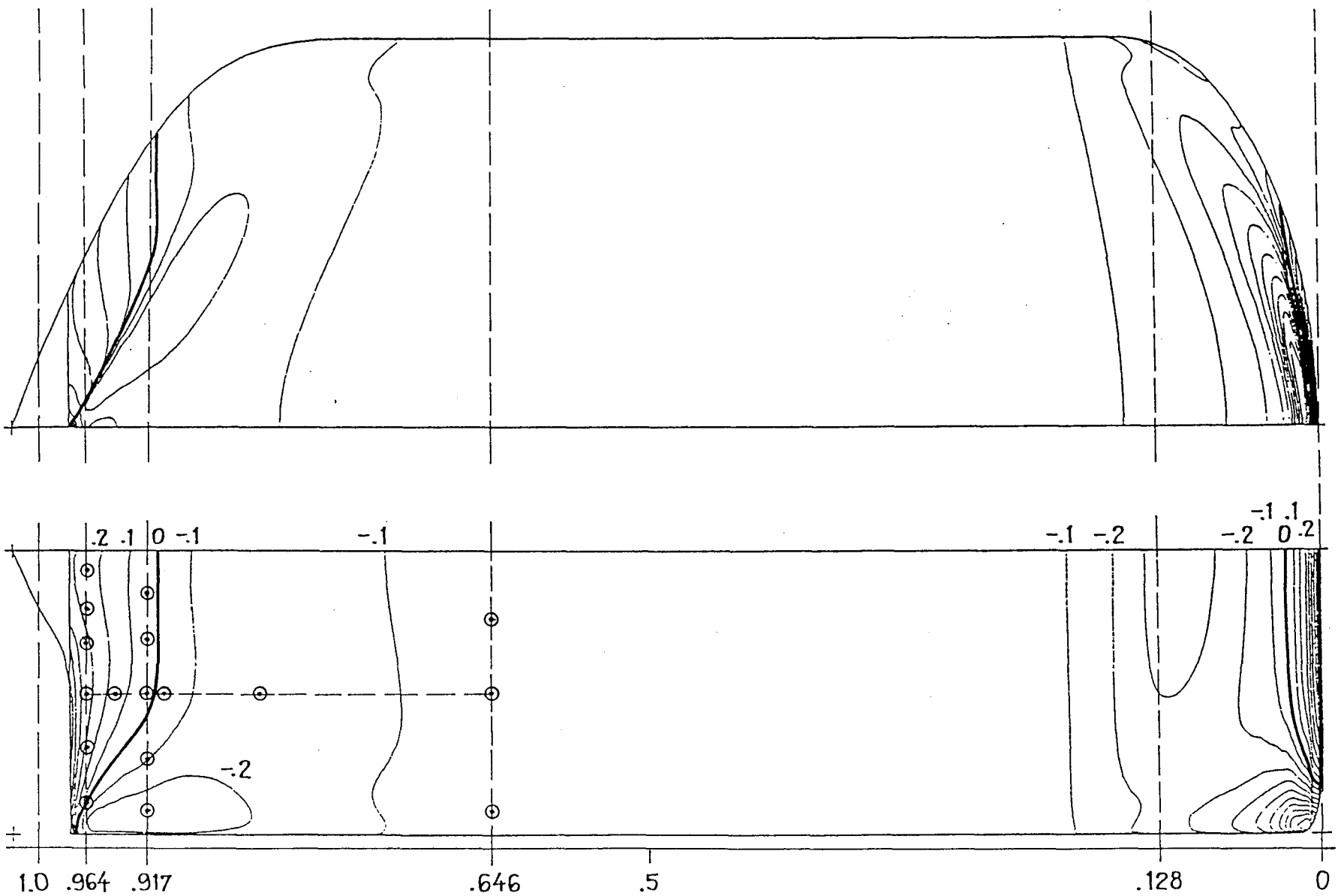

Figure 2: Pressure distribution on the hull (Computation);
Location of pressure taps (Experiment)

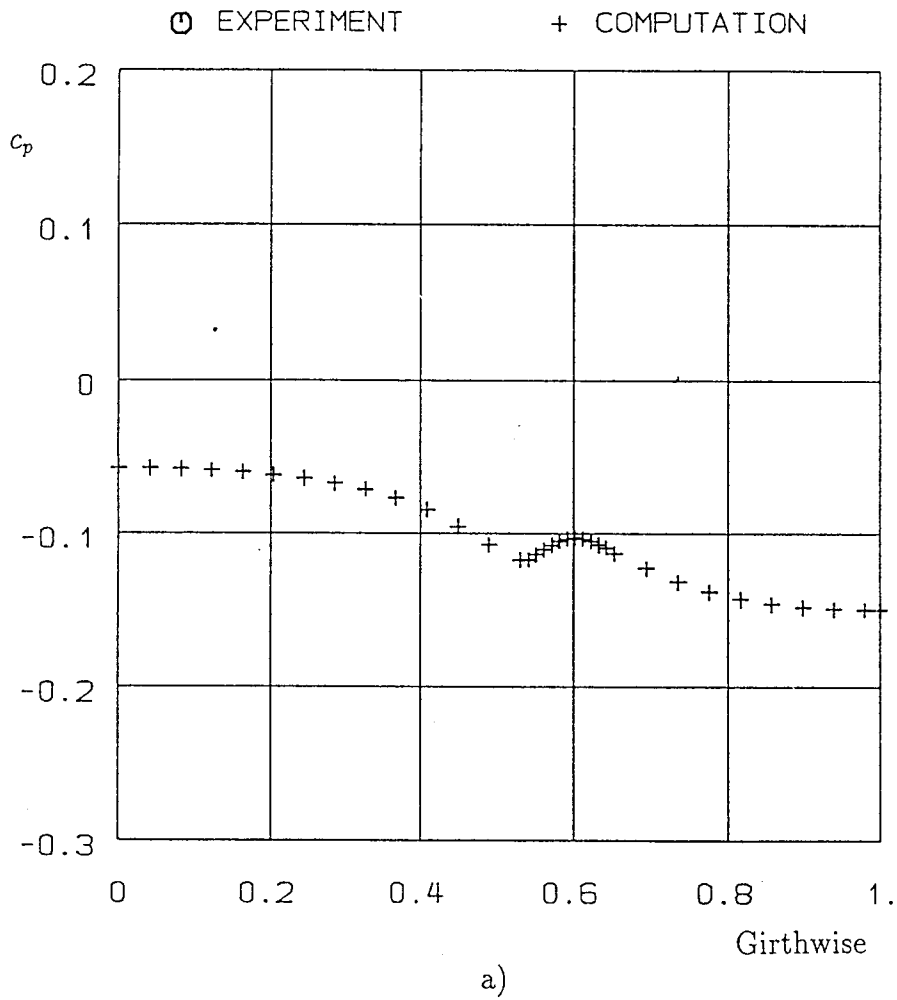

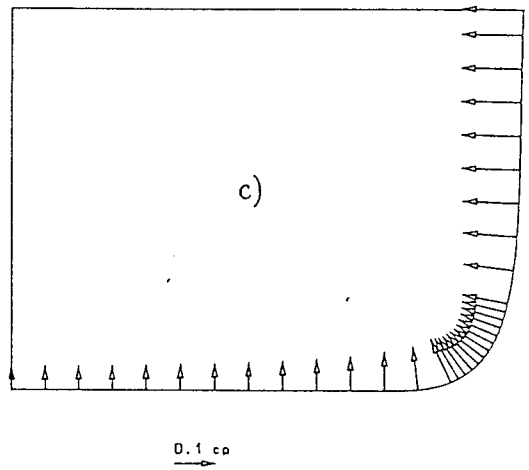

Figure 3: Station X/L = 0.128; c_p; a) Girthwise distribution
c) Computation

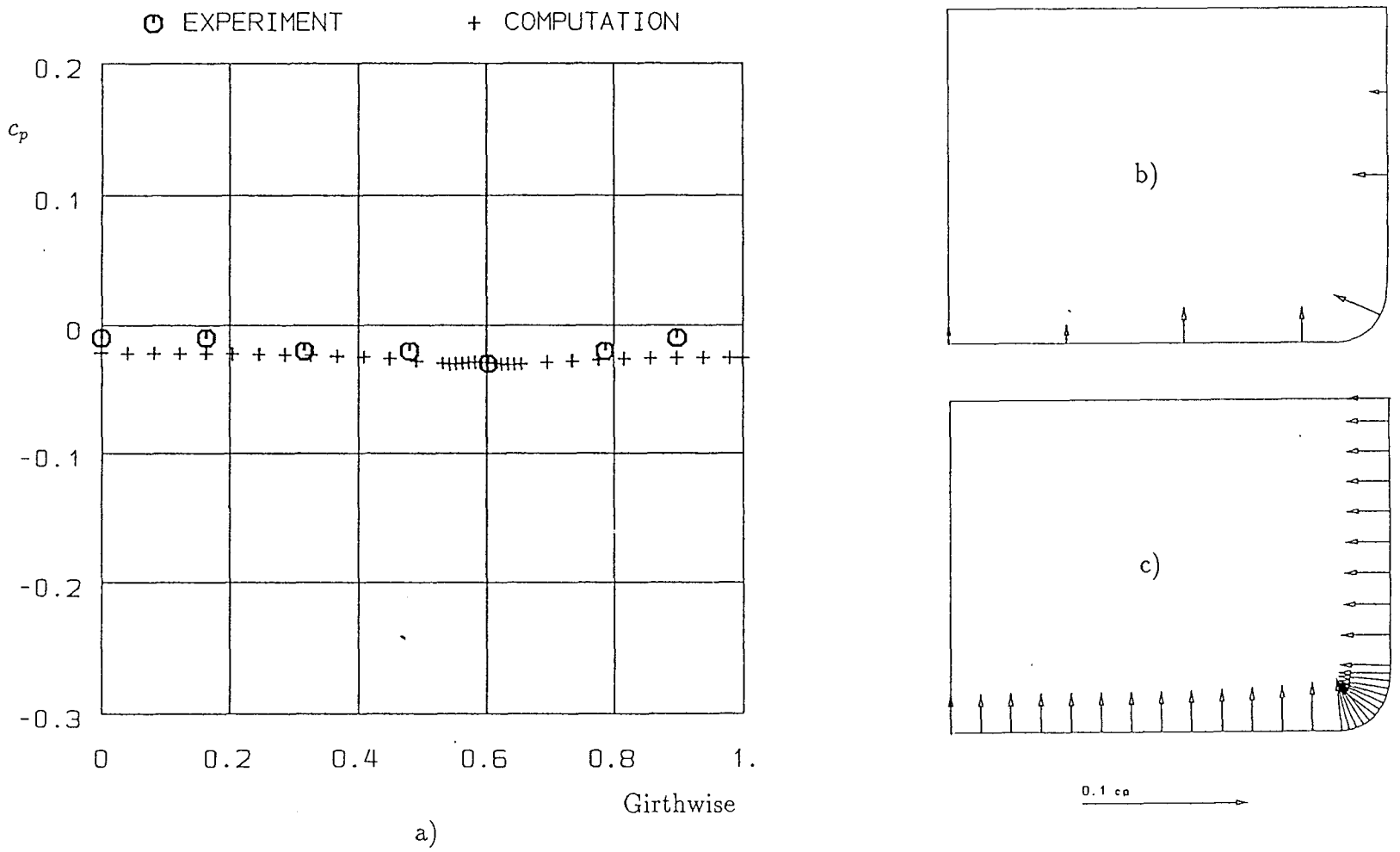

Figure 4: Station X/L = 0.646; c_p; a) Girthwise distribution
b) Experiment; c) Computation

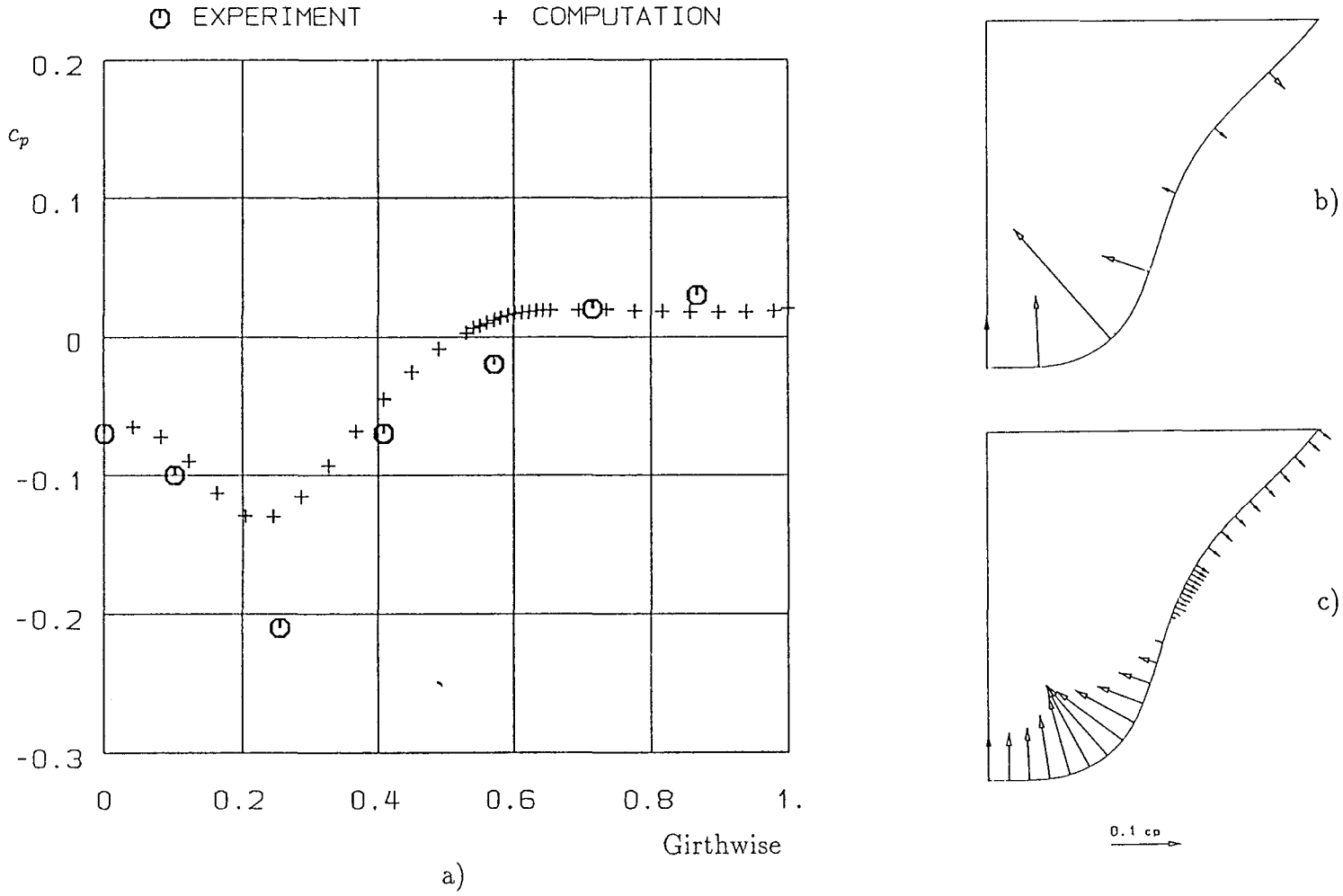

Figure 5: Station X/L = 0.917; c_p; a) Girthwise distribution
b) Experiment; c) Computation

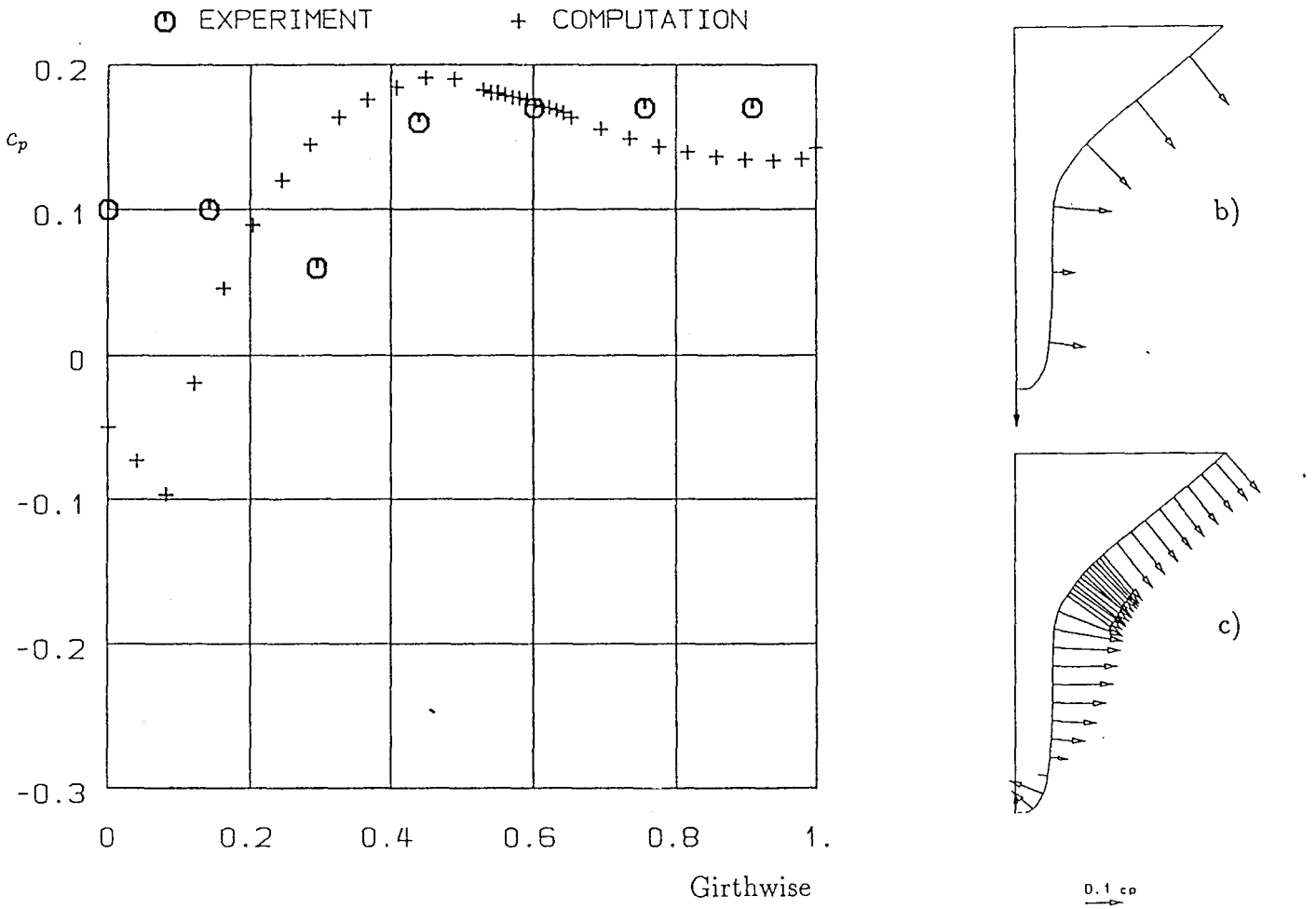

Figure 6: Station X/L = 0.964; c_p; a) Girthwise distribution
b) Experiment; c) Computation

5.2 Velocity

Velocity distributions were investigated at various check stations. An overview on location and different results of investigations was given in table 1 (p. 10). Results of mean velocity distributions are presented in figures 7 to 23 (p. 19 to 35).

Both, experimental data and computed results were transformed to common coordinates in order to be compared. The details are given in appendix A.

In figure 7 lines of constant axial component of "experimental velocity" are displayed at station $X/L = 0.128$, while figure 8 shows the absolute value of "numerical mean velocity vector". Original location of measurements respectively computation are included in both figures.
Girthwise distributions (experimental and computed) of the boundary layer thickness agree well. It decreases around the turn of the bilge, as it is assumed because of divergence of secondary flow to both sides. Secondary flow here is too small to be determined by experiment (ref. app. A). From of the magnification of the figures (ref. to Fig. 9) it can be determined , that minimum of the boundary layer thickness is smaller than 2 mm (model scale) at the turn of the bilge.
Proceeding towards the keel boundary layer thickness increases. Staying constant below the hull in the experimental data, while decreasing in computation approaching to the keel. Maximum of boundary layer thickness below the hull is two times the maximum at the side wall in both investigations.
Velocity profiles in direction normal to the surface give detailed informations about velocity distribution (Fig. 10 and 11). Profiles are numbered starting with no. 1 at the keel. This numbering is obtained e.g. from Fig. 8. Velocity profiles compiled from experimental results form a database for calculating c_f, which will be discussed in section 5.4).
By showing in addition distributions of "experimental turbulence" (axial component $\overline{u'^2}/U_\infty^2$) with each of the profiles of velocity in figure 10 and 11, the edge of the boundary layer can be recognized clearly. Further results of turbulence are presented in section 5.3 (p. 36).

At station $X/L = 0.646$ boundary layer thickness increases near the turn of the bilge because of convergence of secondary flow. Experimental results (Fig. 12) and numerical results (Fig. 13) agree in showing this effect. In both investigations boundary layer thickness below the hull is larger than boundary layer thickness at the side wall.
There are some strange effects in the contour line of constant "experimental velocity" $\overline{u}/U_\infty = 1.0$ at the keel and at the waterline. Decrease of velocity at the keel may be caused by the wire used to support the model in the wind tunnel. But it was not possible to find a cause for the anormal of the velocity near the waterline.
Distributions of velocity on profiles are presented in figures 14 to 17. As in the results at the previous station, distribution of turbulence is included in these figures. Profile no. 19 is located at the turn of the bilge. At this profile experimental boundary layer thickness is larger than that obtained from computation.

In contrast to previous stations at $X/L \geq 0.921$, there are larger transverse components of the velocity, which were determined experimentally (ref. app. A), but there no information about velocity from computation can be obtained (ref. section 4.3).

At station $X/L = 0.921$ contours of axial velocity are shown in figure 18. Vectors of transverse components are displayed in figure 19. In the outer region of this station mainstream velocity corresponds well to potential flow calculation, while near to the hull at 50% of the girth formation of a large lenghtwise vortex can be observed. This vortex increases at the following stations farther downstream.
As mentioned above, wires used to support the model in the wind tunnel are located at $X/L = 0.81$. Two of those are fastened to the model at the keel, in a direction of 45 degree to the vertical. The wake of the wire produces a bulge in the contours of the axial velocity.

In figures 20 to 23, contours of axial component and arrows for the transverse components of the velocity vector at station $X/L = 0.989$ and $X/L = 1.1018$ are presented. The magnitude of the transverse components in the region of the vortex is larger and increases much more than it was determined at the original HSVA-tanker (ref. [4]). Decrease of axial velocity at the center of the vortex confirms the location of the vortex, as deduced from the transverse components arrow plots. Experimental investigations of the center of the vortex and its distance from the vertical plane of symmetry were validated at station $X/L = 1.018$ by measuring on both sides of this plane of symmetry.
Though development of axial velocitys field from station $X/L = 0.989$ to station $X/L = 1.018$ shows, that the distribution of this component of both vortices mix, this does not mean that the two vortices coalesce, as it can be seen from transverse components plots.

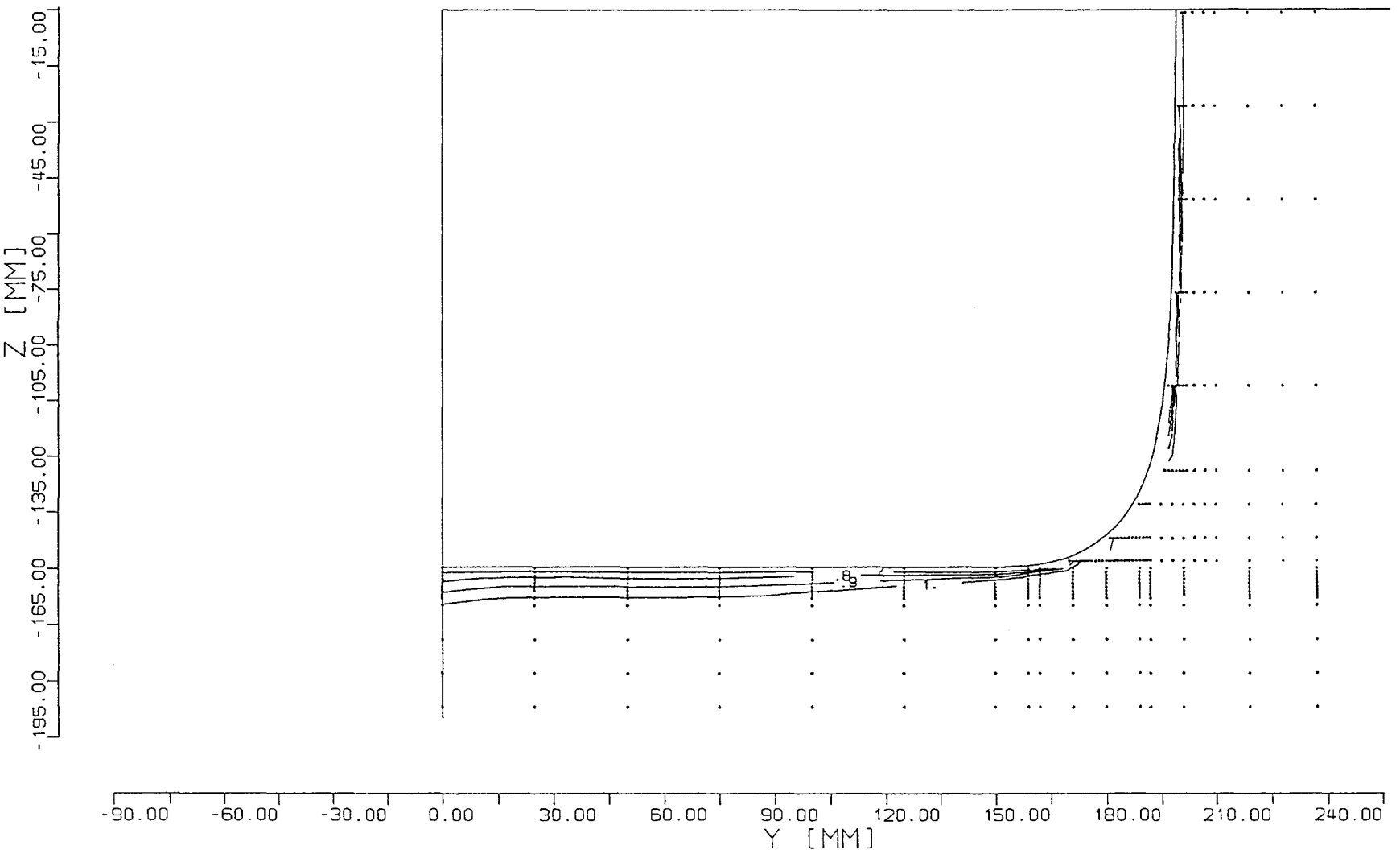

Figure 7: Station X/L = 0.128
Contours of constant axial velocity (Experiment)

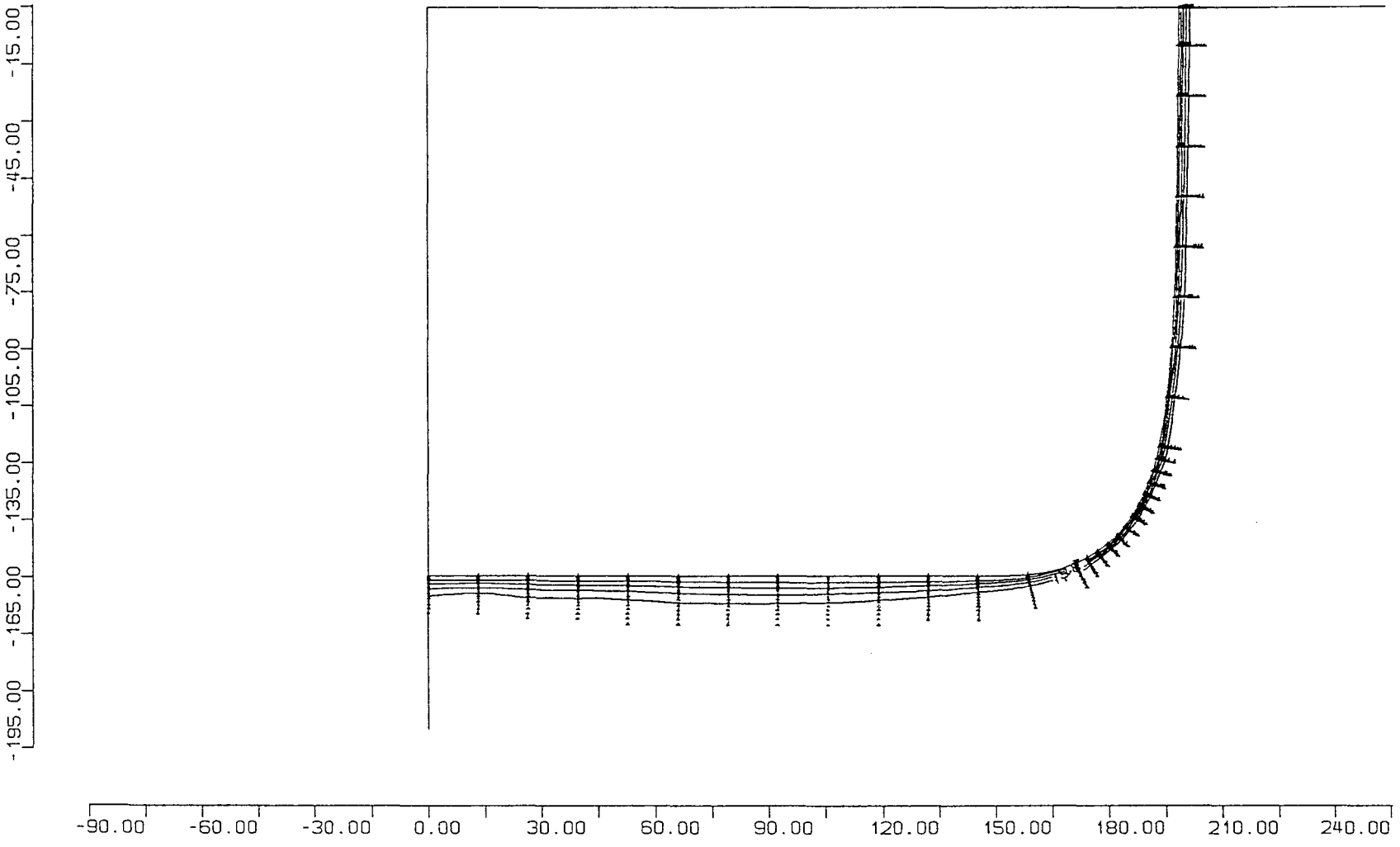

Figure 8: Station X/L = 0.128
Contours of constant absolute value of velocity (Computation)

Figure 9: Station X/L = 0.128
a) Contours of constant axial velocity (Experiment)
b) Contours of constant absolute value of velocity (Computation)

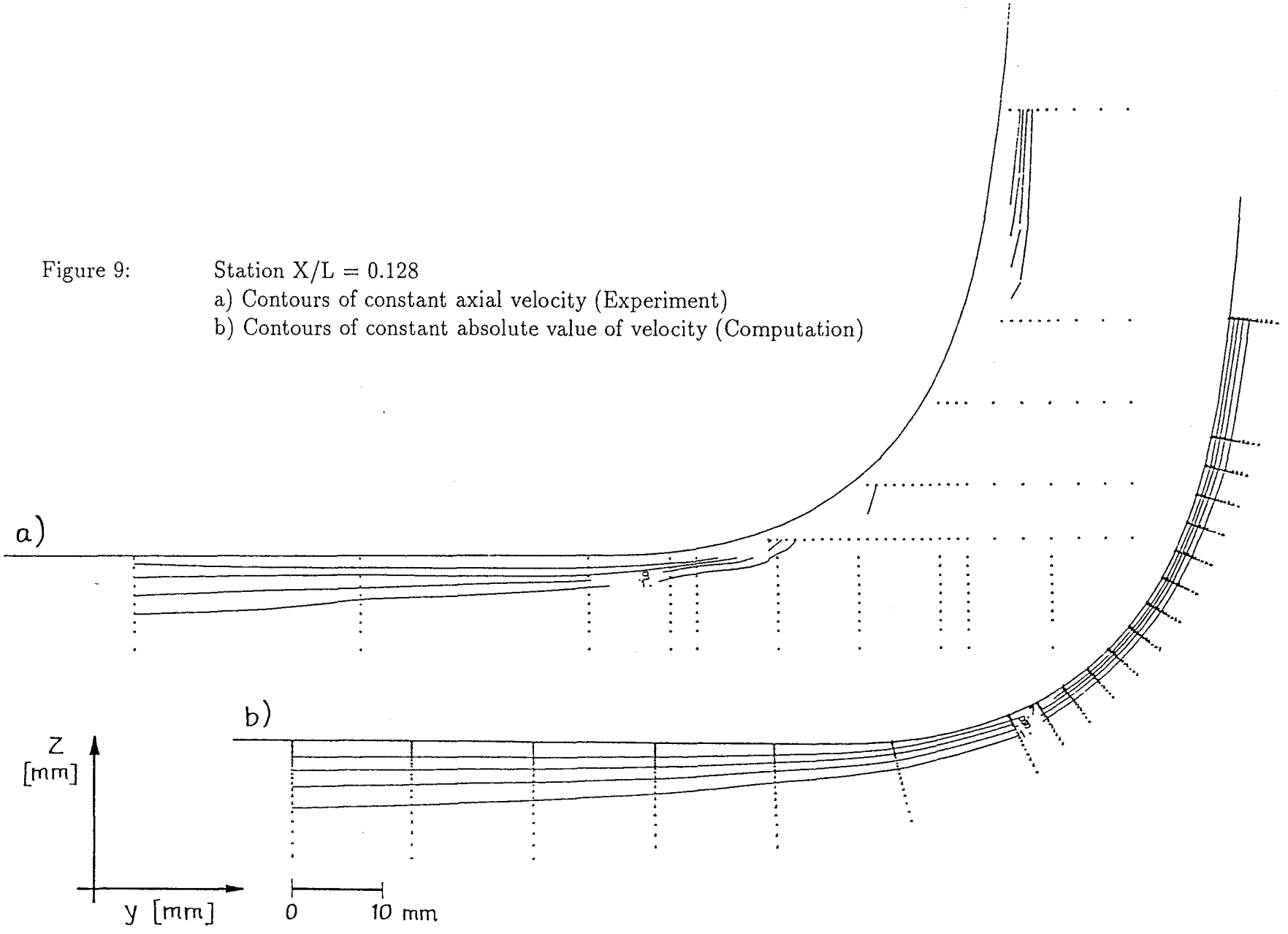

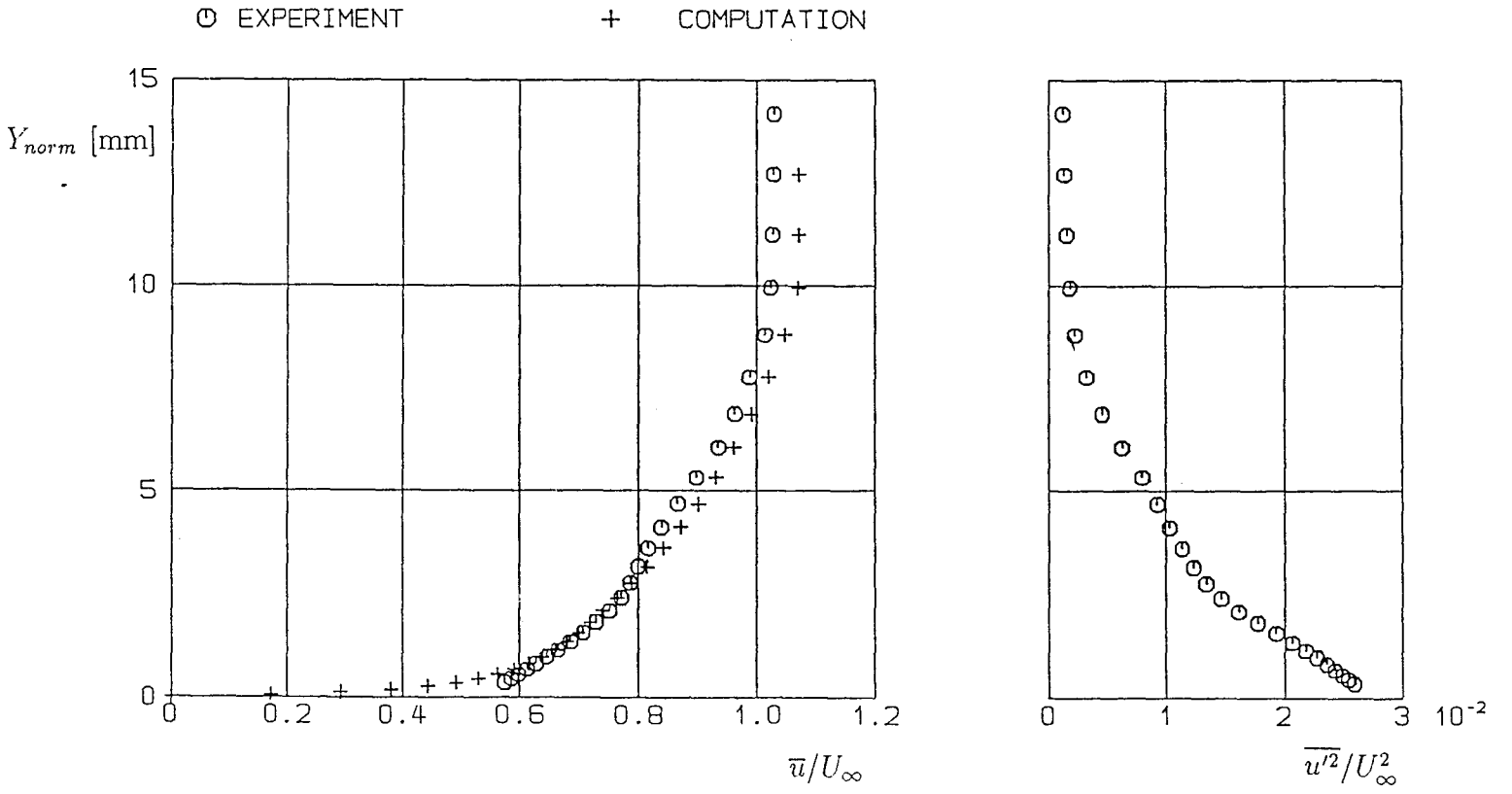

Figure 10: Station X/L = 0.128; Profile no. 6
Profiles of axial velocity and profile of $\overline{u'^2}/U_\infty^2$

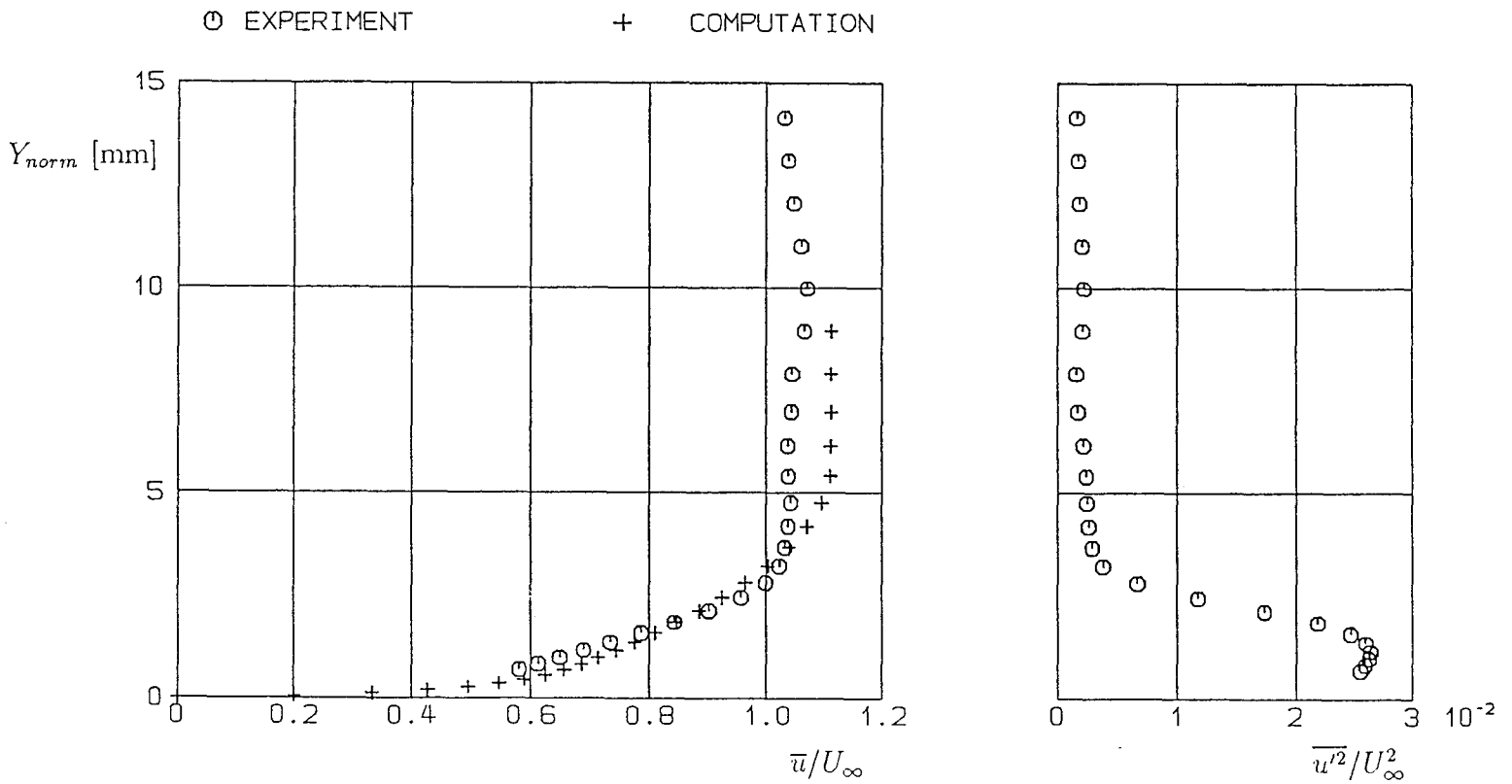

Figure 11: Station X/L = 0.128; Profile no. 13
Profiles of axial velocity and profile of $\overline{u'^2}/U_\infty^2$

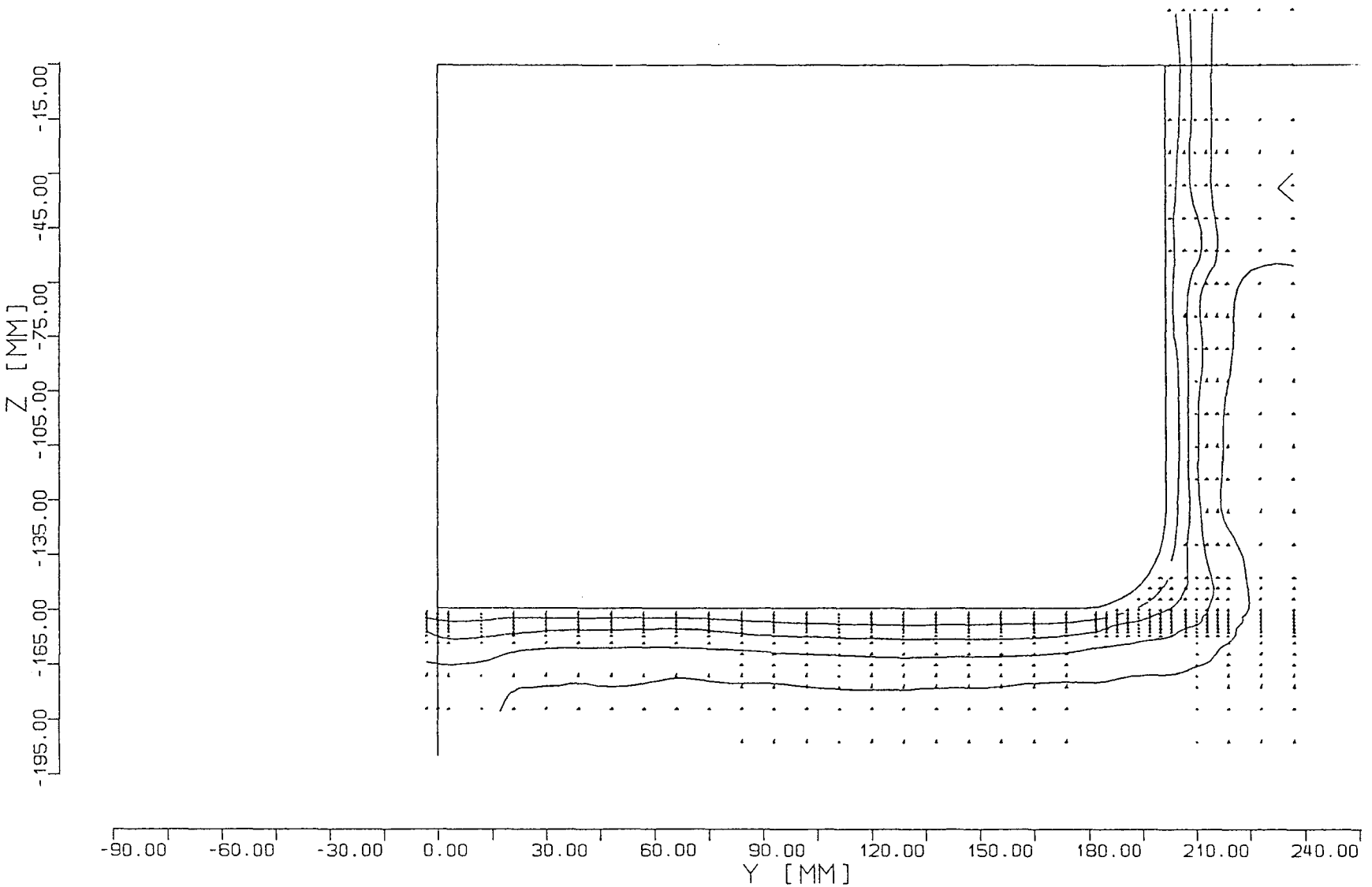

Figure 12: Station X/L = 0.646
Contours of constant axial velocity (Experiment)

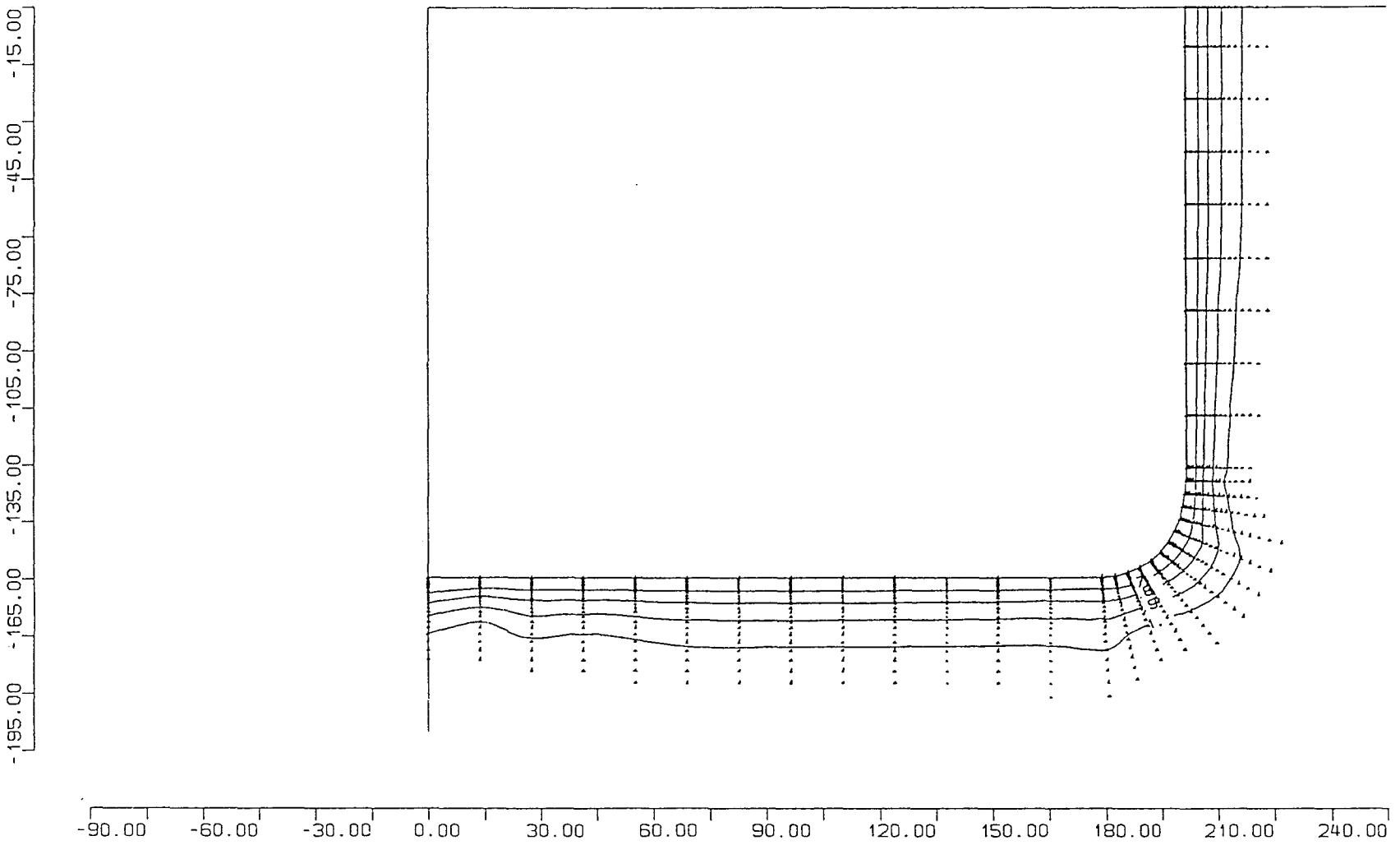

Figure 13: Station X/L = 0.646
Contours of constant absolute value of velocity (Computation)

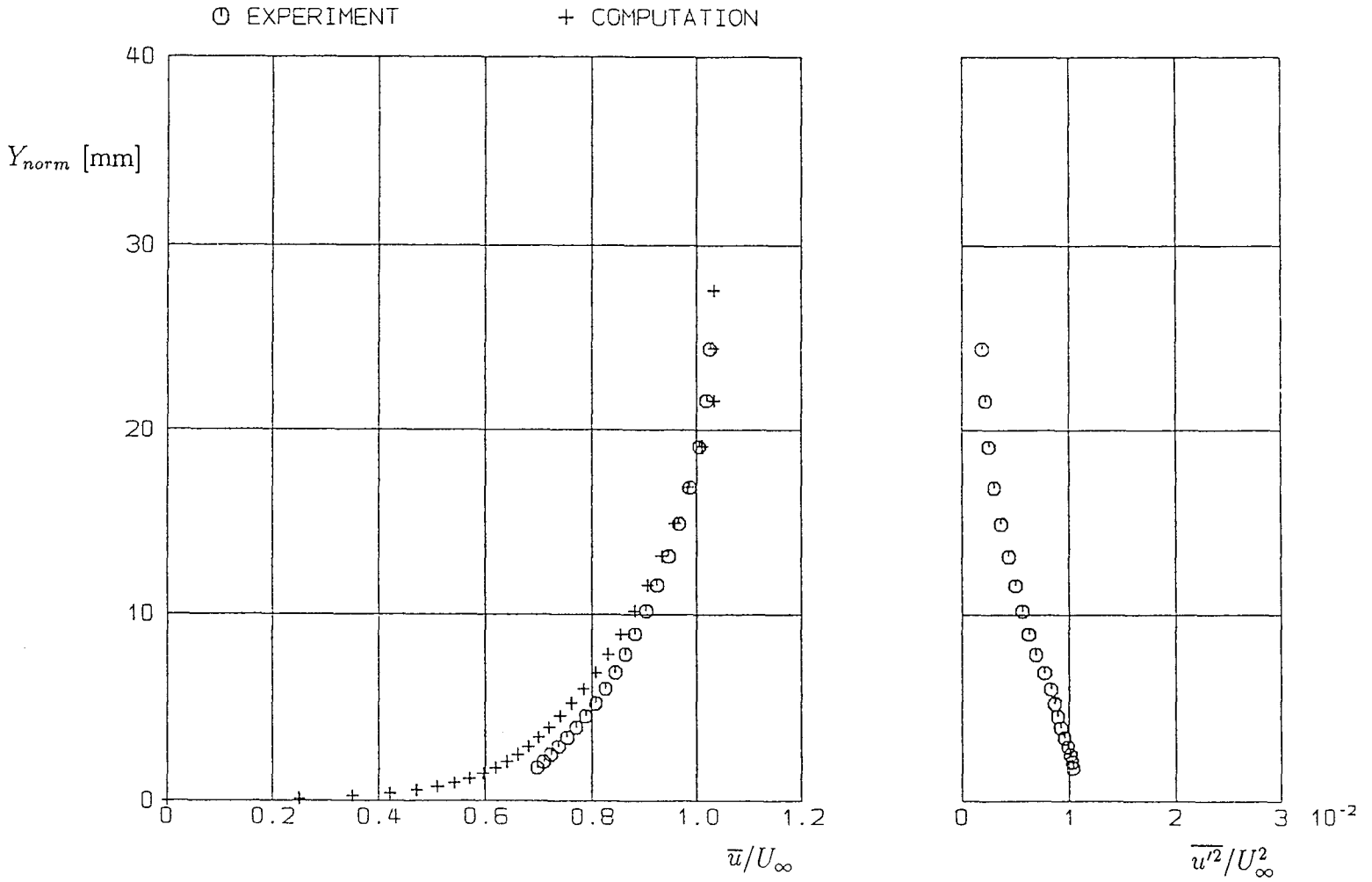

Figure 14: Station X/L = 0.646; Profile no. 6
Profiles of axial velocity and profile of $\overline{u'^2}/U_\infty^2$

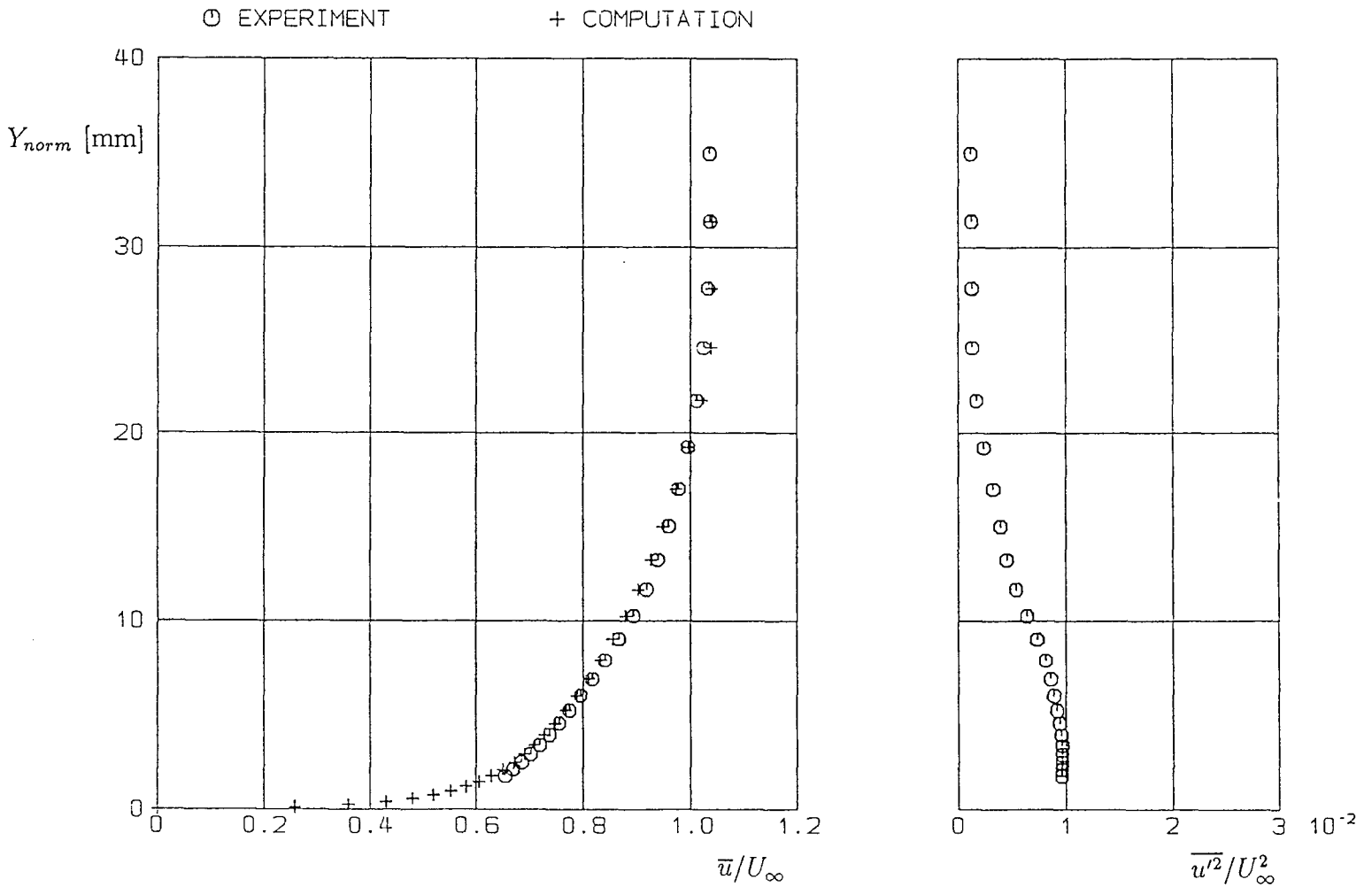

Figure 15: Station X/L = 0.646; Profile no. 14
Profiles of axial velocity and profile of $\overline{u'^2}/U_\infty^2$

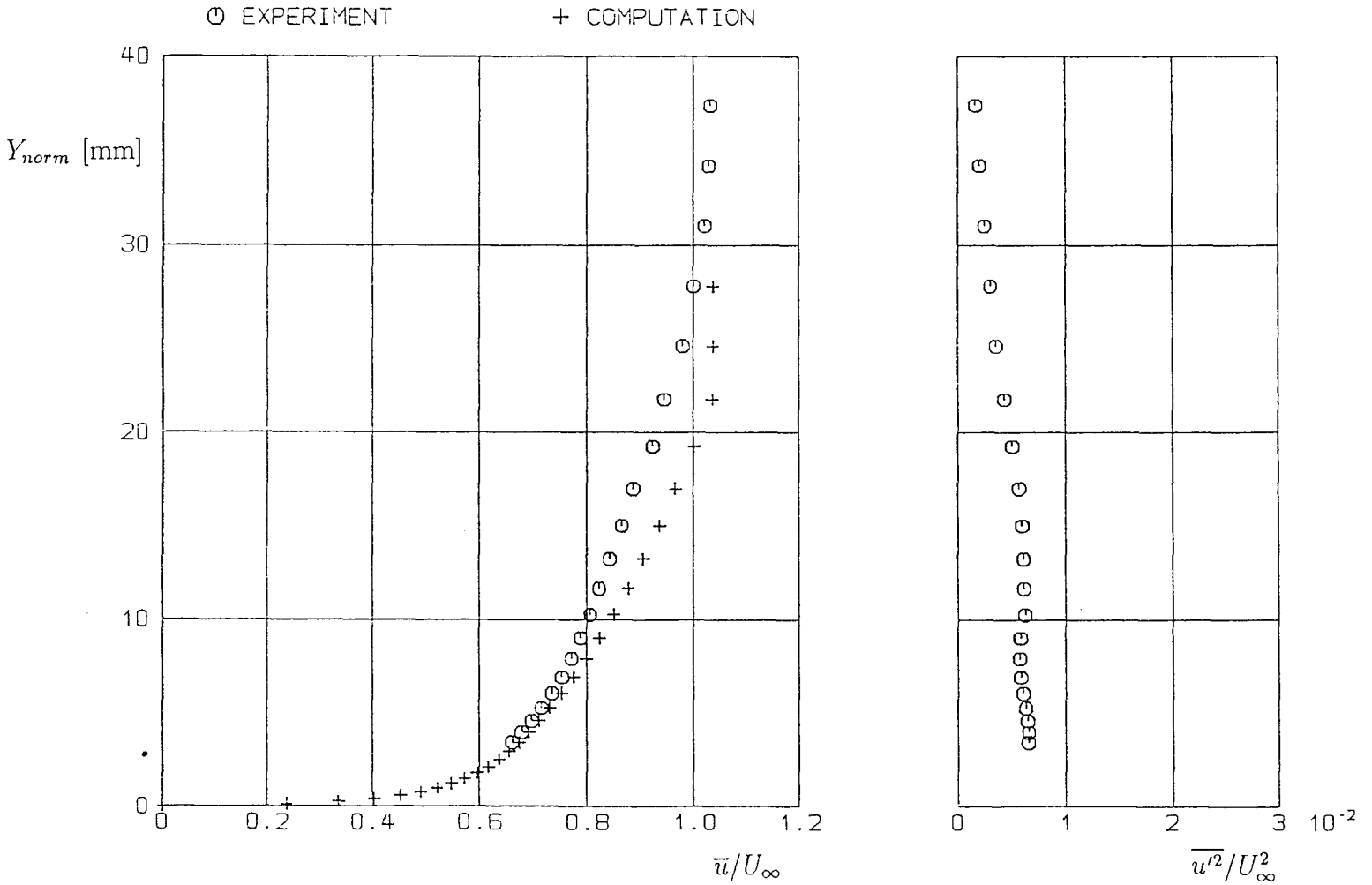

Figure 16: Station X/L = 0.646; Profile no. 19
Profiles of axial velocity and profile of $\overline{u'^2}/U_\infty^2$

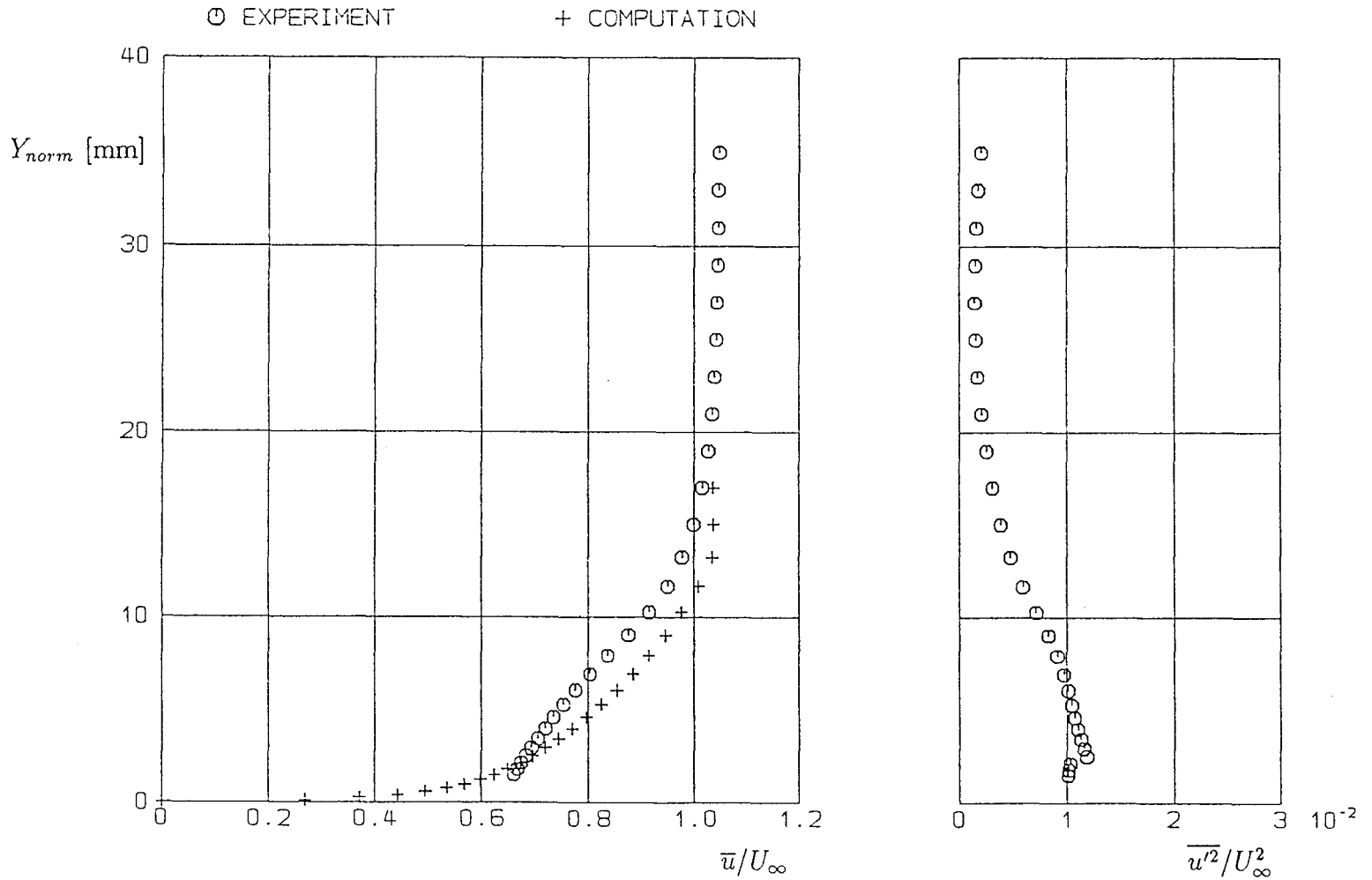

Figure 17: Station X/L = 0.646; Profile no. 26
Profiles of axial velocity and profile of $\overline{u'^2}/U_\infty^2$

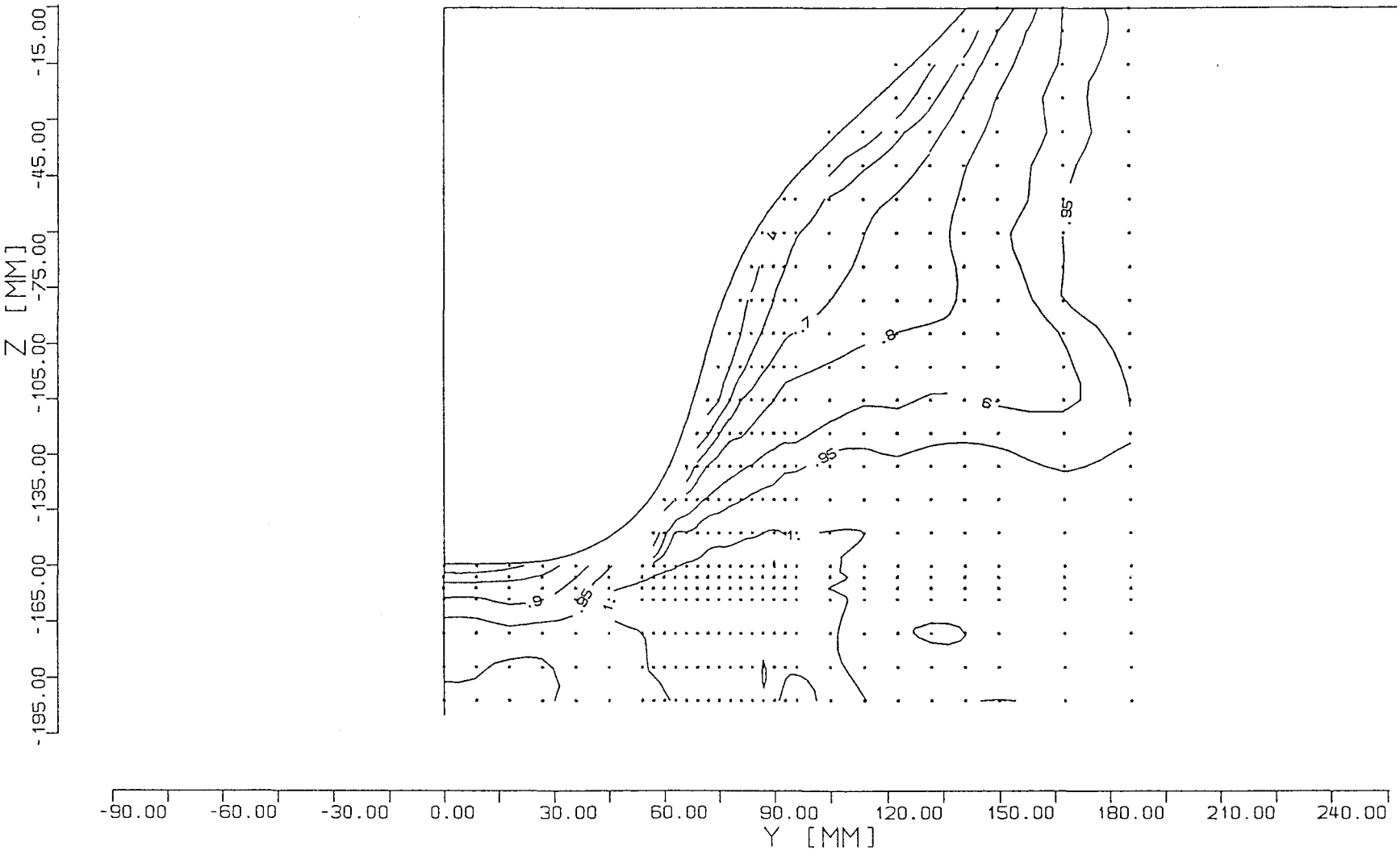

Figure 18: Station X/L = 0.921
Contours of constant axial velocity (Experiment)

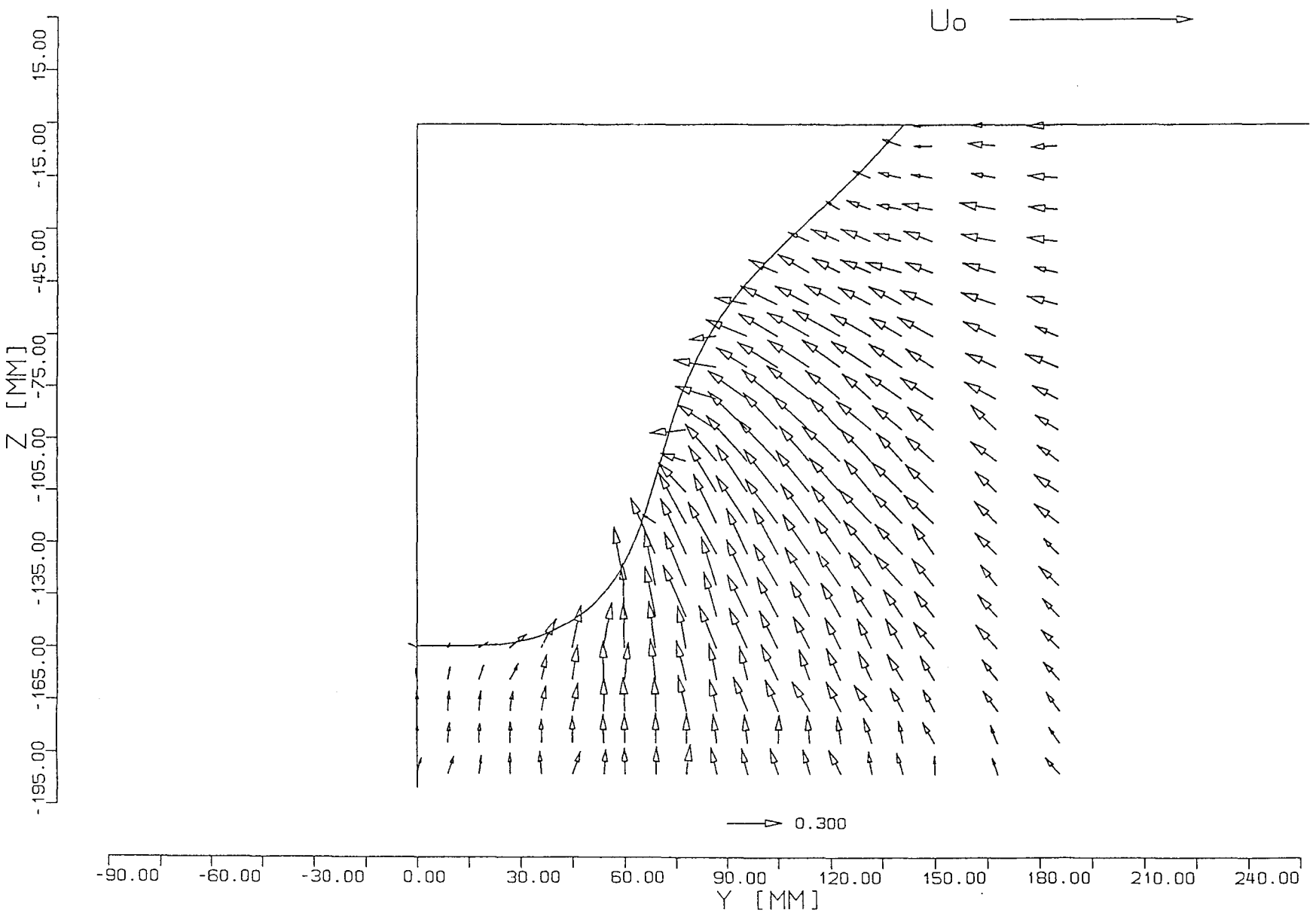

Figure 19: Station X/L = 0.921
Vectors of transverse components (Experiment)

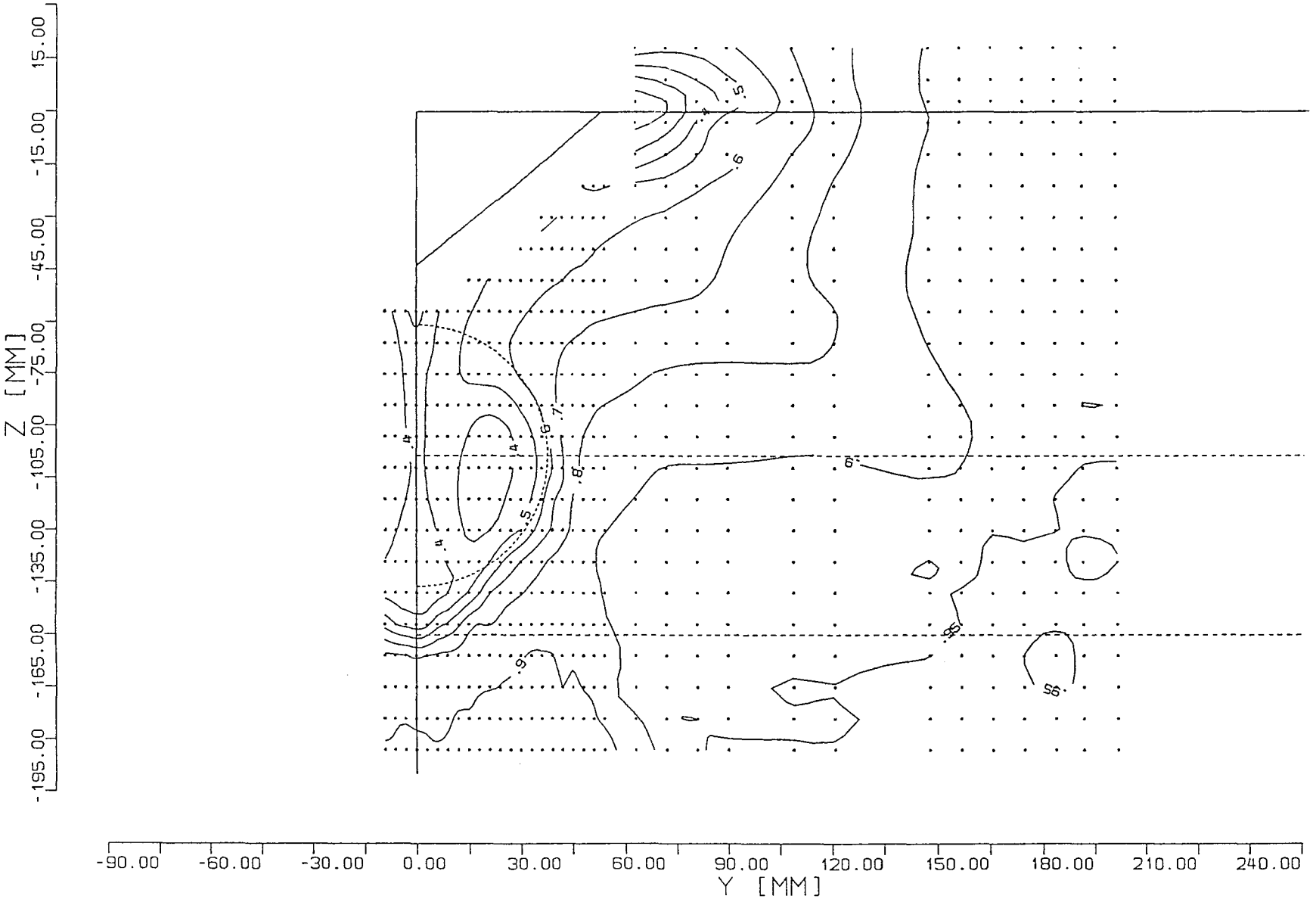

Figure 20: Station X/L = 0.989
Contours of constant axial velocity (Experiment)

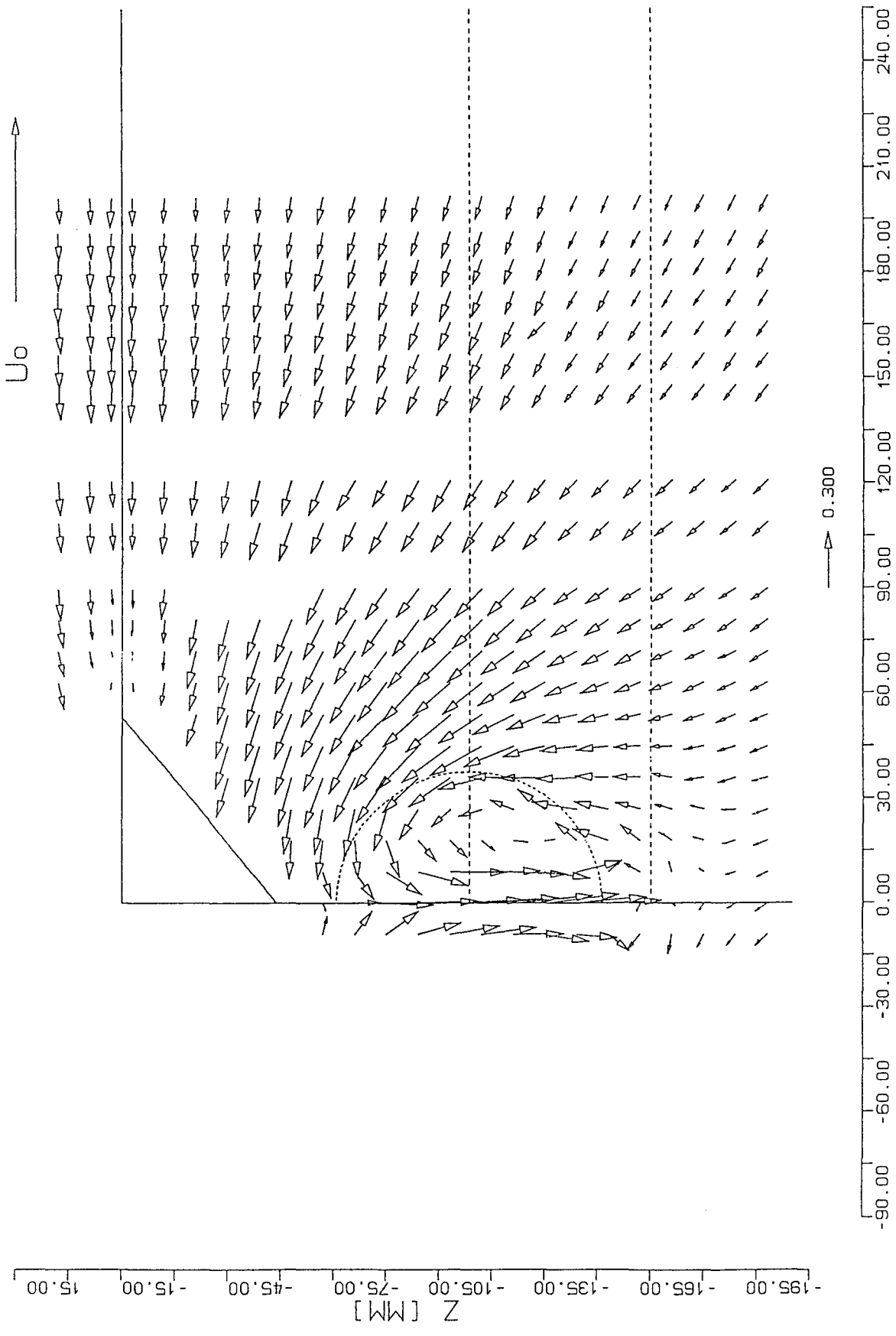

Figure 21: Station X/L = 0.989
Vectors of transverse components (Experiment)

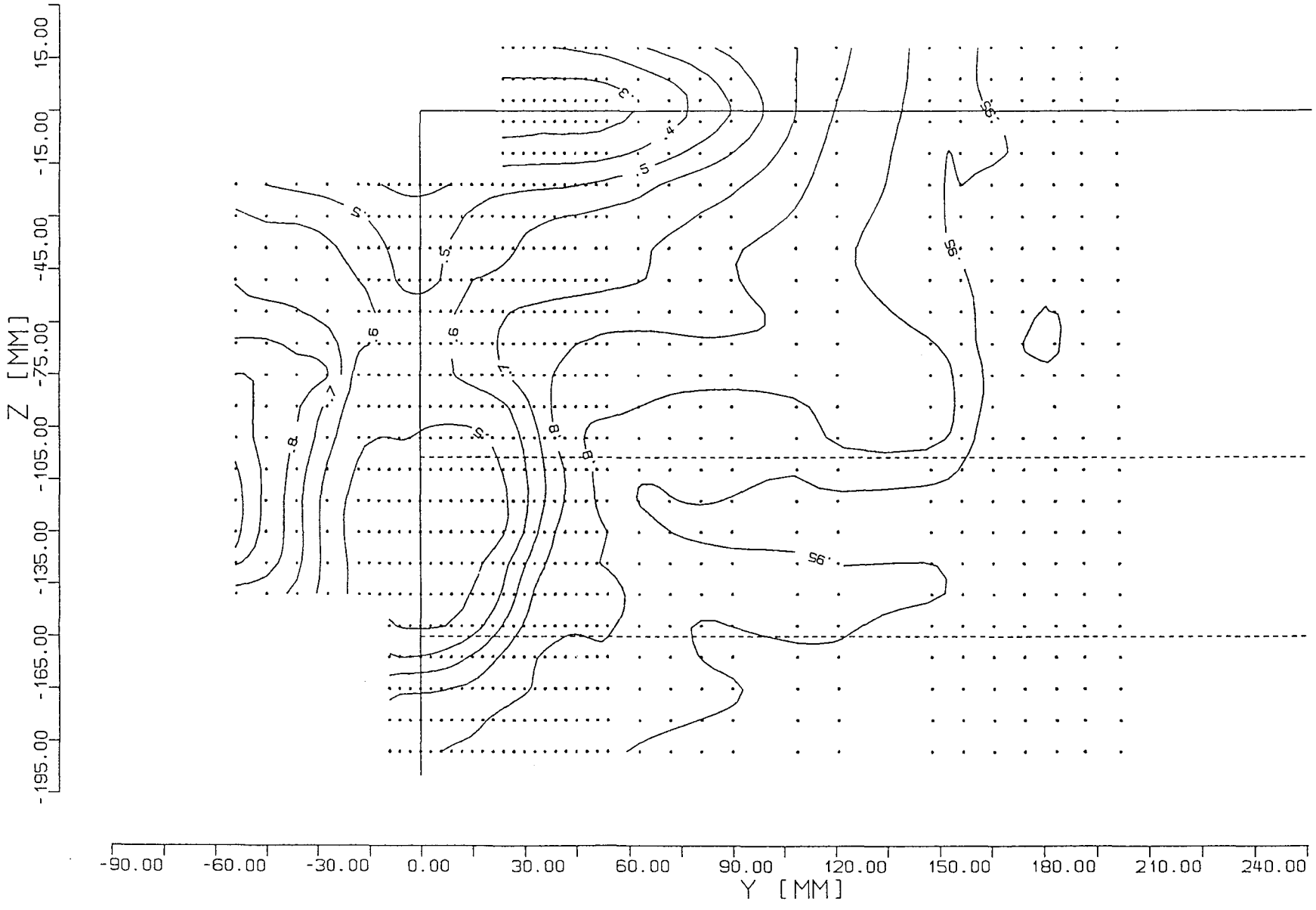

Figure 22: Station X/L = 1.018
Contours of constant axial velocity (Experiment)

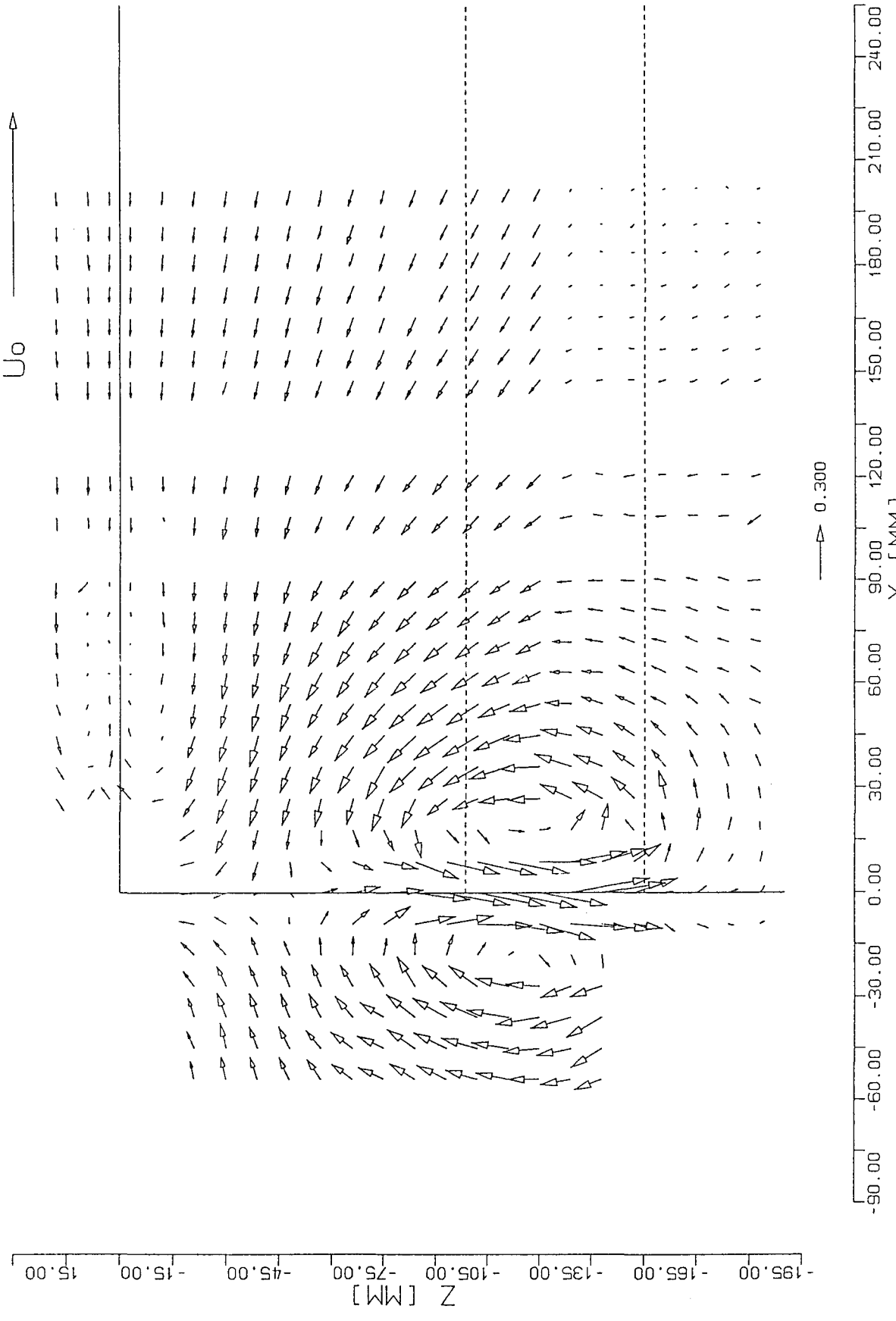

Figure 23: Station X/L = 1.018
Vectors of transverse components (Experiment)

5.3 Turbulence

Different components of the Reynolds stress tensor were investigated in the experiment. While at the first two stations $X/L \leq 0.646$ only measurements of the momentaneous axial velocity component were possible, this lead to $\overline{u'^2}/U_\infty^2$, at stations $X/L \geq 0.921$ measurements of all three components of the velocity made it possible to calculate the kinetic energy of turbulence k (ref. app. A).

At station $X/L = 0.128$ in figure 24 and station $X/L = 0.646$ in figure 25 contours of constant $\overline{u'^2}/U_\infty^2$ are displayed. Distribution of $\overline{u'^2}/U_\infty^2$ is similar to the distribution of velocity (ref. to fig. 7). Due to very small transverse components of mean velocity – approximately two dimensional flow – it is possible to neglect exchange of material between boundary layer and outer flow. Therefore contours of higher values of turbulence are nearly similar to the contours of constant axial velocity in the boundary layer.
Comparing maximum values of turbulence at the two stations we note that maesurements at station $X/L = 0.646$ did not take place as near to the hull surface as at station $X/L = 0.128$. Values of $\overline{u'^2}/U_\infty^2$ greater than 0.02 can be determined at station $X/L = 0.128$ in a wall distance smaller than $1.8mm$ (ref. Fig. 10 p. 22), but there are no measurements at these small wall distances at station $X/L = 0.646$.

At stations $X/L = 0.921$, 0.989 and 1.018 in figure 26 to 28 contours of constant kinetic energy of turbulence k are displayed. At the previous stations upstream there is a characteristic local thickening of the boundary layer (at 60% girth). This thickening develcpes along the hull and at station $X/L = 0.921$ the distribution of k clearly reproduces this feature.

Farther downstream at stations $X/L = 0.989$ and $X/L = 1.018$ two effects have to be emphasized.
Firstly; due to the large lengthwise vortex, undisturbed material from outer regions of the flow field is transported toward the surface of the hull (or rather in direction to the plane y = 0). In other words, there is a region of small values of k, where mean velocity is oriented in direction toward the hull.
Secondly; material from the thin boundary layer below the hull (at the keel) containing concentrated energy of turbulence is transported downstream into the wake by the mean velocity, which is oriented in axial direction. Therefore larger values of k can be determined in the plane $y = 0$ at the depth of the model keel.
Contours of $k = 0.03$ show, that fluctuating material from the boundary layer at the keel combines with fluctuating material from the center of the vortex.

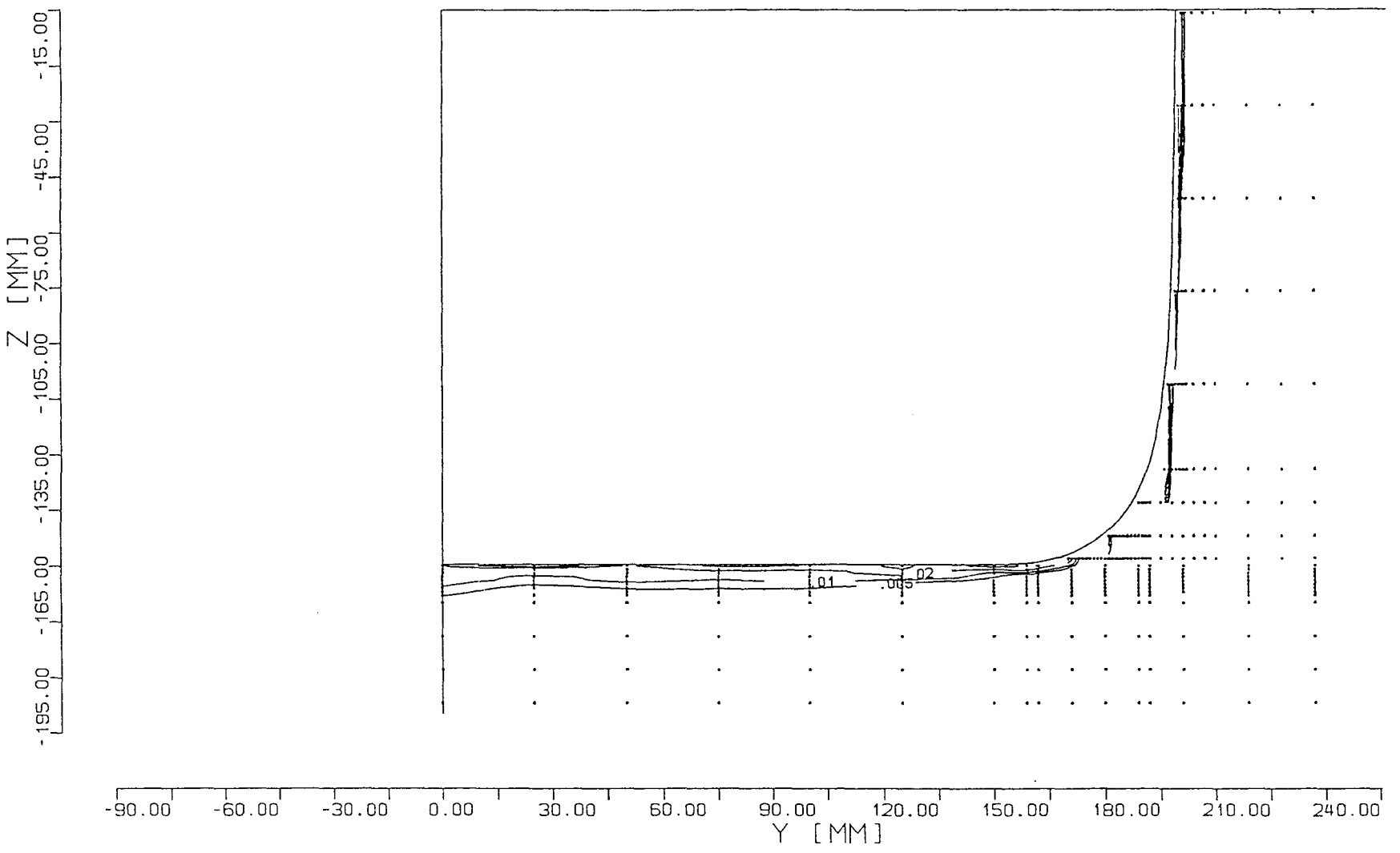

Figure 24: Station X/L = 0.128
Contours of constant $\overline{u'^2}/U_\infty^2$ (Experiment)

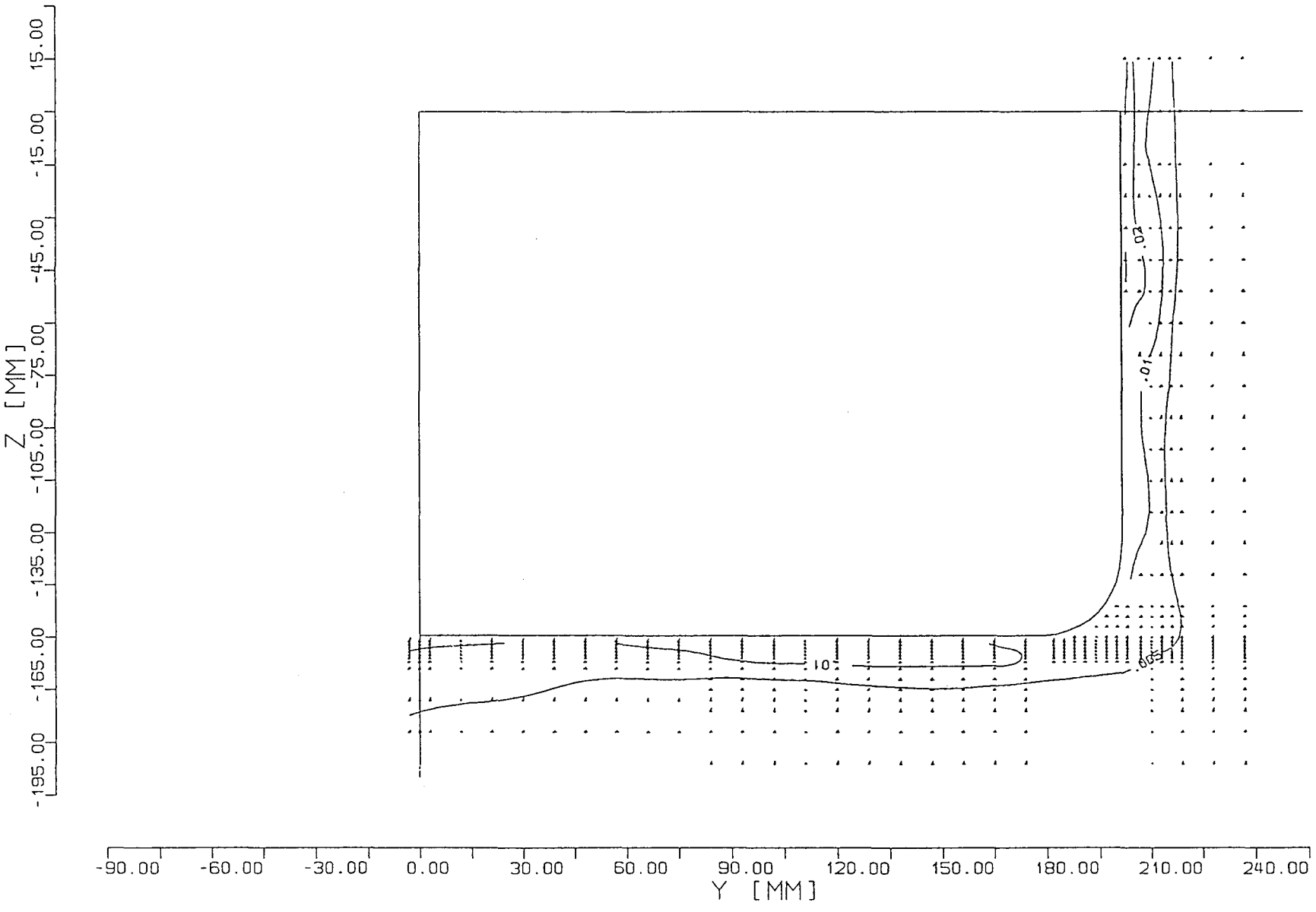

Figure 25: Station X/L = 0.646
Contours of constant $\overline{u'^2}/U_\infty^2$ (Experiment)

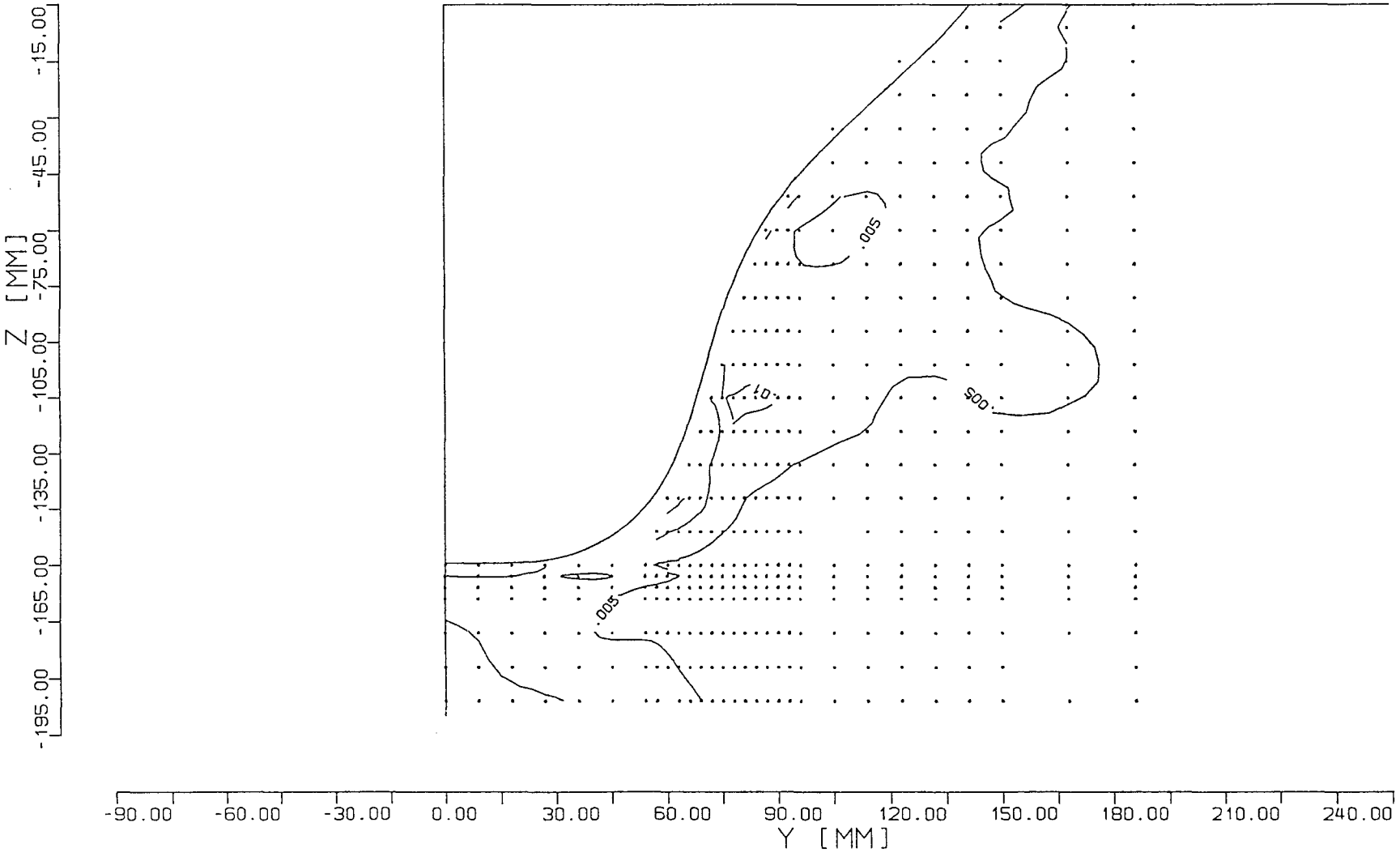

Figure 26: Station X/L = 0.921; Contours of constant normalized kinetic energy of turbulence k/U_∞^2 (Experiment)

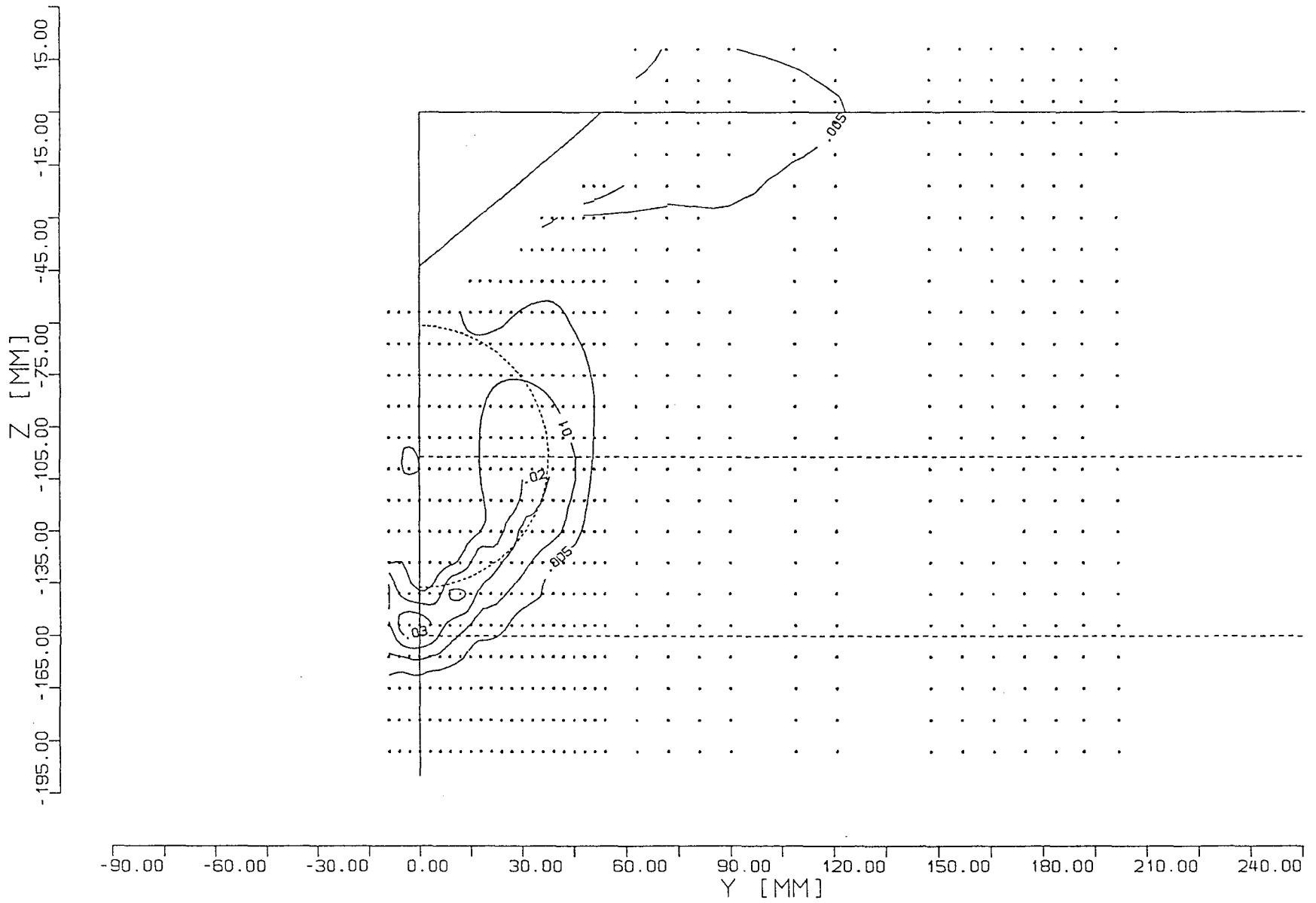

Figure 27: Station X/L = 0.989; Contours of constant normalized kinetic energy of turbulence k/U_∞^2 (Experiment)

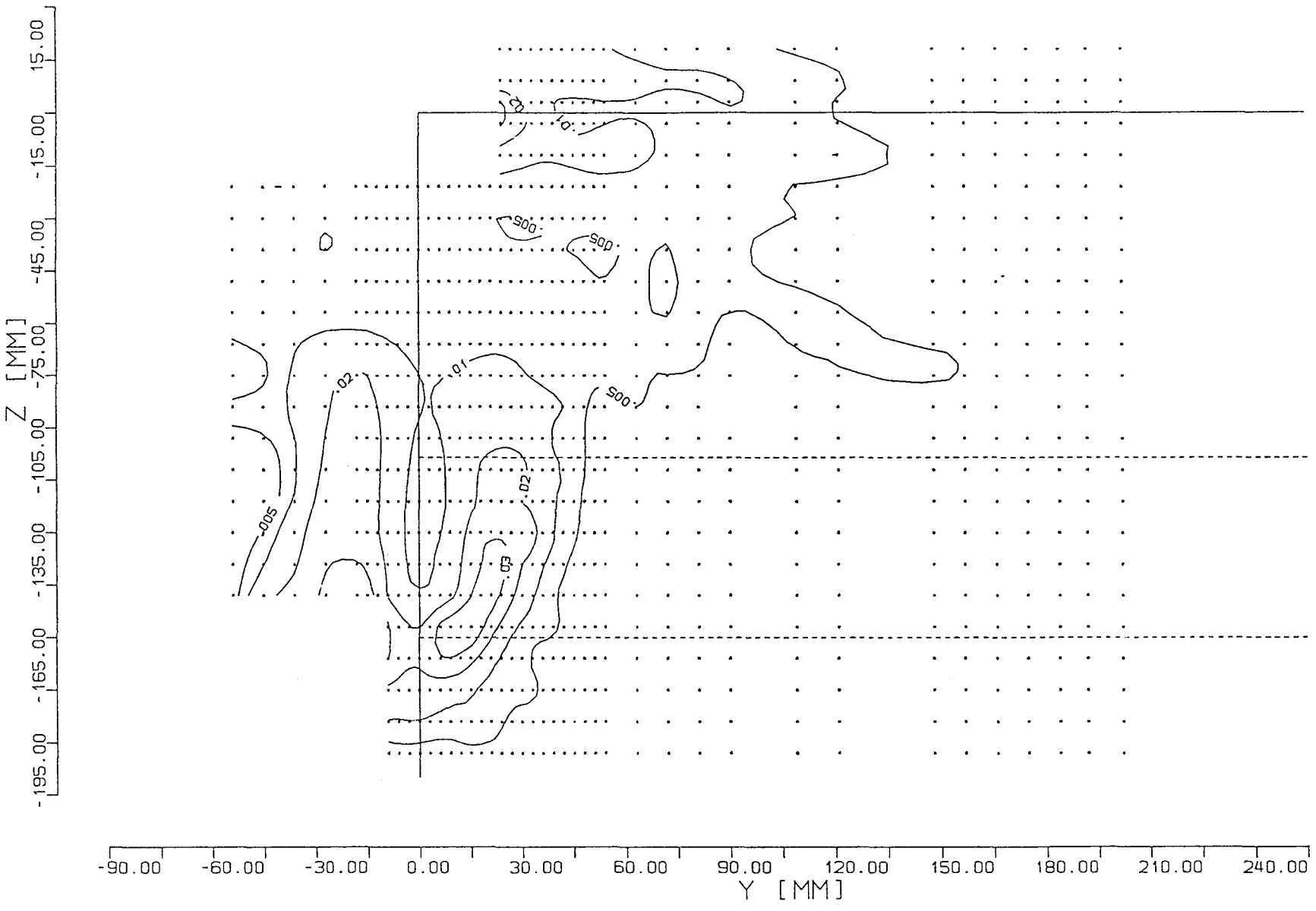

Figure 28: Station X/L = 1.018; Contours of constant normalized kinetic energy of turbulence k/U_∞^2 (Experiment)

5.4 Wall shear stress

Three different investigations of the wall shear stress have been carried out.

- Skin friction coefficient c_f was calculated out of experimental data of the mean velocity using the law of the wall. The method of calculating c_f is explained in appendix A.
- Photographs of flow visualisation show the directional field of wall shear stresses (limiting streamlines) at the stern of the ship.
- Distribution of the skin friction vector along the hull surface was determined by the boundary layer computation, as explained in section 4. At the stern of the ship there is a region where this computation fails. This may be due to negative velocity components in lenghtwise direction or because the range of validity of the boundary layer approximations has been abandoned.

Girthwise distributions of the skin friction are shown in figure 29 and 30. Two vertical axes are plotted. One labeled for the skin friction coefficient c_f and the other labeled for the friction velocity u_τ. u_τ has been obtained at the stations $X/L = 0.128$ and $X/L = 0.646$ by the method explained in appendix A and therefore depends on U_e, the velocity at the boundary layer edge. U_e varies slightly along the girth and since it does not differ from U_∞ by more than 2%, U_e has been substituted by the constant U_∞.
At station $X/L = 0.128$ "experimental c_f" and "numerical c_f" are displayed in figure 29. At girthwise locations greater than 35% "experimental c_f" could not be obtained (the small boundary layer thickness does not allow to calculate u_τ). "Numerical c_f" shows a significant maximum at the turn of the bilge at 60% of the girth, where comparison with experimental data is not possible.
At station $X/L = 0.646$ (Fig. 30) there is a displacement between the otherwise similar distributions of "experimental c_f" and "numerical c_f", which may be caused by the different methods applied in this derivation (Clauser plot is used in the experiment, Ludwieg-Tillmann formula is used in the computation; ref. appendix A). The minimum of c_f at the turn of the bilge appears at the same location in both distributions.

c_f could not be obtained from the experimental data at stations with $X/L \geq 0.646$, because there the distribution measured in transverse planes are not velocity profiles in normal direction to the surface any more (compare app. A).

In figure 31 calculated skin-friction vectors plotted on the surface of the hull (Fig. "b") are compared with a photograph of flow visualisation (Fig. "a"). A line on the surface bounding the region where the computation failed has been plotted in both figures, "a" and "b". This line may thus be interpreted as separation line. Near to the keel at $X/L = 0.921$ the lower branch of this line (result of computation) corresponds to a contour in the flow visualisation, to which limiting streamlines converge.

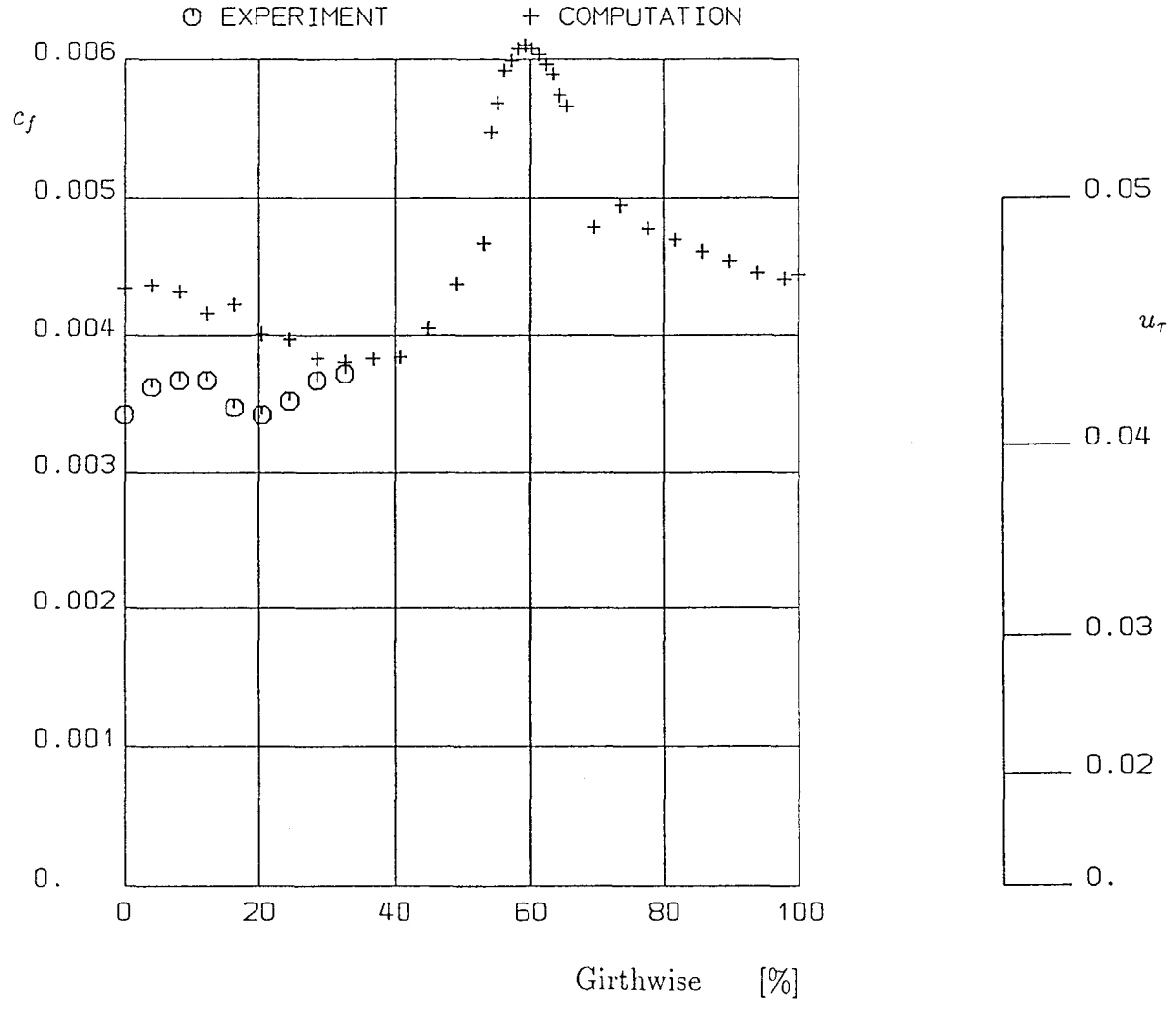

Figure 29: Station X/L = 0.128; c_f; Girthwise distribution

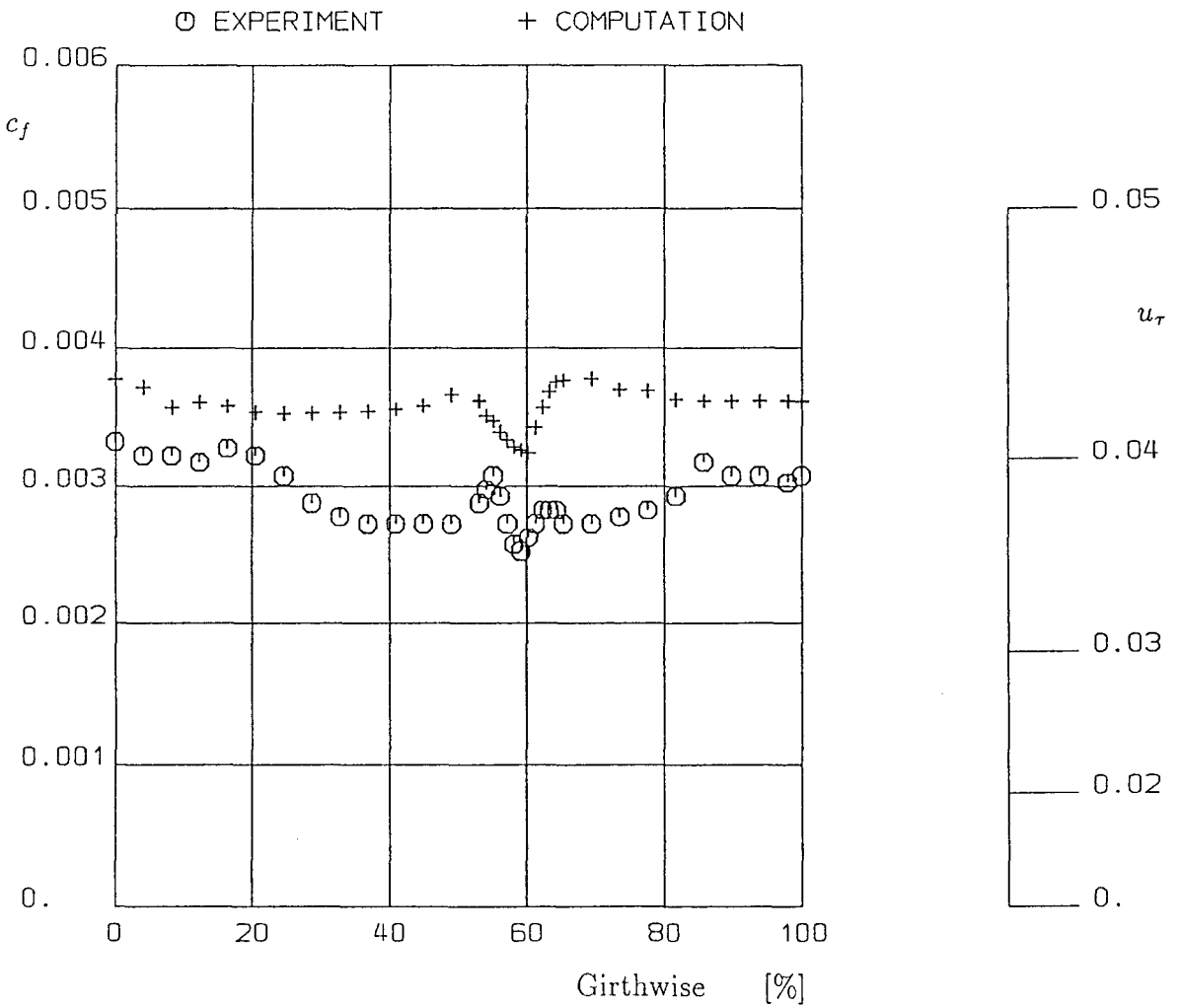

Figure 30: Station X/L = 0.646; c_f; Girthwise distribution

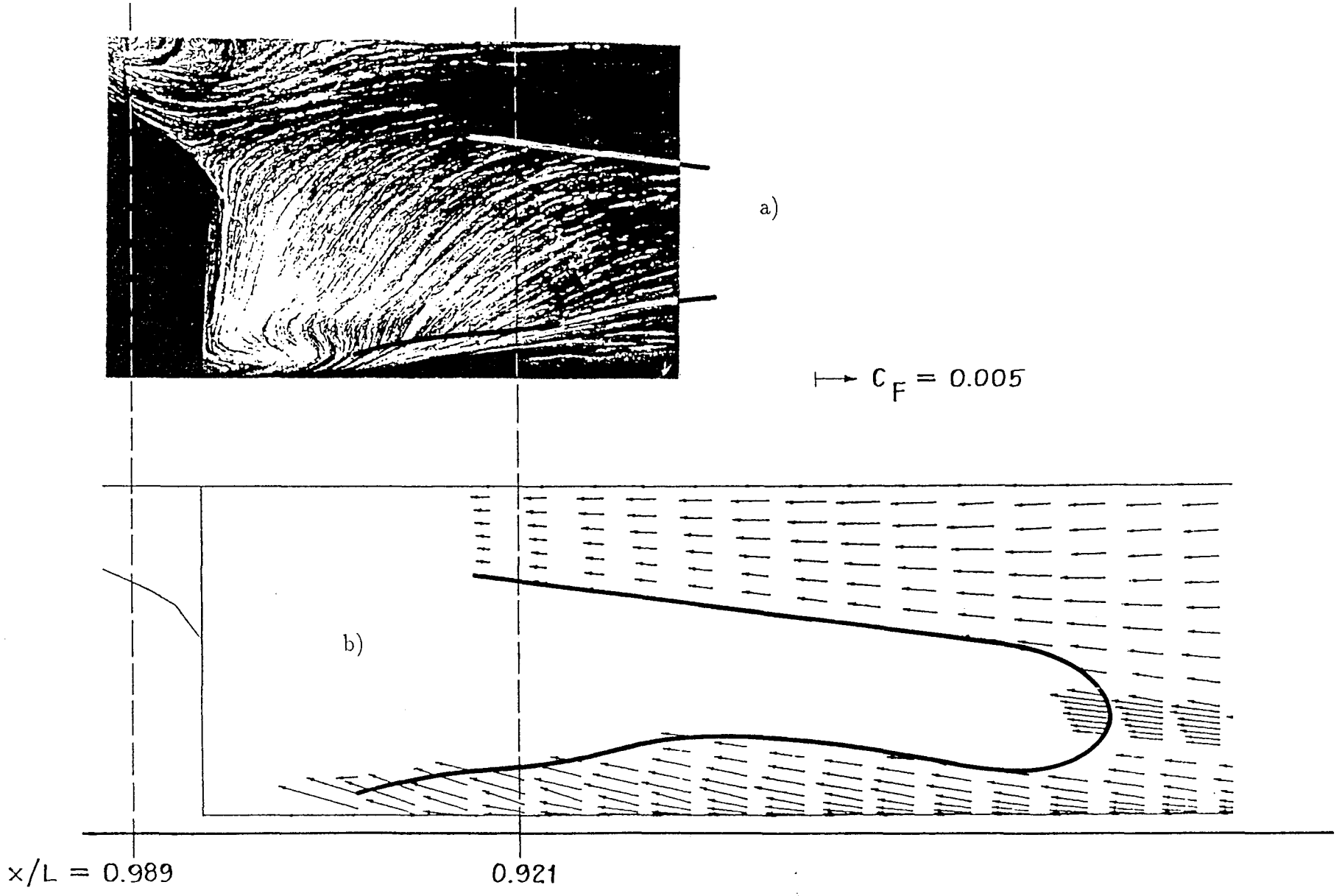

Figure 31: a) Directional field of wall shear stresses (limiting streamlines)
b) Computation of skin-friction vector $\vec{c_f}$

Nomenclature

c_f	skin friction coefficient
c_p	pressure coefficient $\frac{p-p_\infty}{1/2 U_\infty^2}$
k	kinetic energy of turbulence
L, L_{pp}	length between perpendiculars
U_∞	undisturbed velocity
U_e	velocity at the boundary layer edge
$\overline{u}, \overline{v}, \overline{w}$	components of mean velocity vector
$\overline{u'^2}$	first component of the Reynolds stress tensor
u_τ	skin friction velocity
X, Y, Z	global othogonal coordinate system
Y_{norm}	wall distance

δ	boundary-layer thickness
ΔY_{norm}	deviation of the wall distance

Acknowledgements

The authors wish to thank the german research council Deutsche Forschungsgesellschaft for funding the manufacturing of the wind tunnel model.

The body plan of the HSVA-tanker-2 was designed SSPA.

We are especially grateful to Mr. U. Gietz, M. Spohr and E. Schuckert, for their activity during the measurement in the wind tunnel.

Last but not least thanks to all members of the IfS, which contributed to this project.

References

[1] Cebeci T., Chang K.C., Kaups K., "A General Method for Calculating Three-Dimensional Laminar and Turbulent Boundary Layers on Ship Hulls", Report No. MDC J7998, Douglas Aircraft Co., 1978

[2] Hess J.L., Smith A.M.O., "Calculation of Nonlifting Potential Flow about Arbitrary Three-Dimensional Bodies", Douglas Aircraft Co., Inc., Aircraft Division, Report No. E. S. 40622, 1962

[3] Hoffmann H.-P., "Untersuchung der dreidimensionalen, turbulenten Grenzschicht an einem Schiffsdoppelmodell im Windkanal", Institut für Schiffbau, Bericht Nr. 343, 1976

[4] Knaack Th., Kux J., Wieghardt K., "On the Structure of the Flow Field on Ship Hulls", Osaka Int. Colloquium on Ship Viscous Flow, Osaka, 1985

[5] Knaack Th., Kux J., Wieghardt K., "Theoretical Analysis of the Detaching Turbulent Three-Dimensional Flow in the Stern Region of a Hull", Tenth Australasian Fluid Mechanics Conference, Melbourne, 1989, Proceedings, 8.27 - 8.30

[6] Knaack Th., "LDV-Messungen der Reynolds-Spannungen im Nachlauf eines Schiffmodells im Windkanal", IfS-Bericht Nr. 499, 1990

[7] Kux J., "Über dreidimensionale Grenzschichten an gekrümmten Wänden", Institut für Schiffbau, Bericht Nr. 273, 1971

[8] Kux J., Wieghardt K., "Nomineller Nachstrom auf Grund von Windkanaluntersuchungen", Jahrbuch Schiffbautechnische Gesellschaft 74, 1980

[9] Kux J., "Dreidimensionale Schiffsgrenzschichten-Wechselwirkung mit der Nachlaufströmung", Teilprojekt II/2, im Abschlußbericht zum 1. Finanzierungsabschnitt in "Verbundforschungsvorhaben der Stiftung Volkswagenwerk Entwicklung von Berechnungsverfahren für Probleme der Strömungstechnik", zusammengestellt von Durst F. und Kessler R., 1988, S. II.114 - II.144

[10] Kux J., "Dreidimensionale Schiffsgrenzschichten-Wechselwirkung mit der Nachlaufströmung", in "Verbundforschungsvorhaben der Stiftung Volkswagenwerk Entwicklung von Berechnungsverfahren für Probleme der Strömungstechnik", Abschlußbericht des Gesamtprojektes, Oktober 1991, zusammengestellt vom Lehrstuhl für Strömungsmechanik, Universität Erlangen-Nürnberg, S.II/2/1 - 22

[11] Larsson L., Patel V.C., Dyne G., "Ship Viscous Flow: Proceedings of the 1990 SSPA-CTH-IIHR Workshop", Flowtech International AB, Research Report No 2, Gothenburg, 1991

[12] Monnoyer de Galland F., "Calculation of Three-Dimensional Attached Viscous Flow on General Configurations with Second-Order Boundary-Layer Theory", Z.Flugwiss. Weltraumforsch. 14, 1990, S. 95 -108

[13] Wieghardt K.,"On a Characteristic of Threedimensional Free Turbulence", 12th Georg Weinblum Memorial Lecture, in Schiffstechnik Bd. 37, 1990

List of Figures

A Transformation of experimental and numerical data

Experimental data and computed results were transformed to common coordinates and common units in order to be compared. The required calculation of several parameters and approximations, are described in this section.

Wall pressure

"Experimental c_p" was determined by pressure taps at 25 locations, which were built into the wind tunnel model at three stations. "Numerical c_p" was calculated by potential theory at the center of 1820 panels. Results of computation were interpolated onto the locations of the pressure taps.

Velocity

Coordinates

Points of measurement are defined by their coordinates in an orthogonal coordinate system. The computed results are given on points in a wall oriented coordinate system, this points are distributed along profiles in direction normal to the wall. There are 35 profiles at each station. The orthogonal coordinates of the points on a profile, therefore are functions of the wall distance Y_{norm}. The number of computed points on a profile is dependent on the boundary layer thickness. Starting with 20 points on a profile this number is increased automatically, as the boundary layer thickness grows.

A common set of coordinates was defined in order to solve some problems for comparisons.
Profiles in normal direction to the wall are assumed to be located in a plane of constant x (the x component of the normal vector is set to zero). This leads to a small deviation ΔY_{norm} of the wall distance as compared to Y_{norm}. Due to this approximation ΔY_{norm} is less than 0.1% at station $X/L = 0.646$, while at station $X/L = 0.128$ it increases in a determinate region along the girth (the turn of the bilge) up to 1.2% in maximum. ΔY_{norm} becomes greater than 10% at stations $X/L > 0.646$. Based on this approximation:

- At stations $X/L \leq 0.646$ spatial distribution of "experimental velocity" along profiles in direction normal to the wall (constant x) are calculated by interpolation. This is a basis for the calculation of "experimental c_f".
- At stations $X/L > 0.646$ it is not possible to obtain distributions along profiles in normal direction to the wall with sufficient accuracy from experimental data, due to the large ΔY_{norm}, as explained. Therefore no results of "experimental c_f" at these stations are given.
- "Numerical velocity" is presented in planes of constant x for $X/L \leq 0.646$.

Components of mean velocity

The components of the "experimental mean velocity vector" are evaluated in the orthogonal coordinate system. Results of measurements are the axial component of velocity $\overline{u}$ (in direction of the undisturbed velocity U_∞) and transverse components $\overline{v}$ and $\overline{w}$. The accuracy of the components of the mean velocity is 1% in relation to the absolute value this vector (ref. Knaack [6]). At stations $X/L = 0.128$ and 0.646 these transverse components are smaller than this accuracy of 1%. Therefore no detailed information about transverse components at these stations is given.
Though obtained in the original wall oriented coordinate system the output of the computation is a mean velocity vector with components given in a coordinate system, which is aligned in the direction of the potential flow streamlines, i.e. one component in direction of the streamline (potential theory) and the transverse components, in normal direction to the wall and as crossflow component.

The mean velocity vector is displayed in its orthogonal components $\overline{u}$, $\overline{v}$ and $\overline{w}$. At station $X/L = 0.128$ and 0.646 it is possible to compare component $\overline{u}$ from the experiment with the absolute value of the velocity vector from computation, because there the transverse components of the mean velocity, as well those obtained in the experiment as those computed, are very small

Turbulence

Diagonal components of the Reynolds stress tensor were determined in the experiment. As mentioned above, at stations $X/L \leq 0.646$ there is no sufficient accuracy measuring transverse velocity components, the corresponding turbulence fluctuations can not be determined, and therefore at these stations the kinetic energy of turbulence k could not be calculated. At these stations the first component of the Reynoldstensor $\overline{u'^2}/U_\infty^2$ is displayed, while for the stations $X/L > 0.646$ isolines of k are displayed.
No details on the turbulence as provided by computation with its turbulence model are presented.

Wall shear stress

Using the law of the wall "Experimental c_f" was calculated by "Clauser plot method" at the profiles of the mean velocity derived as decribed under "Velocity", for station $X/L \leq 0.646$. The value of c_f was determined by adjusting the straight line to experimental data calculating the minimum of the square of the error. In figure 32 the adjusted line is displayed at station $X/L = 0.646$ for profiles no. 6 and 14.
"Numerical c_f " from the boundary layer computation (Cebeci [1]) is displayed without any kind of transformation.

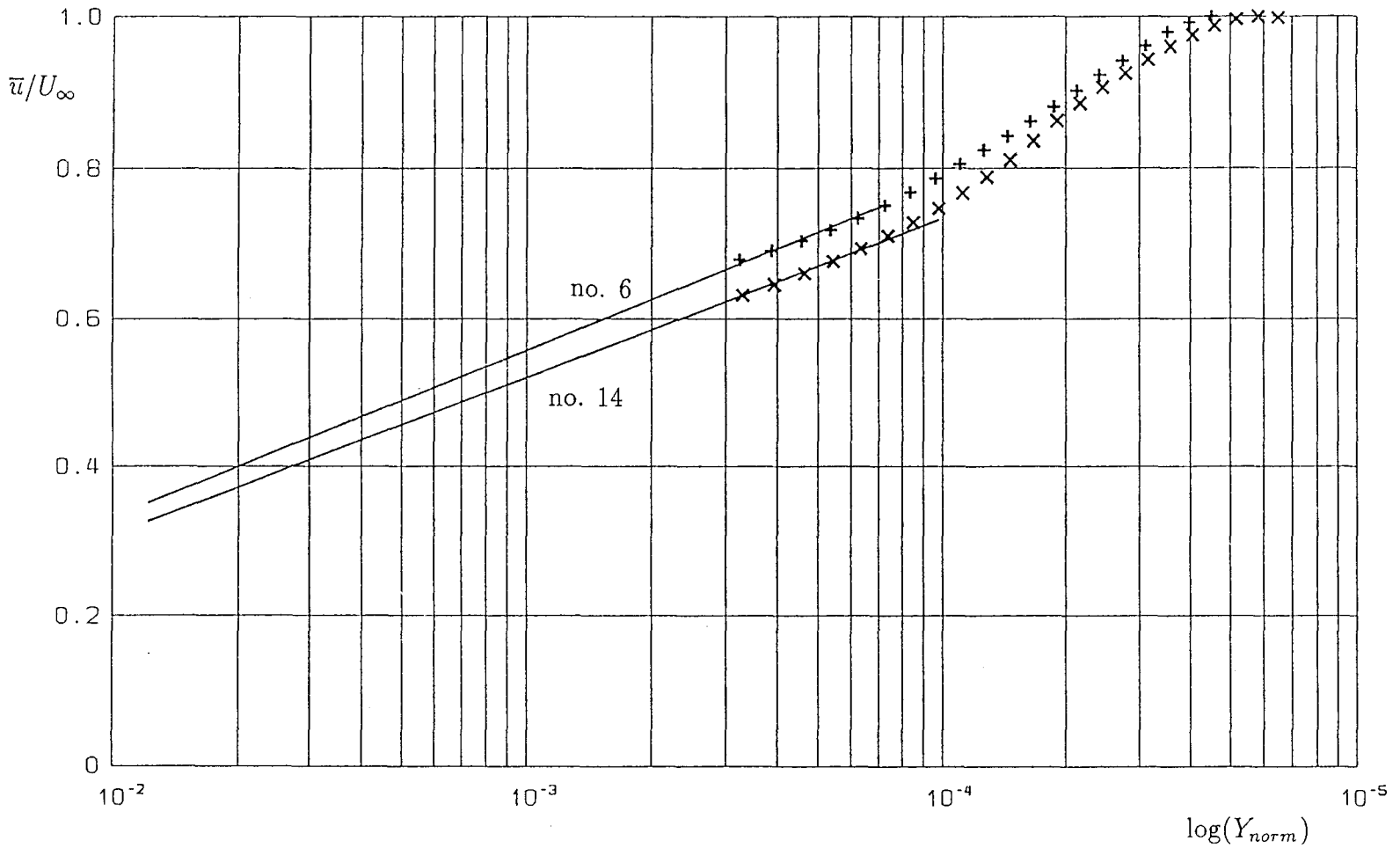

Figure 32: Station X/L = 0.646; Clauser plot;
Profiles no. 6 and 14

B Experimental results of c_p

INSTITUT FUER SCHIFFBAU

DOPPELRUMPF-HSVA-2
DRUCKVERTEILUNG
FEB 91

No	P [Pa]	CP [1]	Pdyn [Pa]	U0 [m/s]	X [mm]	Y [mm]	Z [mm]
1	47.	.10	472.	28.0	2569.0	.0	-149.5
2	45.	.10	474.	28.1	2569.0	-14.0	-130.5
3	30.	.06	475.	28.1	2569.0	-15.6	-101.5
4	75.	.16	473.	28.1	2569.0	-16.2	-74.5
5	82.	.17	474.	28.1	2569.0	-30.3	-48.5
6	81.	.17	474.	28.1	2569.0	-51.5	-30.5
7	80.	.17	473.	28.1	2569.0	-74.0	-12.5
8	22.	.05	473.	28.1	2506.0	-49.0	-74.5
9	-33.	-.07	472.	28.1	2443.0	.0	-149.5
10	-49.	-.10	475.	28.1	2443.0	-23.0	-149.5
11	-100.	-.21	472.	28.0	2443.0	-54.1	-137.5
12	-34.	-.07	474.	28.1	2443.0	-71.0	-108.5
13	-11.	-.02	474.	28.1	2443.0	-82.9	-74.5
14	8.	.02	473.	28.1	2443.0	-100.0	-46.5
15	15.	.03	472.	28.0	2443.0	-123.8	-22.5
16	-25.	-.05	473.	28.1	2412.0	-98.3	-74.5
17	-66.	-.14	472.	28.1	2210.5	-170.6	-74.5
18	-39.	-.08	473.	28.1	1968.4	-199.1	-74.5
19	-7.	-.01	473.	28.1	1720.0	.0	-149.5
20	-6.	-.01	471.	28.0	1720.0	-54.0	-149.5
21	-9.	-.02	471.	28.0	1720.0	-108.0	-149.5
22	-11.	-.02	473.	28.1	1720.0	-162.0	-149.5
23	-13.	-.03	472.	28.1	1720.0	-198.4	-137.5
24	-9.	-.02	474.	28.1	1720.0	-201.7	-74.5
25	-7.	-.01	474.	28.1	1720.0	-201.7	-37.5

CFO =0.00500

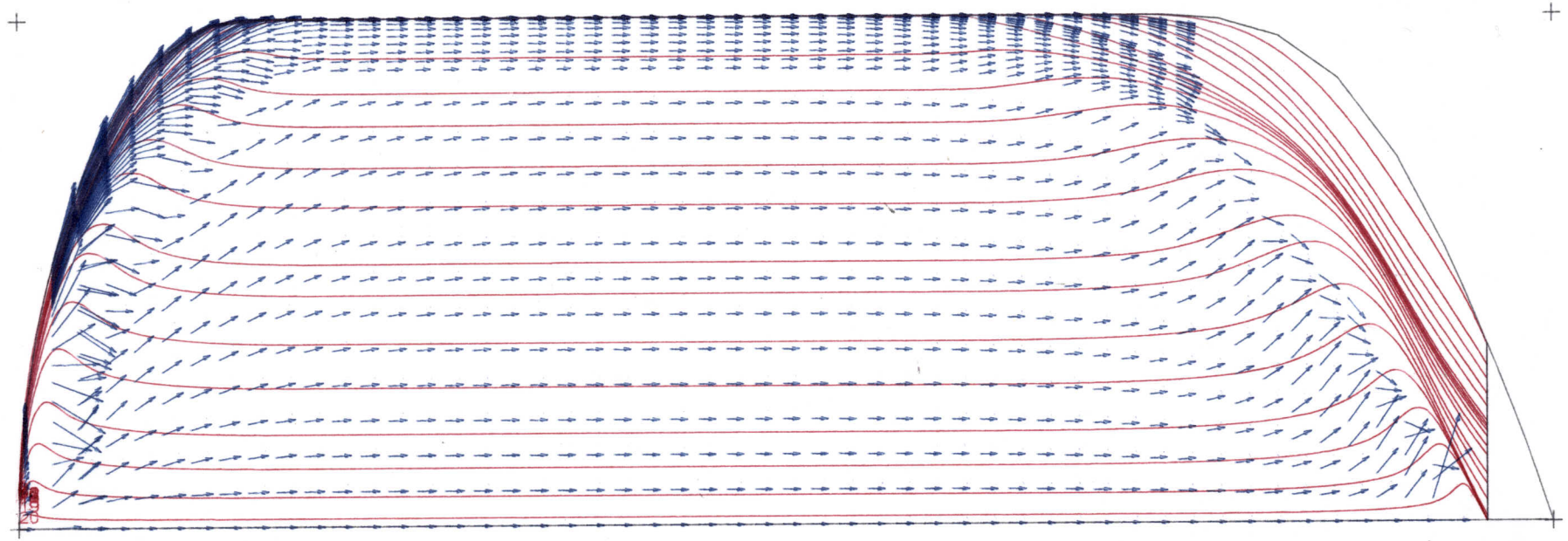

VF= 750.000
FX= 0.0900 FY= 0.4000 XY-Ebene

HSVA-TANKER2/L95

WINDKANAL DOPPELMODELL: 3D-GRENZSCHICHTBERECHNUNG NACH CEBECI
LAENGE=2.72 m, BREITE= 0.40 m, HOEHE = 0.30 m; NETZ: LARSSON2
REYNOLDSZAHL = 4.9*10Δ6 , Anstroemgeschwindigkeit = 27 m/s
Dargestellte Groesse : Wandschubspannungsvektor CF plus
Potentialtheoretische Stromlinien

CFO =0.00500

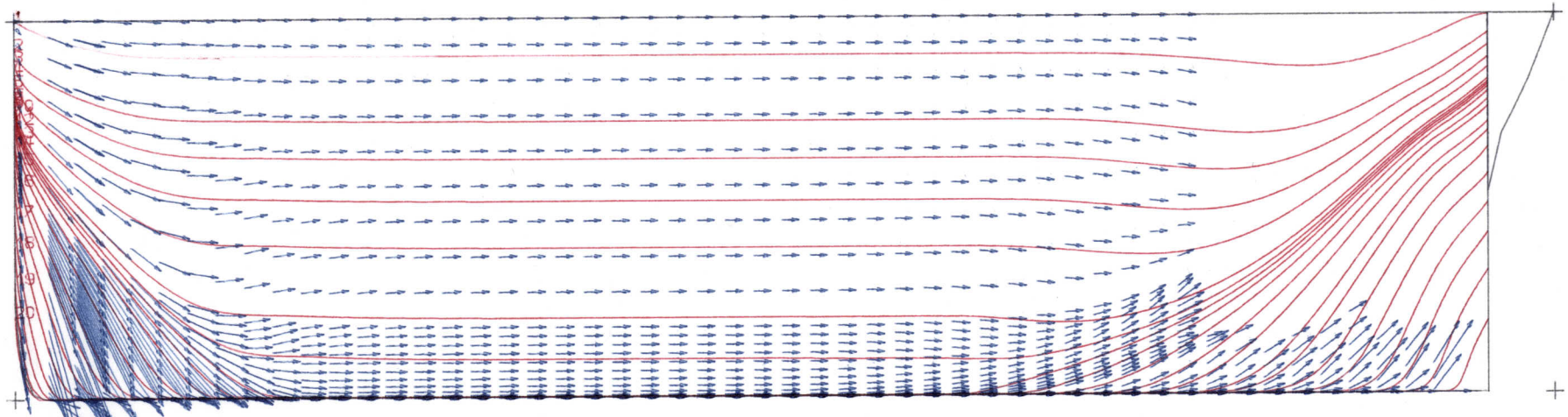

VF= 750.000
FX= 0.0900 FY= 0.4000 XZ-Ebene

HSVA-TANKER2/L95

J.DENKER/IFS/06.91

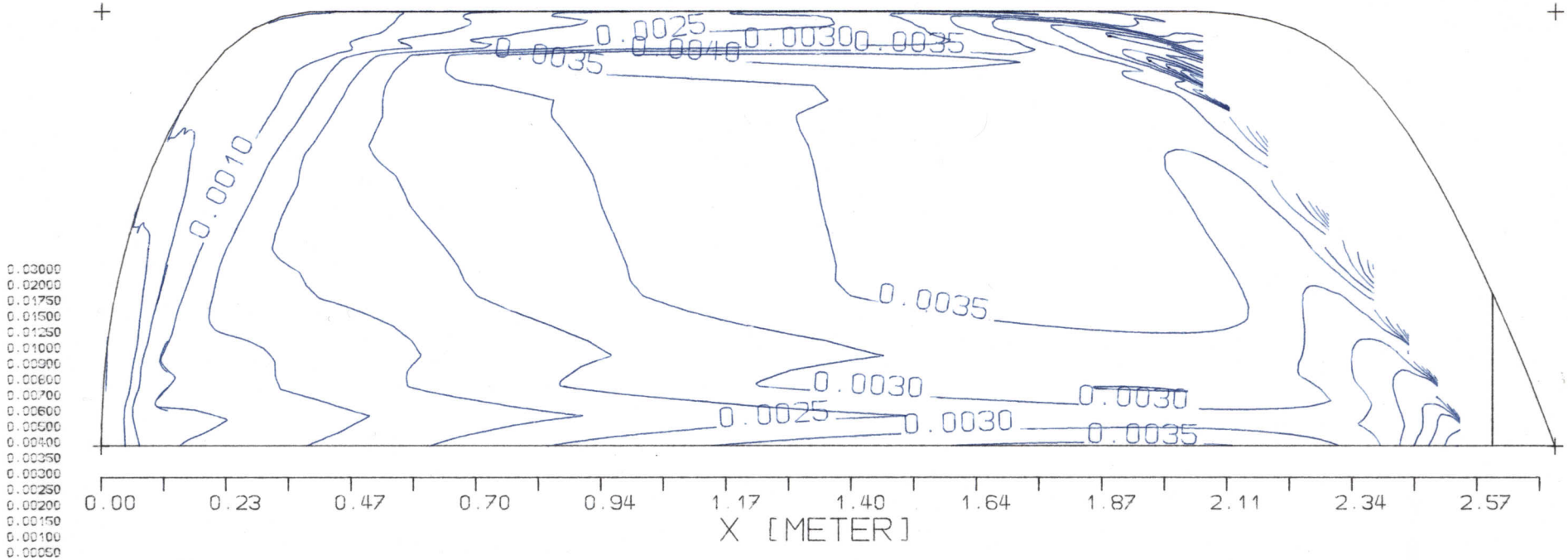

0.03000 0.02000 0.01750 0.01500 0.01250 0.01000 0.00900 0.00800 0.00700 0.00600 0.00500 0.00400 0.00350 0.00300 0.00250 0.00200 0.00150 0.00100 0.00050 0.00030

DLSTS

FX= 0.0900 FY= 0.3600 XY-Ebene

HSVA-TANKER2/L95

WINDKANAL DOPPELMODELL: 3D-GRENZSCHICHTBERECHNUNG NACH CEBECI
LAENGE=2.72 m, BREITE= 0.40 m, HOEHE= 0.30 m; NETZ: LARSSON2
REYNOLDSZAHL = 4.9*10Δ6 , Anstroemgeschwindigkeit = 27 m/s
Dargestellte Groesse : Isolinien der Verdraengungsdicke DEL1

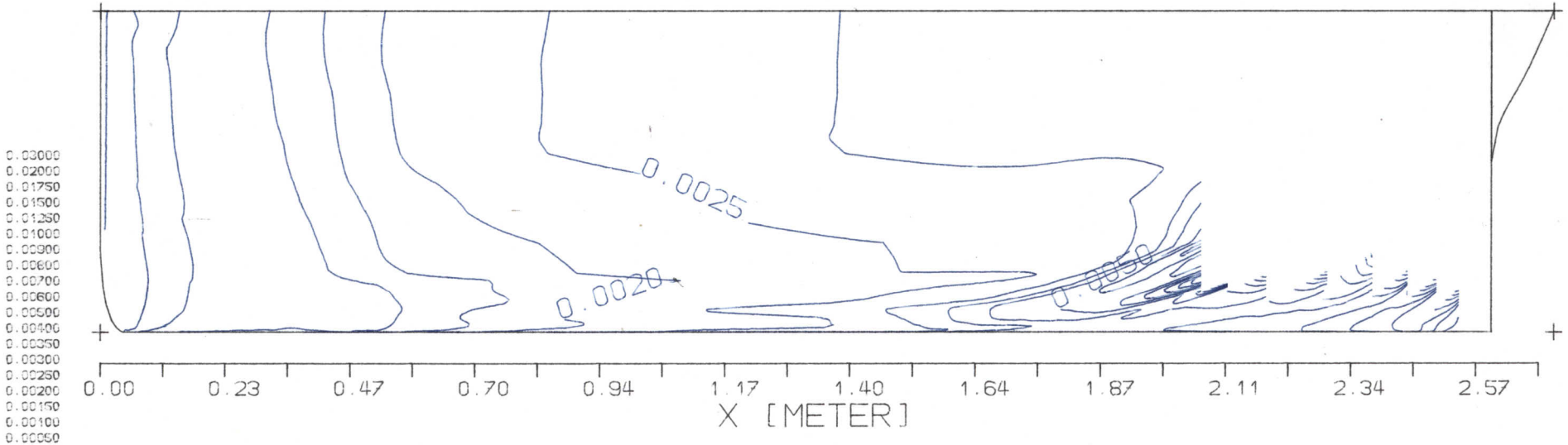

0.03000 0.02000 0.01750 0.01500 0.01250 0.01000 0.00900 0.00800 0.00700 0.00600 0.00500 0.00400 0.00350 0.00300 0.00250 0.00200 0.00150 0.00100 0.00050 0.00030

DLSTS

FX= 0.0900 FY= 0.3600 XZ-Ebene

HSVA-TANKER2/L95

J.DENKER/IFS/05.91

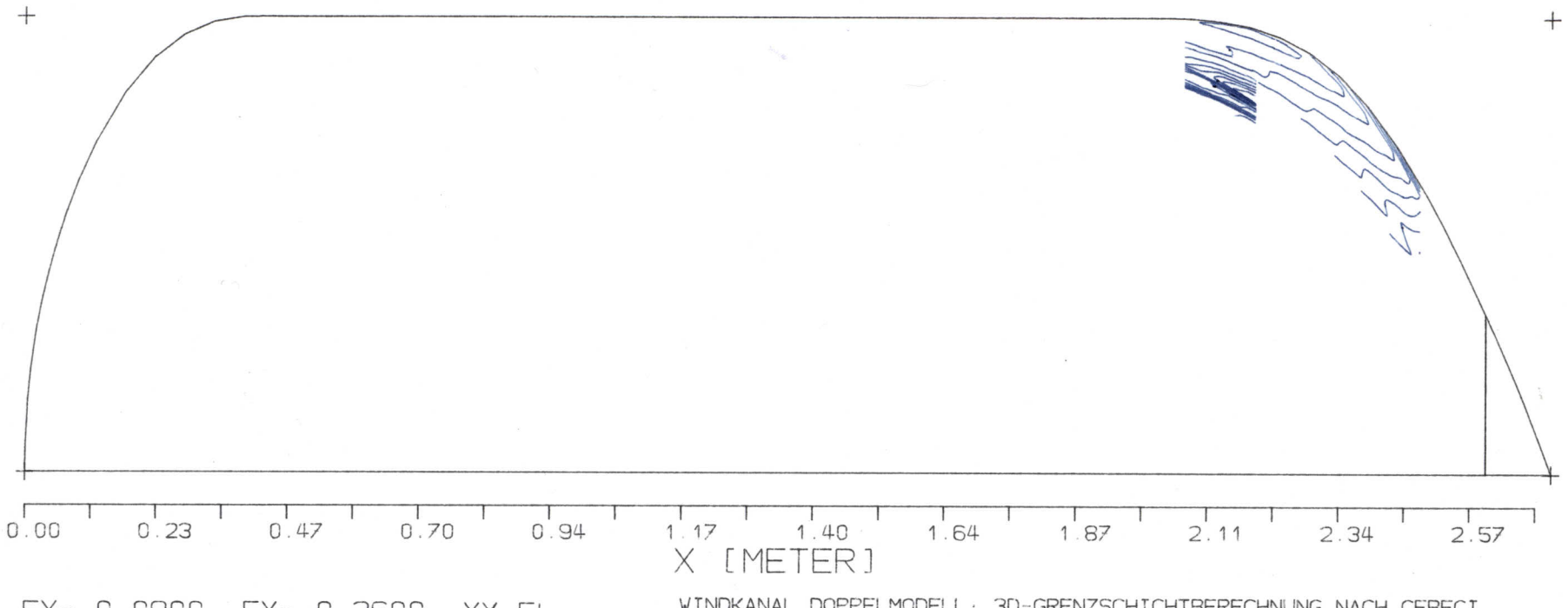

FX= 0.0900 FY= 0.3600 XY-Ebene

HSVA-TANKER2/L95

WINDKANAL DOPPELMODELL: 3D-GRENZSCHICHTBERECHNUNG NACH CEBECI
LAENGE=2.72 m, BREITE= 0.40 m, HOEHE= 0.30 m; NETZ: LARSSON2
REYNOLDSZAHL = 4.9*10Δ6 , Anstroemgeschwindigkeit = 27 m/s
Dargestellte Groesse : Isolinien der Verdraengungsdicke DEL1

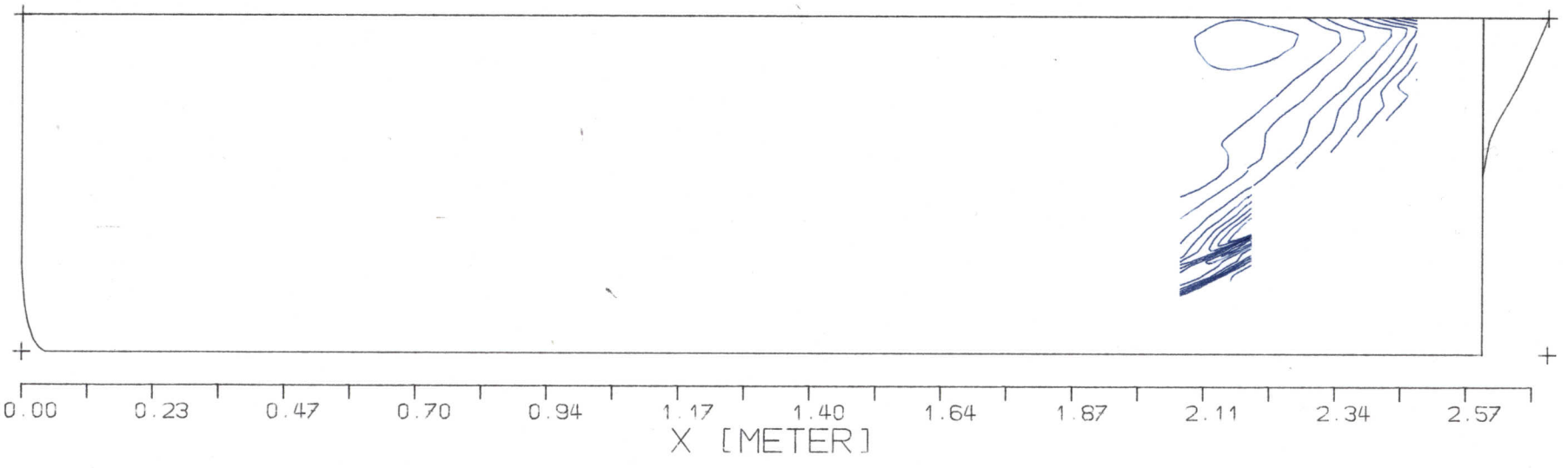

FX= 0.0900 FY= 0.3600 XZ-Ebene

HSVA-TANKER2/L95

J.DENKER/IFS/05.91

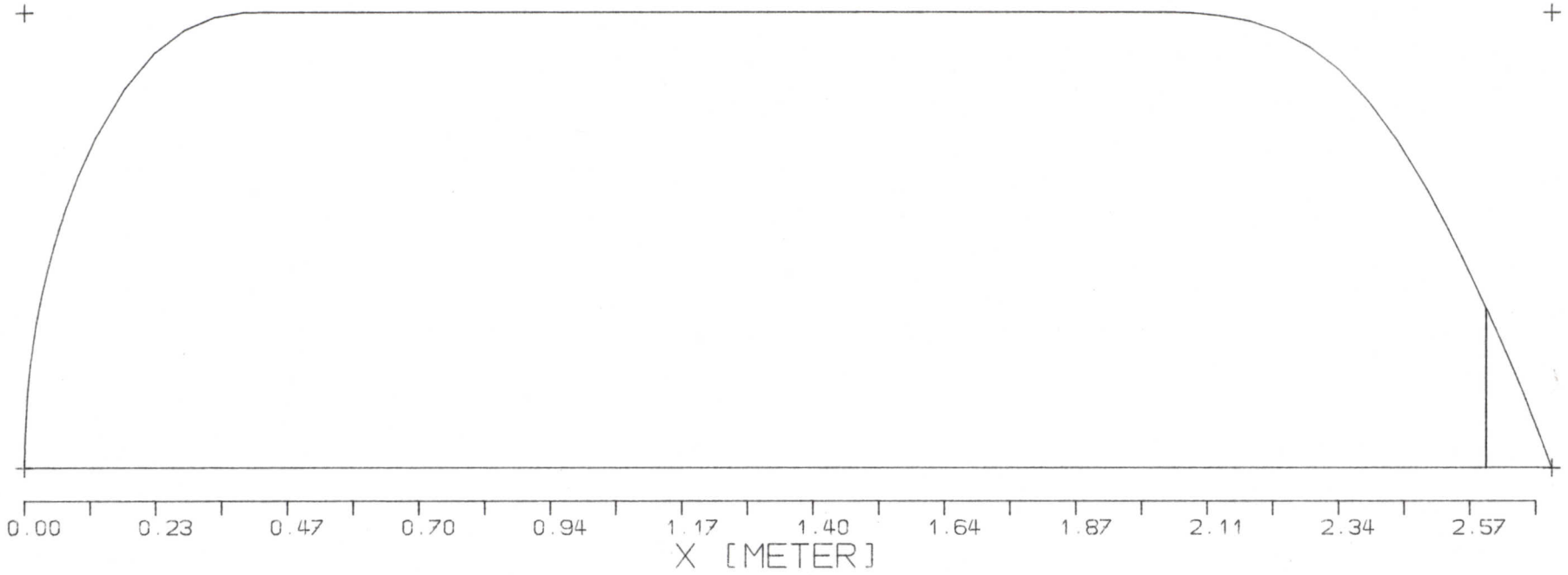

FX= 0.0900 FY= 0.3600 XY-Ebene

HSVA-TANKER2/L95

WINDKANAL DOPPELMODELL
KONTUR

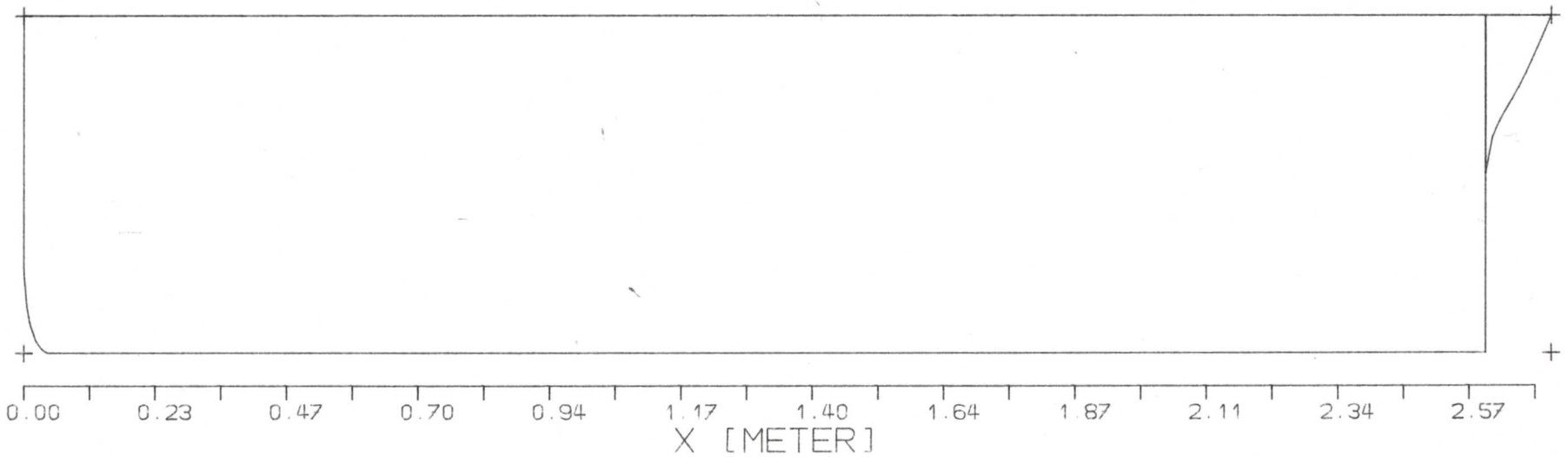

FX= 0.0900 FY= 0.3600 XZ-Ebene

HSVA-TANKER2/L95

J.DENKER/IFS/05.91

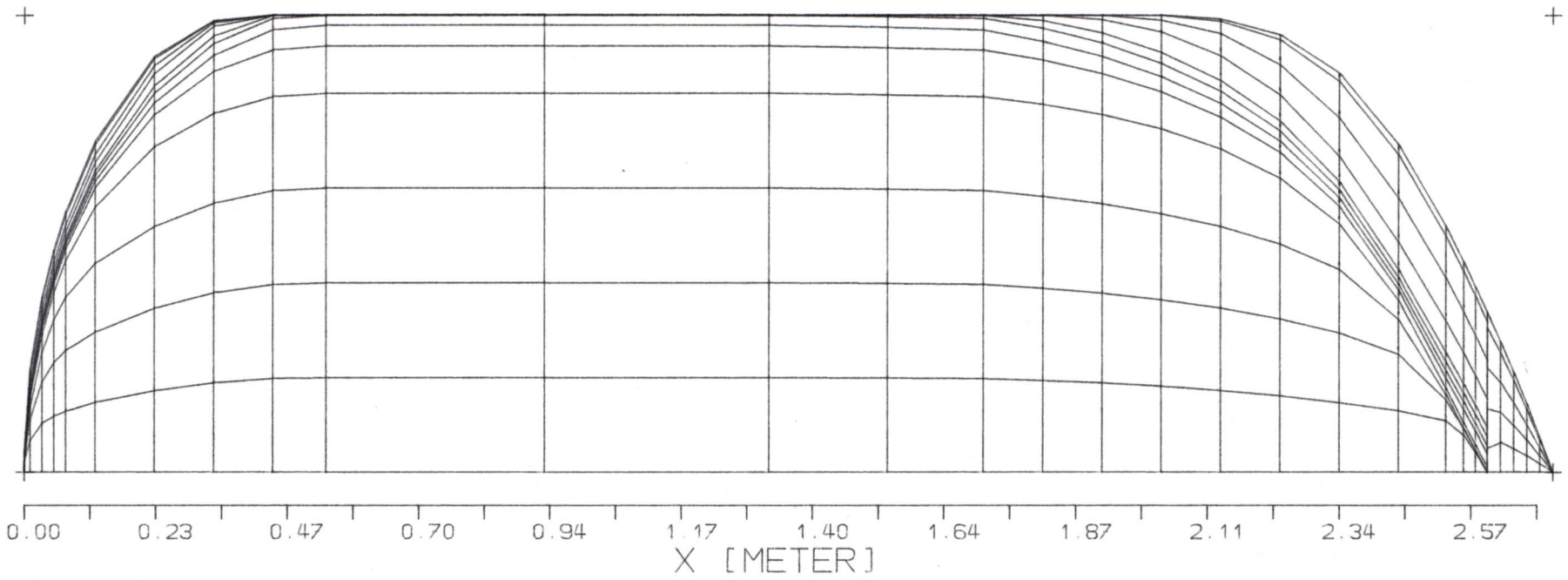

FX= 0.0900 FY= 0.3600 XY-Ebene

HSVA-TANKER2/L95

WINDKANAL DOPPELMODELL :
AUSGEDUENNTES LARSSON-NETZ
JEDER 2.SPANT UND JEDE 3.WASSERLINIE IST DARGESTELLT

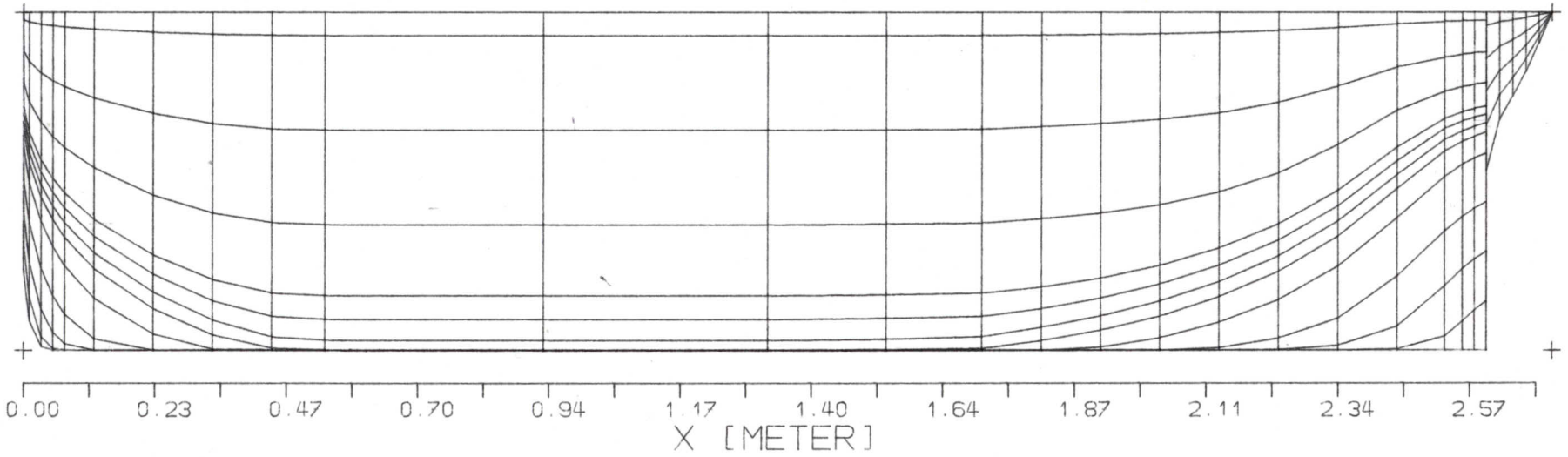

FX= 0.0900 FY= 0.3600 XZ-Ebene

HSVA-TANKER2/L95

J.DENKER/IFS/05.91

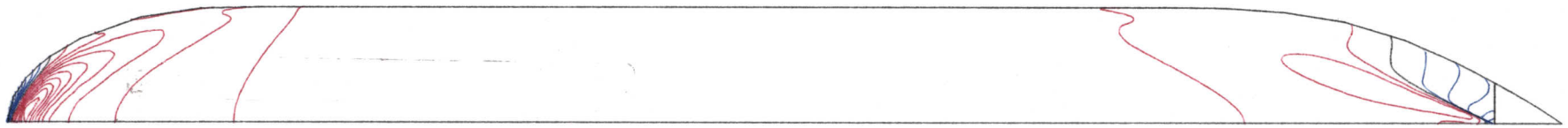

WINDKANAL DOPPELMODELL :
NETZ : LARSSON2
Dargestellte Groesse > Isolinien des Druckbeiwertes CP

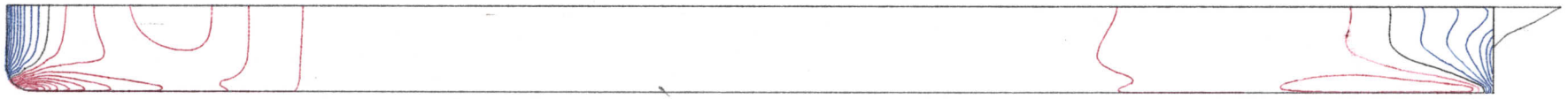

J.DENKER/IFS/05.91

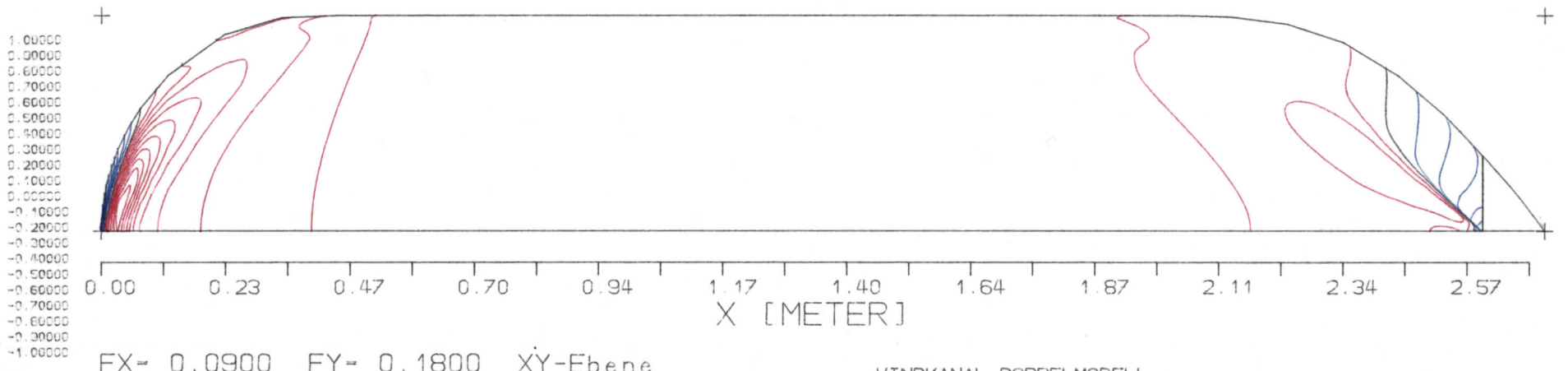

FX= 0.0900 FY= 0.1800 XY-Ebene

HSVA-TANKER2/L95

WINDKANAL DOPPELMODELL :
NETZ : LARSSON2
Dargestellte Groesse > Isolinien des Druckbeiwertes CP

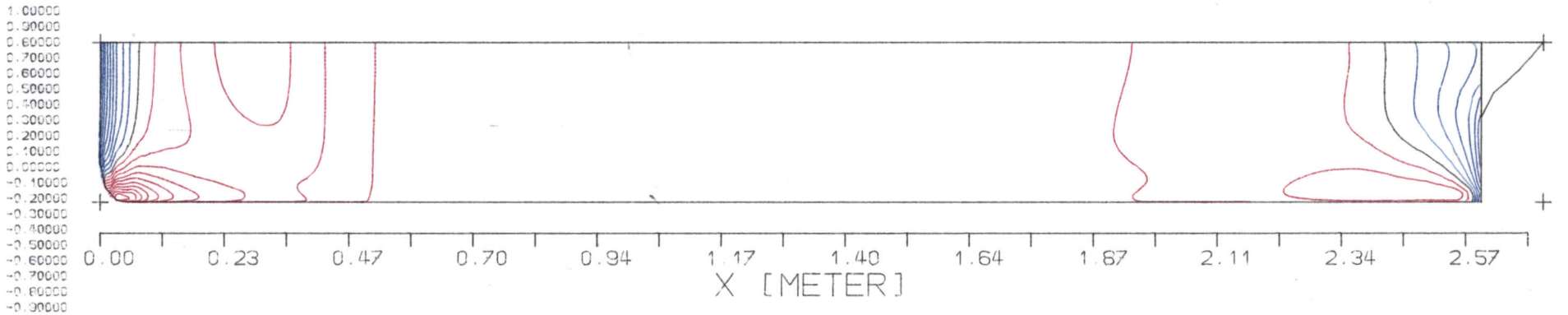

FX= 0.0900 FY= 0.1800 XZ-Ebene

HSVA-TANKER2/L95

J.DENKER/IFS/05.91

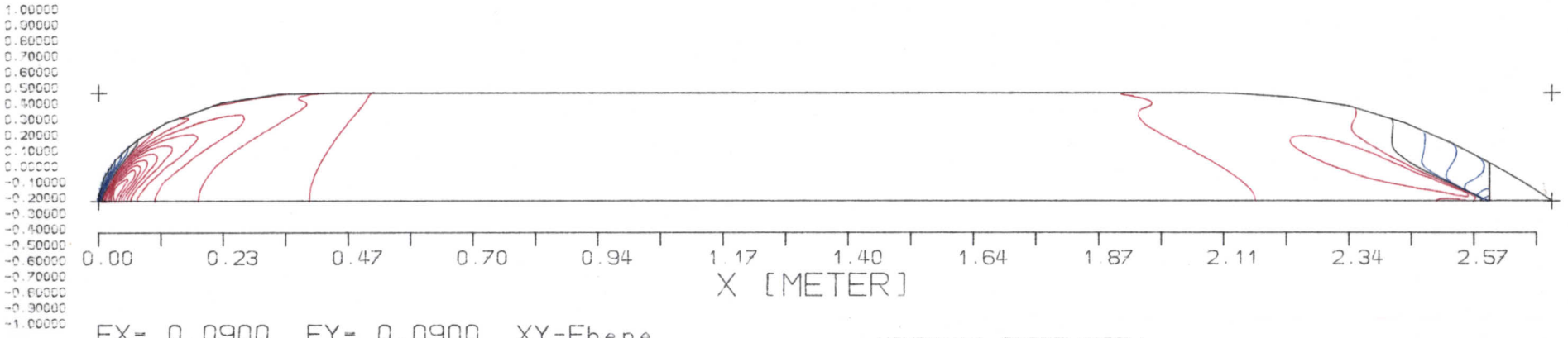

FX- 0.0900 FY- 0.0900 XY-Ebene

HSVA-TANKER2/L95

WINDKANAL DOPPELMODELL :
NETZ : LARSSON2
Dargestellte Groesse > Isolinien des Druckbeiwertes CP

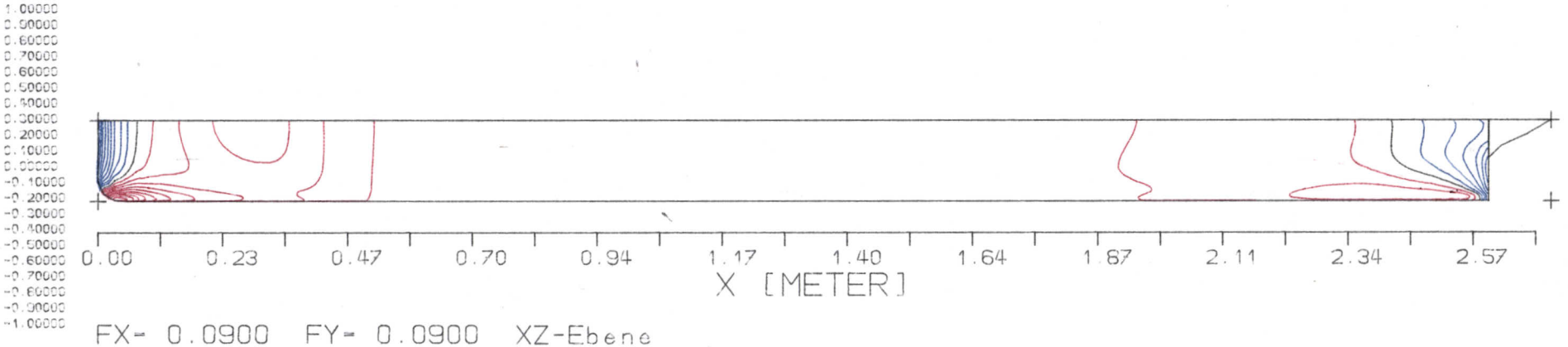

FX- 0.0900 FY- 0.0900 XZ-Ebene

HSVA-TANKER2/L95

J.DENKER/IFS/05.91

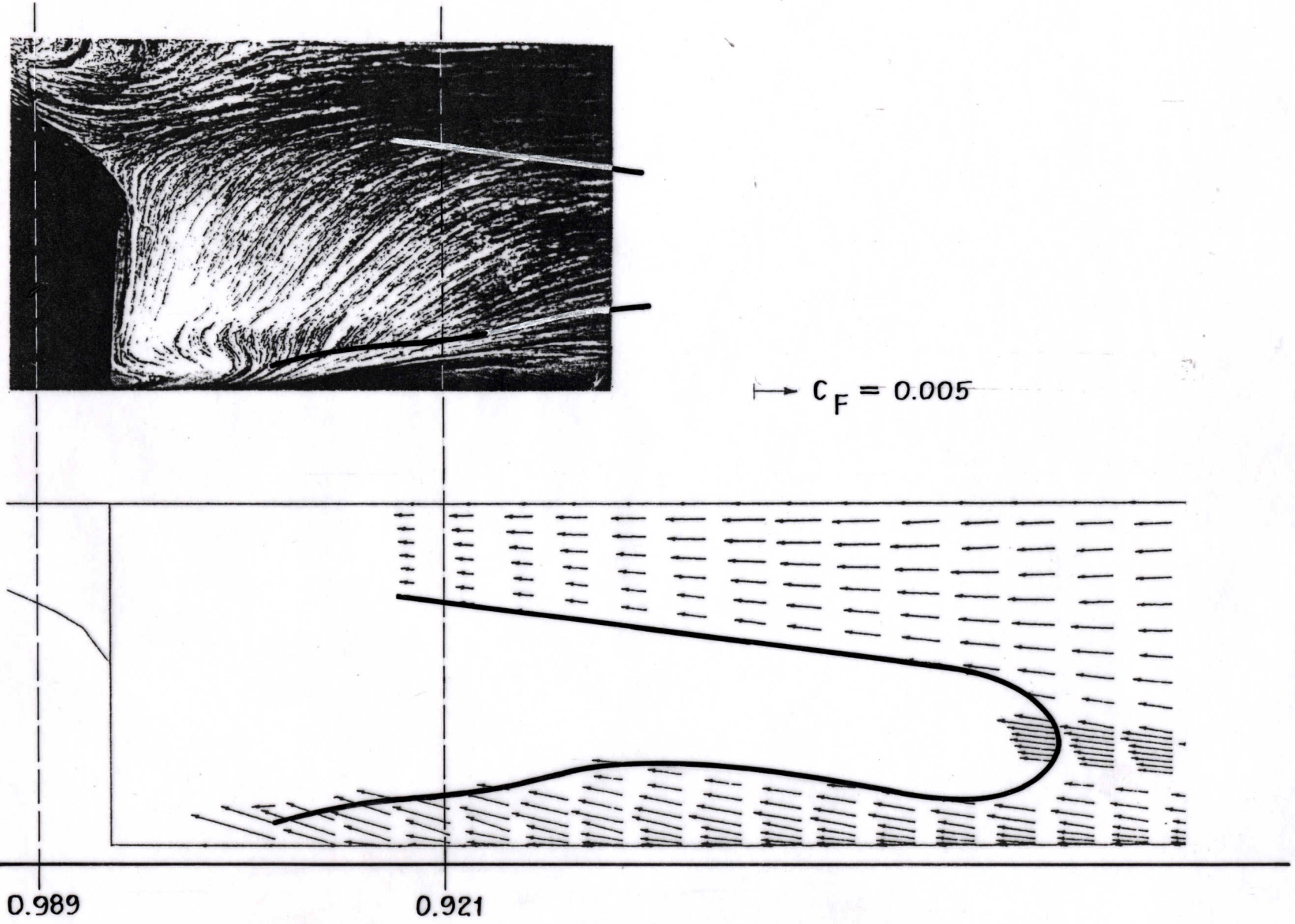
$C_F = 0.005$
x/L = 0.989
0.921

Ende Bilde Seitenverschieben (gegenüber hier)

(siehe Abb. 6)

hier Photo Originalgröße

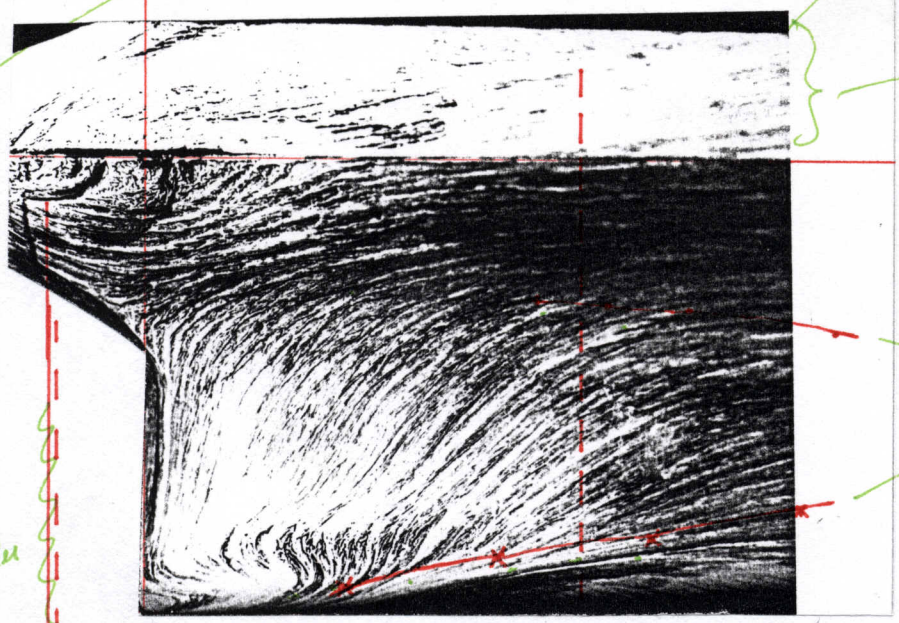

oberen Teil abschneiden

Linien von unten eingetragen

abschneiden

Pfeil! Länge → CF = 0.005

hier Plot a) Seitenverschieben b) 118%

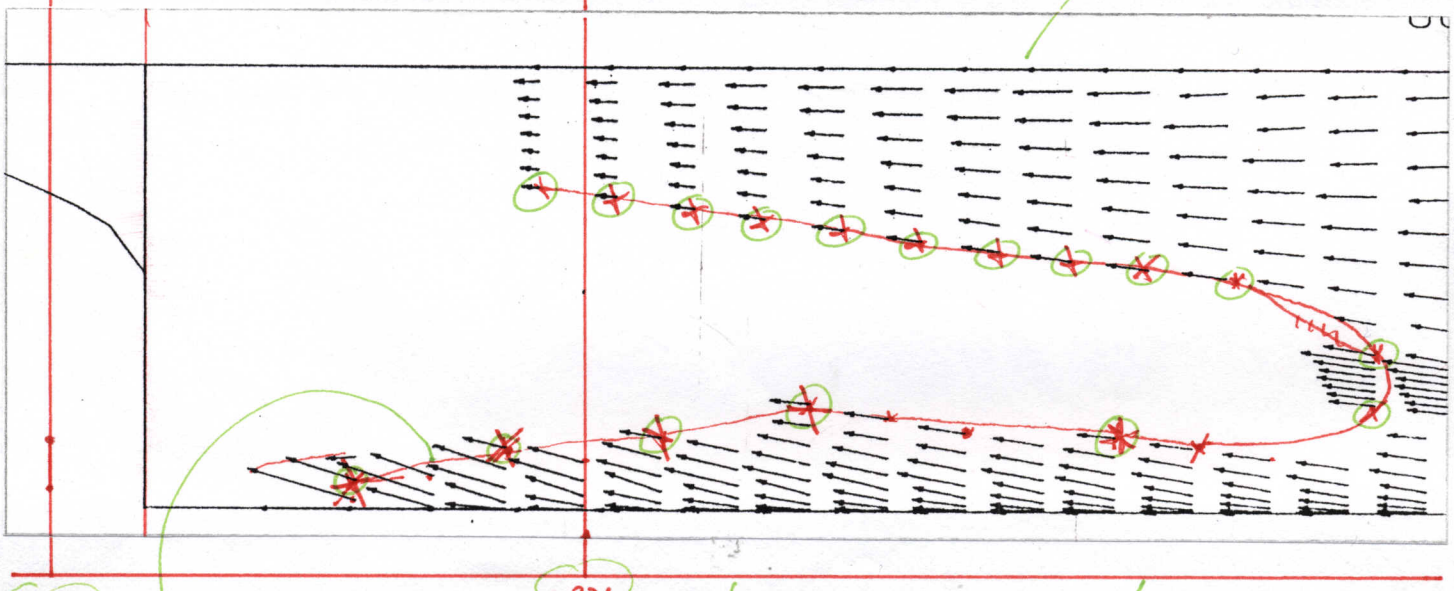

0.989 X/L

0.921

Linie durch die markierten Punkte (X)

Achse + Beschriftung

! Seitenverschieben

CFO =0.00500

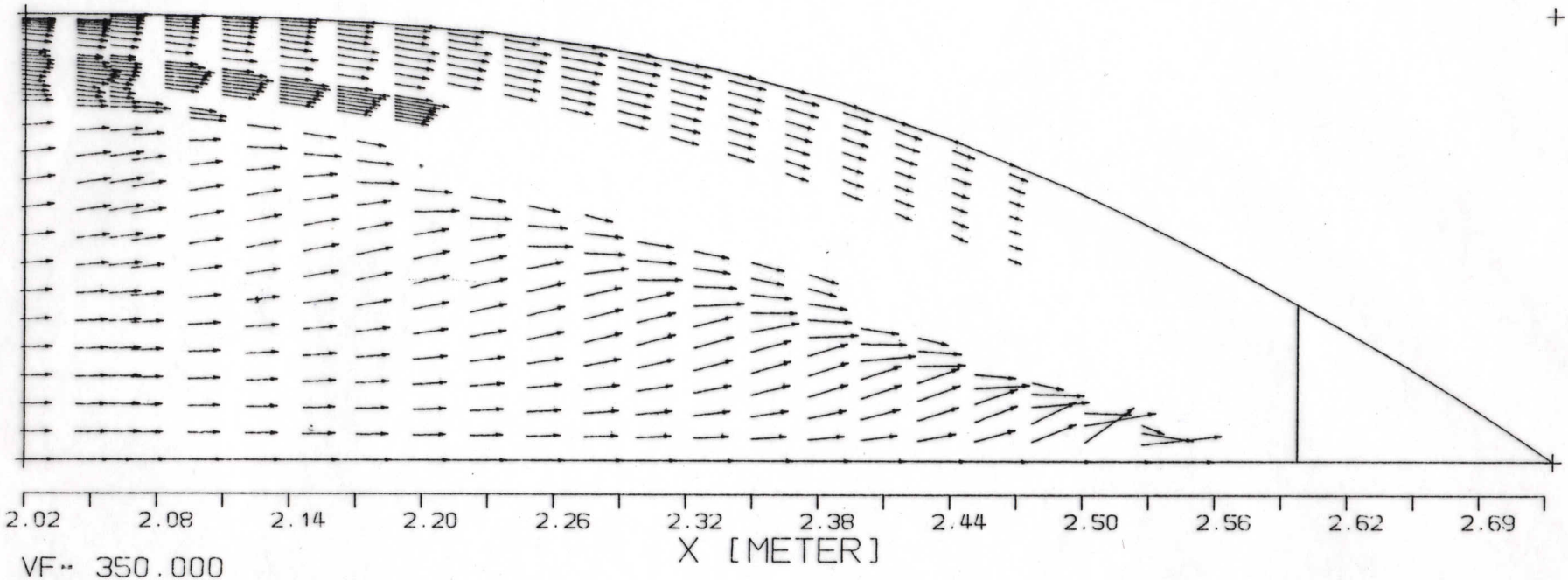

2.02 2.08 2.14 2.20 2.26 2.32 2.38 2.44 2.50 2.56 2.62 2.69

X [METER]

VF= 350.000

FX= 0.3500 FY= 0.3500 XY-Ebene

HSVA-TANKER2/L95

WINDKANAL DOPPELMODELL: 3D-GRENZSCHICHTBERECHNUNG NACH CEBECI
LAENGE=2.72 m. BREITE= 0.40 m. HOEHE = 0.30 m: NETZ: LARSSON2
REYNOLDSZAHL = 4.9*10Δ6 , Anstroemgeschwindigkeit = 27 m/s
Dargestellte Groesse : Wandschubspannungsvektor CF

CFO =0.00500

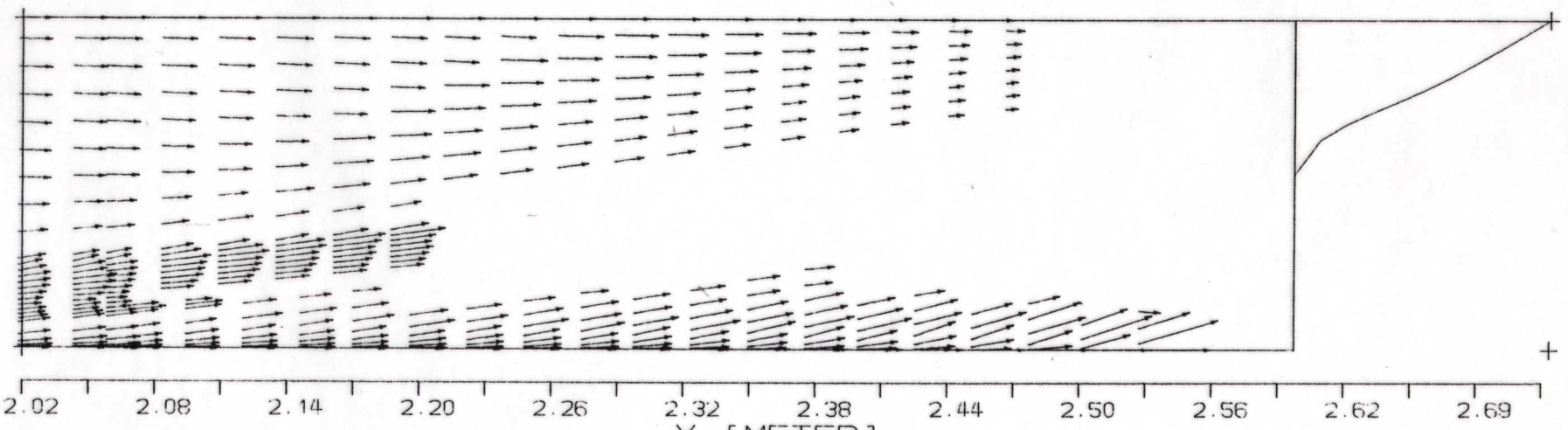

2.02 2.08 2.14 2.20 2.26 2.32 2.38 2.44 2.50 2.56 2.62 2.69

X [METER]

VF= 350.000

FX= 0.3500 FY= 0.3500 XZ-Ebene

HSVA-TANKER2/L95

J.DENKER/IFS/06.91

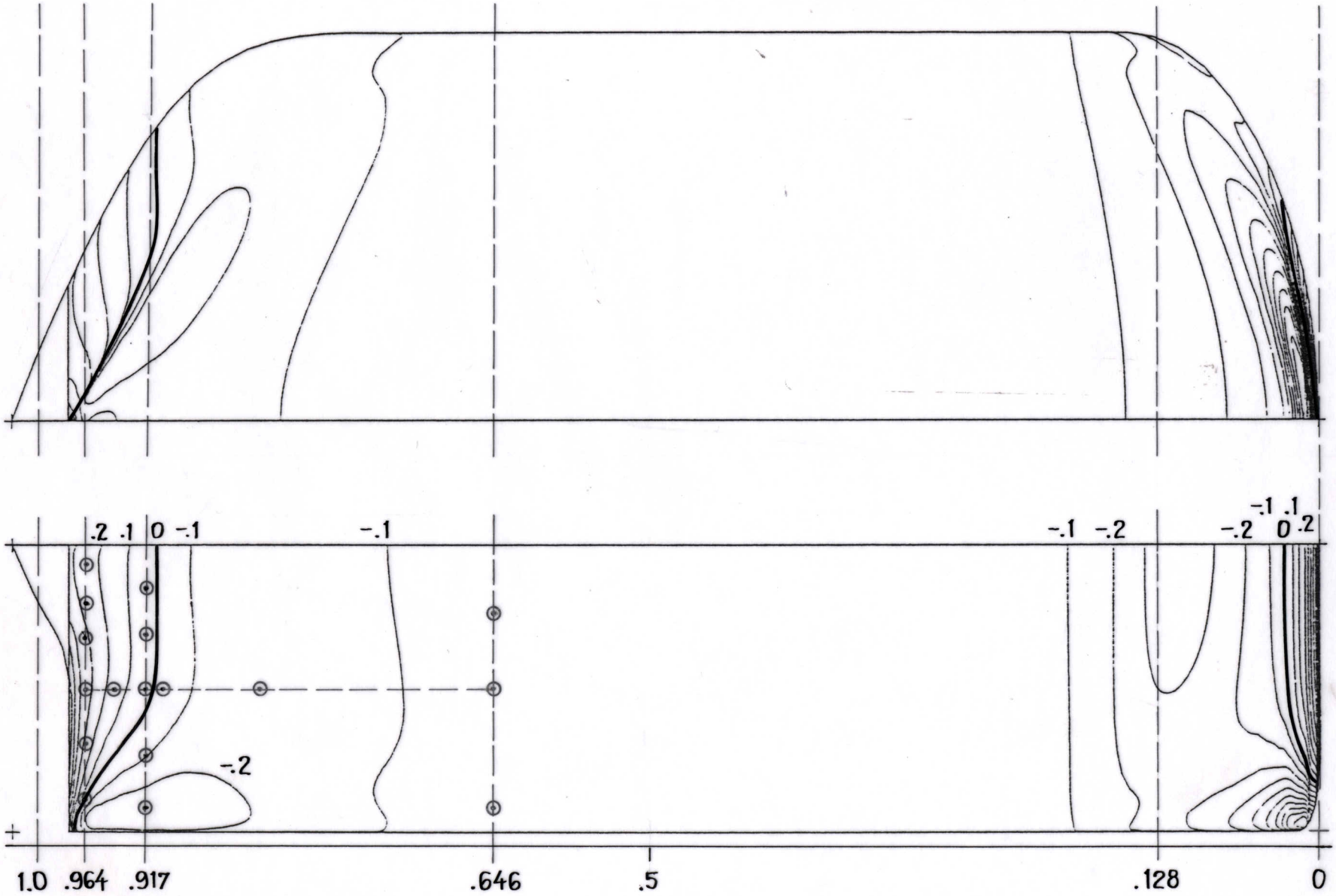
.2
.1
0
-.1
-.1
-.1
-.2
-.1
.1
-.2
0
.2
-.2
1.0
.964
.917
.646
.5
.128
0

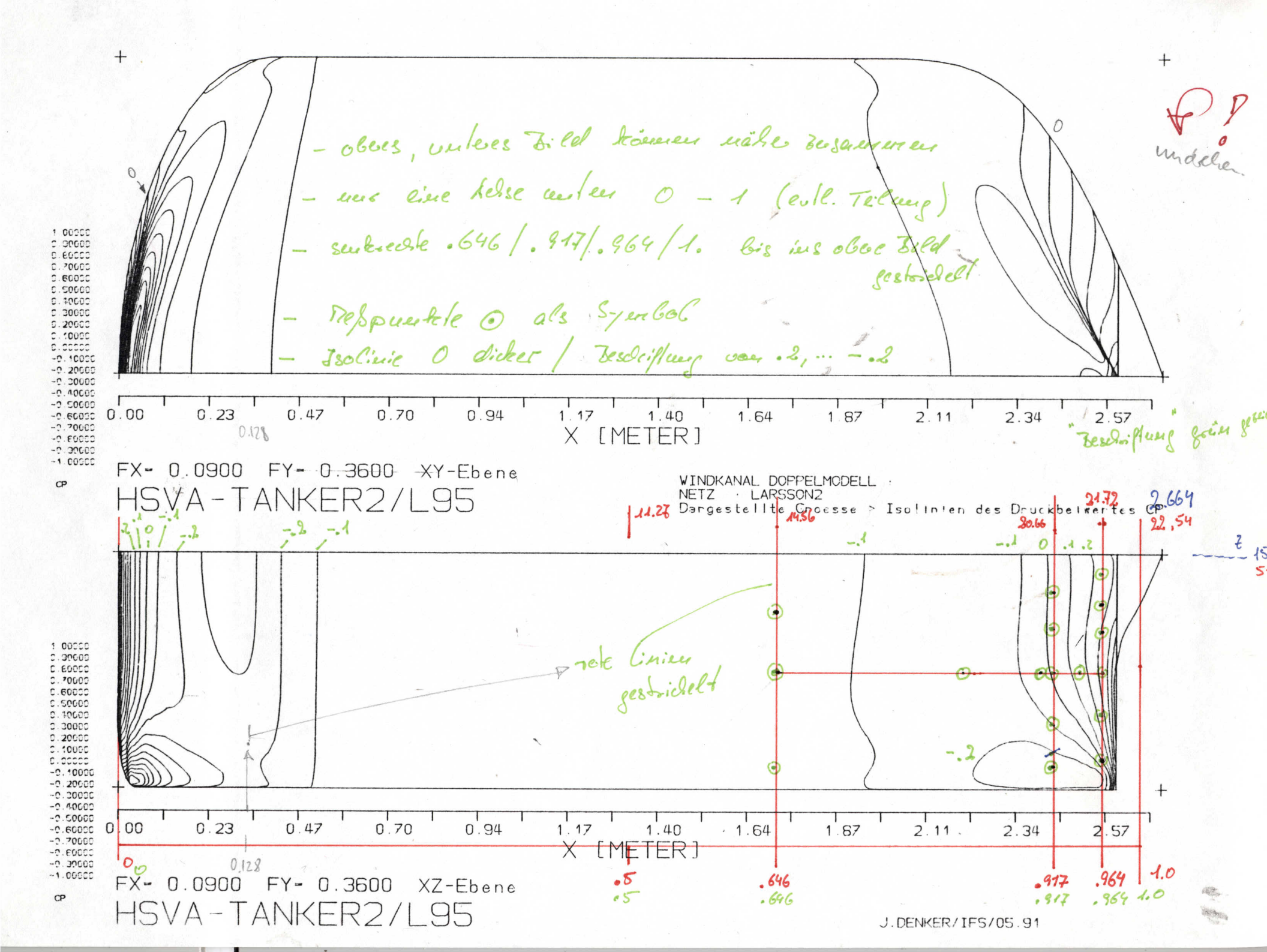
- oberes, unteres Bild können näher zusammen
- neue Reihe unter 0 – 1 (evtl. Teilung)
- senkrechte .646 / .917 / .964 / 1. bis ins obere Bild gestrichelt
- Messpunkte ⊙ als Symbol
- Isolinie 0 dicker / Beschriftung von .2, ... –.2
1.00000
0.90000
0.80000
0.70000
0.60000
0.50000
0.40000
0.30000
0.20000
0.10000
0.00000
-0.10000
-0.20000
-0.30000
-0.40000
-0.50000
-0.60000
-0.70000
-0.80000
-0.90000
-1.00000
CP
0.00 0.23 0.47 0.70 0.94 1.17 1.40 1.64 1.87 2.11 2.34 2.57
0.128
X [METER]
FX- 0.0900 FY- 0.3600 XY-Ebene
HSVA-TANKER2/L95
WINDKANAL DOPPELMODELL
NETZ · LARSSON2
Dargestellte Groesse : Isolinien des Druckbeiwertes CP
11.27
14.56
20.66
21.72
2.664
22.54
rote Linien gestrichelt
FX- 0.0900 FY- 0.3600 XZ-Ebene
HSVA-TANKER2/L95
.5
.646
.917
.964
1.0
J.DENKER/IFS/05.91

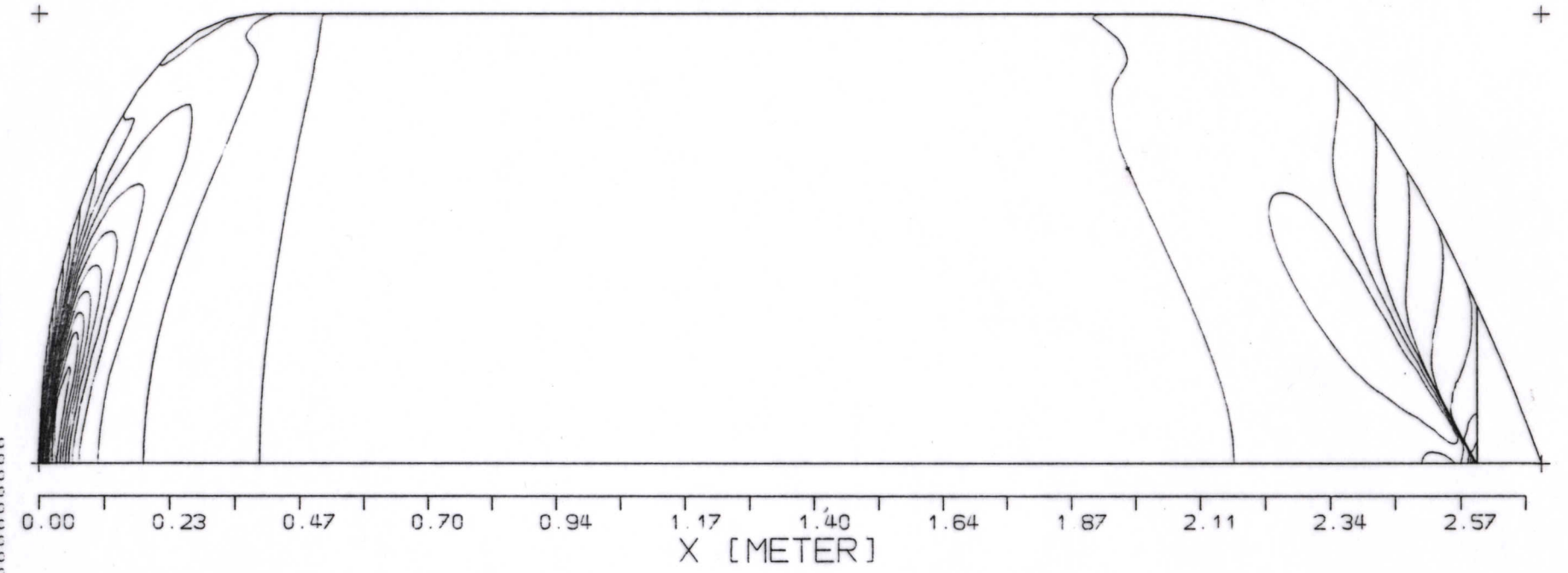

FX- 0.0900 FY- 0.3600 XY-Ebene

HSVA-TANKER2/L95

WINDKANAL DOPPELMODELL
NETZ : LARSSON2
Dargestellte Groesse > Isolinien des Druckbeiwertes CP

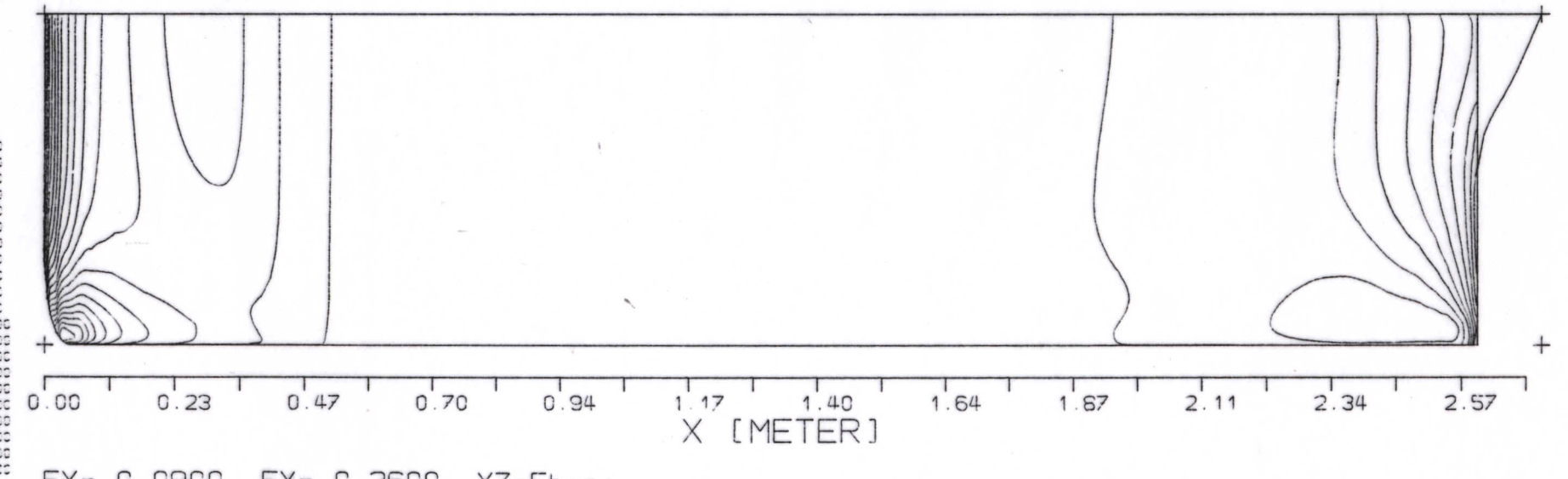

FX- 0.0900 FY- 0.3600 XZ-Ebene

HSVA-TANKER2/L95

J.DENKER/IFS/05.91